Study of the Design Problems of an Integrating Television Tube for Astronomical Research

FINAL REPORT

December 1964

Prepared for Princeton University Observatory
Space Telescope Program, Princeton, New Jersey

Under Subcontract No. 1, NASA Grant NSG-414

By

Westinghouse Electric Corporation
Electronic Tube Division
Box 746
Baltimore, Maryland

TABLE OF CONTENTS

LIST OF ILLUSTRATIONS

LIST OF TABLES

Contributors:

Electronic Tube Division

A. S. Jensen
I. Limansky
W. G. Reininger
M. P. Siedband
G. W. Goetze

Research Laboratories

E. J. Sternglass
A. K. Rigler
M. Green

Aerospace Division

F. B. Marshall
R. A. Lee
J. A. Hall
R. S. Cortesi
G. D. Roane

1.0 INTRODUCTION

The advantages to be gained through the use of an imaging tube have long been appreciated and several investigators* have devoted much time and effort in evaluating the performance and limitations of contemporary tubes. There has been general agreement that a storage tube could have the main advantages of large storage capacity, and the capability of parallel write-in and serial read-out of the information that would be useful in many astronomical applications. Space astronomy is one application where the integrating imaging tube has been seriously considered as a replacement for the scanning photomultiplier, and the Westinghouse UVICON is slated for the Smithsonian experiment of the OAO series.

Even though the concept of an integrating image tube appeared desirable from an analytical point of view, it rapidly became apparent to experimenters that if state-of-the-art imaging tubes were to be used, compromises had to be made which often nullified the advantages that were hopefully expected. Resolution, positional accuracy, signal-to-noise ratio, and sensitivity often had to be traded off one against the other in order to approach the requirements of a particular application. One or more breakthroughs in the imaging tube field were evidently needed to enable the use of these tubes to their maximum capabilities.

Westinghouse Electric Corporation has conducted research and development in the imaging tube field both at the Westinghouse Research Laboratories and at the Electronic Tube Division. As the direct consequence of this work, the SEC Vidicon and the Optechon were developed. These two are the integrating image tubes considered in this study, each having certain advantages to contribute to the problem at hand.

*References 1 through 25 represent a fraction of the total effort expended on imaging devices.

We will consider three main applications of the integrating image tube to astronomical studies. In order of importance for this study:

1) Stellar spectrophotometry
2) Photometry of extended sources
3) Binary resolution - faint point sources.

Stellar Spectrophotometry

This application is one of the main purposes for the Princeton University Observatory OAO experiment. In general, absorption spectra of low contrast are to be expected from faint stars. Spectra in the wavelength range of 1200 to 6000 Å are of primary interest, although the 900 to 1200 Å range is also desirable.

Photometry of Extended Sources

This application generally involves low-contrast signals but may also have a bright point source with a low-contrast surround.

Binary Resolution - Faint Sources

Here, the relative position of two faint sources, or a faint and a bright source, is of interest as well as any intensity fluctuations of these sources.

The goal of any imaging tube used in these applications is its ability to measure 400 photoelectrons per image element with an accuracy of 10 percent, which a photomultiplier can achieve at present. Seldom more than 10^4 photoelectrons per image element should be necessary for a maximum integration time of 100 minutes and the signal-to-noise ratio should permit a one percent accuracy. The contribution of the unresolved star background radiation is considered to be negligible. The maximum readout time of the stored information is one minute at a maximum bandwidth of 62.5 Kc/sec. A total resolution of 500 line pairs at 50 percent response is considered adequate, although better resolution is desirable.

An important consideration is that the data obtained from the imaging tube must be capable of being processed into a digital format: consequently, the data reproducibility is paramount, particularly in photometric applications. No two-dimensional display is required except possibly

for preliminary set up of equipment.

Since eventually the imaging tubes will be used in a spacecraft, ruggedness of the tubes and the weight and volume of the system required will also be of importance.

The SEC Vidicon and the Optechon considered in this study, have been evaluated on the basis of several properties that would have a definite effect either on their performance or their utilization in astronomical work. Some of these properties also limit the applicability of the Vidicon and Image Orthicon; others are peculiar to the two tubes under consideration. Also, as noted previously, the application will often dictate which of these properties is of importance. The properties considered are noted below, not necessarily in their order of importance.

1. Storage Capacity
2. Prestorage Gain
3. Detectability
4. Spatial Resolution
5. Mode of Readout
6. Beam Pulling and Spot Spreading
7. Target Configuration (fixed or movable)
8. Signal-to-noise Ratio vs. Photoelectrons per Image Element
9. Target Disturbance Noise
10. Charge Readout Reproducibility
11. Focusing
12. Integration Time
13. Production Status
14. Ruggedness

In addition to these, the ubiquitous weight-volume-power properties must also be considered. For the two tubes, when Space is considered, these factors will be largely similar.

2.0 SUMMARY OF STUDY AND RECOMMENDATIONS

2.1 Summary

The properties to be compared for the Optechon and SEC Vidicon have been outlined in Section 1.0. Table 2.0 is a brief summary of the performance of the tubes with respect to these properties and the following text references the body of the report for further data.

2.1.1 Storage Capacity

Baum[5] emphasizes storage capacity in an astronomical sensor, giving it more importance than quantum efficiency for extending the threshold of detection. In both cases the Optechon and SEC Vidicon have a storage capacity well in excess of that required ($\approx 10^9$ electrons/cm^2) even at the highest resolution provided by the Optechon (25 micron image element).

In the Optechon, the elemental electrical capacitance is much higher than that of the image orthicon (Section 3.2.4.1), since the latter[1] depends upon the closeness of the target mesh to the storage membrane ($\approx$ 0.001 inch) while the coplanar grating storage target structure permits the elemental capacity to be determined by the thickness of the dielectric[24] ($\approx$ 0.5 micron). The storage capacity for the Optechon is covered in Section 3.1.5.1.

The storage capacity of the SEC Vidicon is a more complex subject, and measurements have implied that it varies as a function of the stored charge, being initially small, and increasing to values higher than can be computed from the image element size and the layer thickness. Section 3.2.4.3 and 3.2.4.6 discuss the observed effects further.

2.1.2 Prestorage Gain

The greater the prestorage gain, the better the signal-to-noise characteristics of the sensor; since noise contributed in later physical

TABLE 2.0 - COMPARATIVE SUMMARY OF PROPERTIES

Property	Optechon	SEC-Vidicon	Image Orthicon	Customer
1. Storage Capacity	2×10^{11} elec/cm^2; 10^{12} electr/cm^2 maximum	10^{10} electrons/cm^2		$\approx 10^4$ elect per image element
2. Prestorage Gain	Range: 7 to 70$^+$	Range: 50 to 200	Range: 6 to 8	-
3. Detectability	10^4 photoelectrons with ELID (limited by target disturbance)	200 photoelectrons		
4. Spatial Resolution	50 lp/mm limiting 20 lp/mm @ 50% response 2000 lp/Diam. limiting	For small signals: 20 lp/mm limiting 500 lp/Diam.limiting (600 TV lines/0.6 in. ht.)	< 10 lp/mm @ 50% resp. 17 lp/mm limiting	20 lp.mm @ 50% resp.
5. Mode of Readout	Non-destructive, with Gain>1; vidicon or return beam orthicon mode	Destructive, with Gain $\approx$1 vidicon mode	Destructive, with Gain <1 vidicon mode	No Pref.
6. Beam Pulling - Spot Spread	Beam pulling <4 microns Spot Spreading - neglig.	$\approx$100 microns centroid shift; Spot Spreading: x7 change over range.	Greater than SEC-Vidicon	-
7. Target Configuration	Rotatable - one-sided	Fixed - two-sided	Fixed - two-sided	No. Pref.
8. Signal-to-Noise Ratio	@ $\bar{\chi} = 10^4$, S/N = 74-85, for $I_b = 10^6$A., $A_y = 0.9$	@ $\bar{\chi} = 10^4$, S/N = 90, for $A_y = 0.9$, G = 150.	$\approx$30	2% error @ $\bar{\chi} = 10^4$
9. Target Disturbance Noise	10^5 photoelectr/25μ elem. measured on old tube	$\approx 10^3$ photoelectrons/ elem	Small	< J-N noise
10. Charge Readout Reproducib.	Dependent upon circuit stability, possibly on target disturbance for point sources.	2% measured, using special circuit techniques of data reduction.		< 2%

TABLE 2.0 - COMPARATIVE SUMMARY OF PROPERTIES (Continued)

Property	Optechon	SEC-Vidicon	Image Orthicon	Customer
11. Focusing	1. Magnetic - gives best results. 2. All-electrostatic tube possible, with target redesign.	1. Magnetic - gives best results. 2. Hybrid possible with 30% resolution loss at the edges.	Same as SEC-Vidicon	Lightest in weight sys.
12. Integration Time	>1 hour with properly processed tube	> 1 hour with properly processed tube		At least 1 hour
13. Production Status	< 30 tubes made by Dec. '64	> 100 tubes made by Dec. '64	>>> 100 tubes made	
14. Ruggedness	WL-7198 ruggedized gun used - ruggedization work needed on target structure	UVicon is space qualified WX-30152 by 1966, WX-5419 not planned	Good history	Eventual Space Qualificat

processes (such as readout, electron multiplication) can be overridden by a large stored signal. In the Optechon, the EBIC prestorage gain is typically 7, although higher gains of 10 have been achieved.[29] ELID gain is another source of prestorage gain (Section 3.1.2.1 and Appendix D), which enhances the amount of stored charge due to the input signal without enhancing the target disturbance, or other noise, appreciably. ELID gains of 10 have been easily achieved. A minimum prestorage gain of 70 is therefore available with some loss in dynamic range.

The SEC Vidicon, due to its target gain mechanism,[35,36,37] is capable of gains of the order of 200 at high target voltages and therefore has exhibited good signal-to-noise characteristics at low light levels.

2.1.3 Detectability

For the purposes of photometry or spectrophotometry this property is relatively unimportant. Detectability implies that the presence of the signal is detected (usually defined at a signal-to-noise ratio of unity) and gives the minimum number of photoelectrons necessary to do this. For the SEC Vidicon this has been reported[35] as 200 photoelectrons.

In the Optechon, if ELID is used, 10^4 photoelectrons minimum can be detected. This estimate was based upon a measurement of the target disturbance (Section 3.1.4) performed upon one of the first tubes made. Subsequent target fabrication processing improvements have shown markedly better results, but no comparative measurements exist at present. It is thought that the improvement of the new targets over the old is of the order of one to two orders of magnitude.

While detectability is not of primary importance in this study, this figure gives a feeling for the photometric accuracy possible with low level signals, since it establishes the unity signal-to-noise value at a certain minimum number of photoelectrons incident on the storage target.

2.1.4 Spatial Resolution

The implications of this property are often neglected. Although it is felt intuitively that high resolution is important, compromises

are often made that not only degrade the ability of the sensor to distinguish between neighboring sources, which may be of secondary importance, but also impair the signal-to-noise ratio. To illustrate, it is necessary to argue on a per - reading element basis, where the "element" in this case is an area defined on the target by the dimensions of the reading beam. The image element, or the extent in area of the charge stored on the target, must be larger than the reading element so that the aperture response is reasonably large, but not so large that the area defined by the reading element contains too few stored charges to insure a good signal-to-noise ratio. This is as true for the SEC Vidicon as it is for the Optechon, although different modes of reading are used.

Where photoelectrons are at a premium, particularly when faint-star spectra photometry is performed, it is imperative that they be concentrated at one location on the target as much as possible so that their greatest effect on the reading beam can be realized no matter what the reading process is. The penalty for low resolution is therefore a lowered signal-to-noise ratio: in the SEC Vidicon destructive reading mode, as the result of fewer readout electrons per reading beam element; in the Optechon nondestructive reading mode, through a lowering of the potential difference between adjacent elements.

The resolution of the Optechon is high: 50 line pairs per millimeter limiting resolution has been achieved consistently, so that 20 line pairs per millimeter at 50% response has been measured. The SEC Vidicon resolution for small signals is 20 line pairs per millimeter limiting, so that the 50% response is only 1/3 as high as a specially-made image orthicon, or is approximately the same as a 7198.

The SEC Vidicon resolution is limited primarily by the target and is a function of the stored charge (through spot spreading), and the "contrast" of the object being viewed (through beam bending). Since stellar spectra are usually of relatively low "contrast" (i.e., the absorption lines vary only by a factor of two or three in brightness), the change in resolution may not be a problem for low-intensity star spectra. For binary star resolution however, where the difference in brightness is high, spatial resolution can be expected to suffer (Section 3.2.4.5 and also Section 2.1.6). Photometry of extended sources, if of

slowly-varying intensity, can be expected to be accurately reproduced spatially. If bright stars are present within the extended source, some inaccuracy will be present, using the SEC Vidicon. The resolution of the Optechon is constant with varying stored charge over a wide range and is limited primarily by the reading beam width (Section 3.1.5.2).

In both cases, the resolution will depend upon the focusing and deflection used, being the highest with magnetic deflection and focusing. In general, all electrostatically focused tubes are degraded 30% in resolution at the edges.

2.1.5 Mode of Readout

The SEC Vidicon reads out the stored signal on the target by replacing electrons in the positively-charged written areas with the electron beam. The reading is therefore destructive, in that the target is 90% recharged during the readout of the signal, and the gain of the reading process is less than unity.

The nature of the Optechon target suggests and measurements verify that the stored signal on the target modulates the reading beam: a reading gain can therefore be realized for values of reading beam current greater than 0.01 microamp (Section 3.1.5.3). Since the reading beam does not strike the dielectric surface, but samples the potential fields above it, the reading is nondestructive.

In this application, the nondestructive mode is not of prime importance, except in the preliminary setup operation. However, detection of very faint sources could be aided by a combination of multicopy readout and statistical decision methods.

One point of importance is that the scanning speed does not affect the amplitude of the output signal in the Optechon: the amplitude is determined solely by the triode-like reading transfer curves operating on the reading beam current. In the SEC Vidicon, since the number of electrons in the reading beam striking a resolution element, must be greater than the number of vacancies representing a stored positive charge, faster or slower scanning speed would respectively give a false (smaller) indication, or give rise to noise, respectively.

2.1.6 Beam Pulling - Spot Spreading

This has been partially covered in 2.1.4 as relating to the spatial resolution. Of course, these phenomena also affect the positional accuracy of the readout signal, and the actual size of bright point images in addition to the signal-to-noise. Both tubes are superior to the image orthicon,[2] since in both tubes the secondary electron redistribution effect is suppressed by the particular nature of each target. The Optechon due to the limited extent of the electrostatic fields above its surface, has negligible effects due to beam bending and spot spreading (Section 3.1.5.4). The SEC Vidicon effects are approximately an order of magnitude greater than the Optechon, but still better than the image orthicon by a factor of two (Section 3.2.4.2). The Optechon has a total effect of 3 microns, while the SEC Vidicon effect is a 100 micron motion of the centroid and 200 micron movement of the edge with increasing exposure.

2.1.7 Target Configuration

The target in the Optechon must be rotated between the writing and reading operation, since it is a light-and electron-opaque structure. Whereas this has the disadvantage that special care must be taken in the mechanical design and ruggedization of a rotatable target, two advantages are gained: first, the photocathode is shielded from the light emitted by the thermionic cathode; and second, the target can be made concave and permit electrostatic focusing and deflection with comparatively less resolution loss.

The SEC Vidicon target accepts photoelectrons from one side, and establishes a potential distribution representing the stored charge to be read out on the other side. The target is somewhat translucent to light, so that it is necessary to decrease the thermionic cathode voltage during integration. The small mass of the target and its fixed position within the tube make ruggedization much simpler.

2.1.8 Signal-to-Noise Ratio

The theoretical signal-to-noise properties of the SEC Vidicon

are discussed fully in Section 3.2.3, resulting in Table 3.2.1 and Figure 3.2.7. It is seen that the best signal-to-noise ratios are obtained at high values of aperture response, gain and equalization ratio, and the maximum signal-to-noise ratio that can be obtained at the maximum gain and a resolution corresponding to 0.9 aperture response is 100 for a 50 micron diameter element. For $\bar{\chi}$ equal to 10^4 photoelectrons per image element the signal-to-noise ratio for the best conditions is 90, or an error slightly over 1%. If the aperture response is decreased to 0.5, the error degrades to 2% at 10^4 photoelectrons.

The theoretical signal-to-noise properties of the Optechon are discussed in detail in Section 3.1.3, tabulated in Table 3.1.1 and plotted in Figures 3.1.9 through 3.1.12. It is found that the vidicon mode of readout gives a slight advantage over the return-beam orthicon mode, that a large beam current is desirable, as is a large value of aperture response, and that ELID prestorage gain will accomplish at low numbers of photoelectrons per image element, what increasing the equalization ratios does for the SEC Vidicon. For $\bar{\chi}$ equal to 10^4 photoelectrons per 50 micron image element the signal-to-noise ratio is 85 with ELID and 74 without, so that the accuracy is better than 1.5% for both cases. Changes produced by changes in beam current are insignificant at this level of input. At low numbers of photoelectrons, the ELID gain may make the difference between 90% error or 15% error, where the lowest error is 10%. Also, at these low numbers an order of magnitude increase in reading beam current can make the difference between 90% error and 25% error where the lowest error is 16%. The maximum signal-to-noise ratio that can be attained is 600 (without ELID).

It should be emphasized that the above figures for signal-to-noise are the result of a theoretical analysis which makes certain assumptions with regard to noise sources in each tube, but does not include all possible sources. One such source is the fixed pattern, or target disturbance noise. The effect of such a source of noise is to move the horizontal line representing signal-to-noise equal to unity up to a higher level, thereby limiting the minimum signal capable of being detected to that equivalent to the fixed pattern noise. Also, the additional noise produced when it is necessary to integrate over several scans for the SEC

Vidicon, is not included.

2.1.9 Target Disturbance Noise

The Optechon target disturbance noise, measured on an early-model tube was 10^5 photoelectrons per 25 micron square image element, and it is believed that current targets being made are one or two orders of magnitude below this value as the result of better processing. The character of this noise is such that it remains approximately constant in amplitude with changes in stored signal (see Figure 3.1.16). Whatever decrease in amplitude that exists is due to changes in the reading point on the transfer curves. Also, the process of ELID does not increase the apparent target disturbance noise, so that this method of prestorage gain is useful in bringing up below-threshold signals out of the target disturbance noise (Figure 3.1.18).

Target disturbance noise in the SEC Vidicon (Section 3.2.4.7) is present, but at this time it is not completely understood. It appears to be affected by the processing, history of the tube, and the target voltage; and has the strange property that it increases in rms value with higher numbers of incident photoelectrons (Figures 3.2.23, 3.2.25), a situation unlike that found in the Optechon. This suggests that it may be caused by statistical variations in the gain of the target structure.

Since target disturbance noise places a restriction on the detectability of these tubes, it is important that it be minimized.

2.1.10 Charge Readout Reproducibility

The error in reading out the accumulated charge in the SEC Vidicon has been measured as better than 2 percent by R. J. Davis of the Smithsonian Observatory* and checked against data obtained with Uvicons in Westinghouse Research Laboratories by R. R. Beyer (Section 3.2.4.1).

*Private communication to E. J. Sternglass

Assuming that the reading beam current is adequate, the written portion can be almost completely discharged in one scan, and small changes in focus of the reading beam do not affect the reproducibility, if the proper provisions are made in the circuitry.

No such documented history exists for the Optechon, but there is no reason to believe that like accuracies cannot be achieved for this tube if proper care is taken in the design of stable circuitry. An experiment conducted during this program showed fair reproducibility for extended sources (Figure 3.1.19) and erratic reproducibility for point sources (Figure 3.1.20). It is conceivable that the target disturbance played a significant role in the erratic readings of the latter experiment.

2.1.11 Focusing

For both tubes, the best ultimate resolution is provided by all-magnetic focusing and deflection fields. Since the SEC target is not rotatable, the proper electron-optic configuration cannot be presented to both image section and reading section. The Optechon, with a rotatable target, could possibly be made in an all-electrostatic electron optic configuration but several problems would need to be resolved before this could be implemented.

2.1.12 Integration Time

This property depends upon the dark current characteristics of the photosurface and the tube construction. Tests performed on the SEC Vidicon (Section 3.2.4.4) during this study have permitted integration for fifteen minutes, this being limited by the poor vacuum in the particular tube used. Tests with the Optechon (Section 3.1.4) showed that fifty minute integration was possible. It is believed that with proper processing both tubes would be capable of integration times well in excess of an hour.

2.1.13 Production Status

The number of tubes made is a reasonable indication of the

experience that has gone into the fabrication and testing of a given tube type, as well as the amount of effort that must be applied to bring the various processes of tube manufacture under control. The image orthicon has had a long history of successful production, while the SEC Vidicon and Optechon are in their adolescence and infancy respectively. As the result of in-house contracts, both tubes can be expected to advance in their respective states of technology, and improve in performance considerably.

In particular, future Optechon development must solve several problems, including mechanical stability, target processing, and optimum operational doctrine.

2.1.14 Ruggedness

The ruggedness of the SEC target structure has been tested during the course of the UVicon program for the Smithsonian Observatory, and the UVicon has passed its space qualification tests.

The Optechon has not been considered for space use and hence has had no need to prepare for it. The main problem would involve the ruggedization of the target support structure and the attendant problem of a reliable target rotating mechanism. The WL-7198 ruggedized image orthicon gun structure would be employed.

2.1.15 Estimate of Performance

The conclusion of this study is that both the SEC Vidicon and the Optechon represent a palpable advance in the state of the imaging and storage tube art, and it is felt that they would be most useful as astronomical sensors. At present, neither of these tubes is considered at the ultimate as an astronomical sensor, mostly because of their relative youth and the lack of experience in their use in this particular application. Both show excellent potential in the field of astronomy, not only in space (for which the UVicon has already been considered) but in ground-based installations as well.

While the photomultiplier remains the basic photometric measuring instrument in astronomy due to its excellent signal-to-noise

characteristics and large dynamic range, there are cases where it may be more expedient to use an imaging tube. Spectrophotometry and the photometry of extended sources are better served with imaging tubes. Photographic emulsions also remain standard in the astronomical field, but suffer from the inconvenience of chemical development and thermal preprocessing, as well as problems involved in the energy conversion and storage process itself. Garden-variety image orthicons and vidicons suffer from limited dynamic range, poor sensitivity, and positional inaccuracies.

While not all of these problems are solved by either the SEC Vidicon or Optechon, several are considerably eased. For example, in stellar spectrophotometry either the SEC Vidicon or Optechon could be used gainfully. The Optechon could be used to determine the position and relative intensities of the spectral absorption lines by virtue of its excellent positional accuracy property. In like fashion the SEC Vidicon could perform the same task if the spectrum was a faint, low-contrast type. In addition, the SEC could provide an absolute photometric measure of the line intensities. It is believed that the Optechon could also be calibrated to give absolute photometric readings with reasonable circuit design. However, not enough substantiating experimental data exists to permit a firm statement of fact.

Extended source photometry could be performed satisfactorily with either tube due to their large dynamic ranges. If bright stars are imbedded in the extended source however, the preference is for the Optechon due to the absence of spot spreading in this tube. The same principle applies to spectra having high contrast, high resolution lines.

Resolution of binaries can be carried out with either tube, although if one of the members is considerably brighter than the other and positional accuracy is important, the choice again lies with the Optechon.

Star cataloging in densely-populated sections of the sky could best be served by the Optechon due to its positional accuracy and freedom from point-source interaction. Sparsely-populated sections of the sky could be examined with either tube.

In short, the SEC Vidicion would be useful in any application where charge readout reproducibility is important, where the objects are of relatively low contrast, and themselves of low resolution. The Optechon is useful in applications where high-contrast images are required, where

positional accuracy and high resolution are important, and where relative intensity measurements are acceptable.

Of the two tubes, the SEC Vidicon with its rigid target structure, and production status, is closest as a deliverable space-qualified tube. The Optechon requires further work in ruggedization, and upon its target-rotating means. Both tubes can be "hybridized" with a corresponding loss in edge resolution. The Optechon can be made all-electrostatic, but only after a reasonably intensive effort was applied to this design problem.

Both tubes require further information regarding the compatibility of the S-20 photosurfaces with lithium fluoride, and possible extension of the response to shorter wavelengths.

2.2 Recommendations

In the following study, Westinghouse has endeavored to gather enough data from prior and contemporary programs and perform enough experiments on this program to be able to answer with authority the majority of the questions put before us, with respect to the applicability of the SEC Vidicon and Optechon to space and ground-based astronomy in the near future. While all the questions have not been resolved, and indeed additional questions have been raised as the result of this study, it is clear to us that both tubes are applicable to the present problems of astronomical research, and have a considerable potential for the resolution of future problems as experience with the tubes increases.

It is difficult to piece together data, and design experiments to establish definitely the advantages and shortcomings of a device in a certain application. This is best done by applying the tube if possible, and comparing the results obtained with supplemental data such as has been provided herein, or obtained concurrently with the application.

We therefore recommend that a camera, capable of accepting either the SEC Vidicon or Optechon, be built and applied to a program of ground-based astronomical measurements. At the same time it is recommended that effort be directed toward the gathering of supplemental data on target disturbance, feasibility of an all-electrostatic Optechon, improvement of resolution and positional accuracy in the SEC Vidicon, photometric

reproducibility of the Optechon, investigation of the compatibility of S-20 photosurfaces with lithium fluoride; in short, effort on unresolved problems outlined in this report and preparatory work leading to a space-qualified sensor.

Application of these tubes to astronomical problems can be expected to ferret out unsuspected shortcomings quickly, permitting remedial measures to be applied to tube design quickly to prevent holdups in future production scheduling. The preparatory tube design and development work is important to insure that all processes are well under control when the first tubes for space use are delivered.

3.0 DETAILS OF STUDY

The supporting information for Section 2.0 is presented herein, and includes not only a description of the two tubes considered in this study, but a discussion of their applicability to astronomical measurements.

3.1 Optechon

The first tube to be considered is the Optechon, a storage tube utilizing a unique type of storage target in place of the conventional mesh, or thin-metal-oxide-film targets.

3.1.1 History of Accomplishments Prior to Start of Program

Since 1959, under contracts AF33(616)6666 and AF33(657)8715 with the Air Force, RTD Reconnaissance Laboratory, Electro-Optical Section, Westinghouse Electronic Tube Division, Special Electron Devices Laboratory has conducted an applied research program that has demonstrated the feasibility of a storage camera tube suitable for reconnaissance under adverse illumination conditions and having both high resolution and large total information storage capacity. It has a photoemissive retina with an image section that provides high sensitivity through high quantum efficiency and prestorage gain. The information can be stored on a unique grating electrostatic storage tape of metal and refractory dielectric reeled within the vacuum envelope, or upon a movable rigid grating storage target. Reading is accomplished electronically and nondestructively with a relatively high modulation ratio independent of reading data rate.

During the course of the Air Force contracts, the work was aimed toward demonstration of the grating storage tape concept, and the techniques and methods required by it, rather than the implementation of a particular device. The camera storage tubes (WX-5074 and WX-5023) made with rigid grating storage targets, pivoted to face sequentially either the photocathode for writing or the electron gun for reading, erasing, and priming,

were considered only to be simple test vehicles for the tape concept. However, it was realized after they performed so well, that they have useful applications in their own right. Hence, for simplicity of nomenclature, it has recently been decided to call such a grating storage camera tube by the name OPTECHON.

The Optechons made on the Air Force contract were operated at both 30 frames per second and one frame per five seconds reading rate, and demonstrated the following: limiting resolution of 75 line pairs per millimeter, 50 percent response resolution of 25 line pairs per millimeter, no reduction of resolution after 41 hours storage; signal current to noise ratio greater than 100 at Mc/second reading data rates; and with a poor nine-microampere per lumen S-20 photocathode, a sensitivity corresponding to a photographic speed index of ASA 12. This was done both with bar patterns and A-scope output and with full-frame photographs with photographed kinescope output.

3.1.2 Theory of Operation

3.1.2.1 Summary

The WX-5074 Optechon, a grating storage camera tube consists of an image section for photoelectron writing, a rigid storage target, and a reading electron gun. The storage target is in the form of a disc, pivoted on a transverse axis so that it may be rotated to face the image section for writing during the optical exposure, or to face the electron gun for the reading, and erase/prime action. Figure 3.1.1 is a schematic representation of the WX-5074 and Figure 3.1.2 is a photograph of the tube.

The tube is operated in the following way:

1) The grating surface is turned toward the reading gun and it is bombarded with electrons having energies well in excess of the first crossover of the dielectric secondary emission curve. This process is called erasing and effectively discharges the dielectric surface until it is at the target potential.

2) The dielectric is then bombarded by electrons and charged to the potential of the cathode, which has now been set several

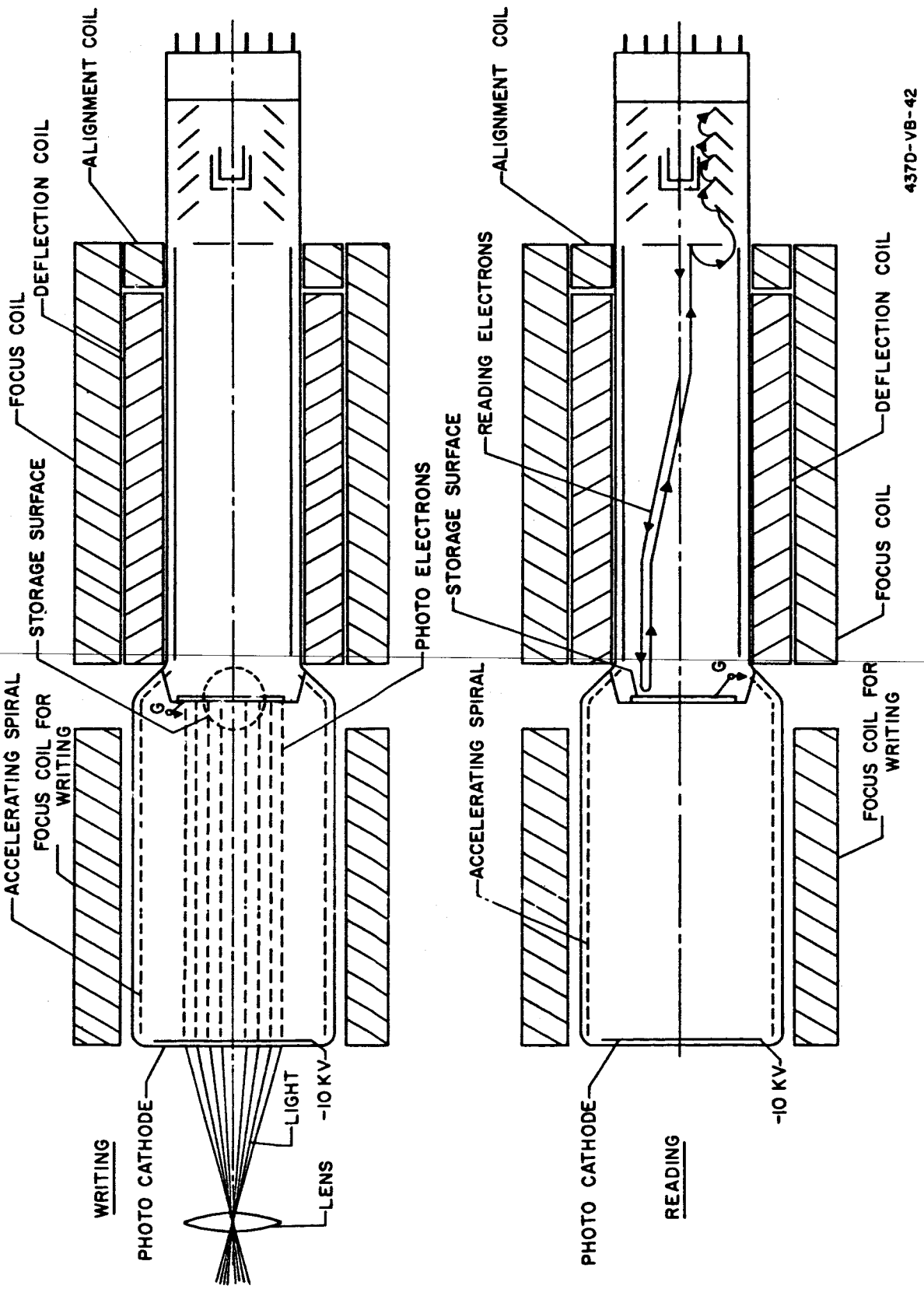

Figure 3.1.1 WX-5074 Optechon - Schematic Representation

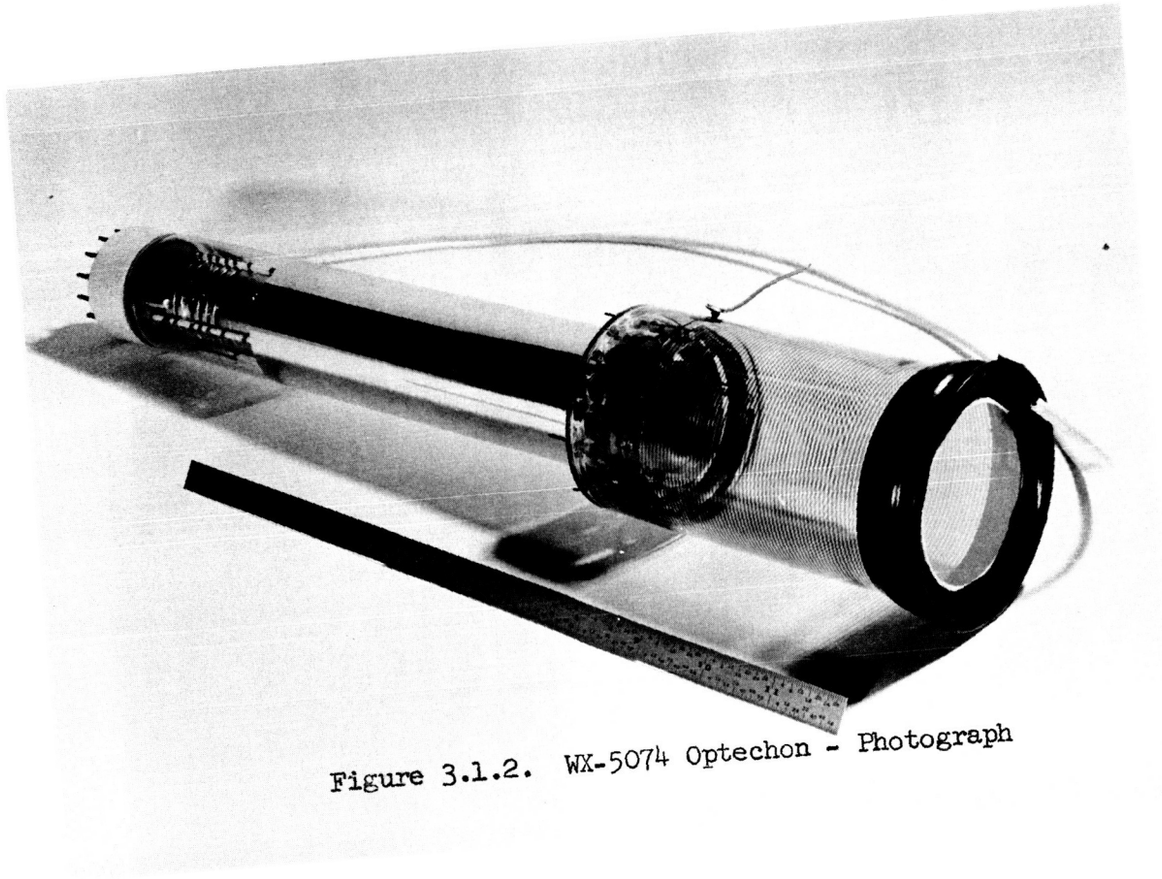

Figure 3.1.2. WX-5074 Optechon - Photograph

volts negative with respect to the metallic target surface. This process is called priming, and causes to be deposited upon the dielectric, a negative electronic charge.

3) The grating surface is then turned toward the image section and exposed to the action of released photoelectrons from the illuminated portions of the photoemissive surface. The photoelectrons are accelerated to energies of the order of 10 keV so that writing occurs as the result of Electron Bombardment Induced Conductivity (EBIC); i.e. the impinging high-energy electrons cause localized conduction in the dielectric target, thereby causing some of the charge on the surface of the dielectric, placed there as the result of the priming process, to leak off.

The dielectric potential therefore varies over the target surface: the written portions are more positive than the unwritten portions in proportion to the number of photoelectrons incident upon the target.

4) The target is then turned to face the reading gun and the potential variation of the target is read out.

3.1.2.2 Details of Operation

The heart of the Optechon is the grating storage target, a unique method of achieving a coplanar target structure. The target consists of a relatively coarse (from the optical standpoint) diffraction grating having approximately 6000 lines per inch. The cross-section of the target surface is shown in Figure 3.1.3. It may be seen that the dielectric is deposited by vacuum shadow evaporation within the grooves so that it covers the long dimension of the groove to a depth of 1/4 to 1/2 micron. A field plot of the potential above the target surface is seen in Figure 3.1.4, and the advantages of this type of structure can be inferred from observing the extent of the fields above the target surface. The guarding action of the metallic short dimensions of the groove essentially confines the field variations to the groove width (4 microns for a 6000 line per inch grating). While not quite that effective in the direction parallel to the grooves, no difference in resolution has been noticed in this direction.

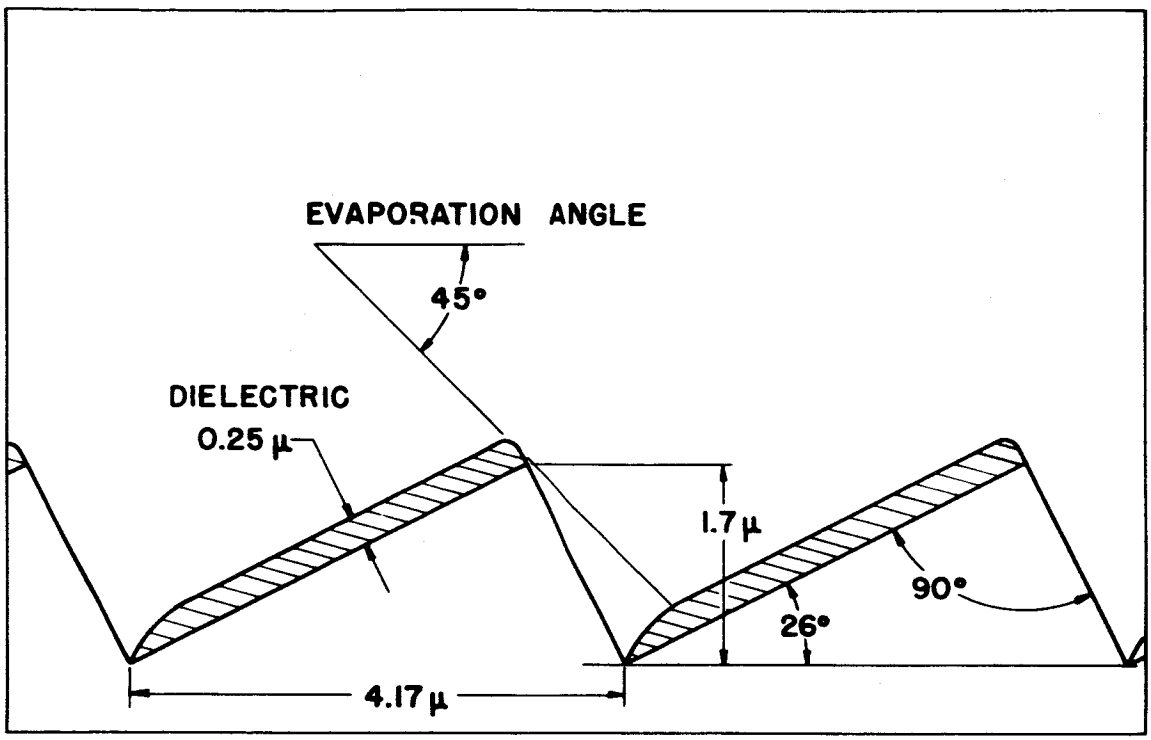

Figure 3.1.3. Magnified Cross Section of Target

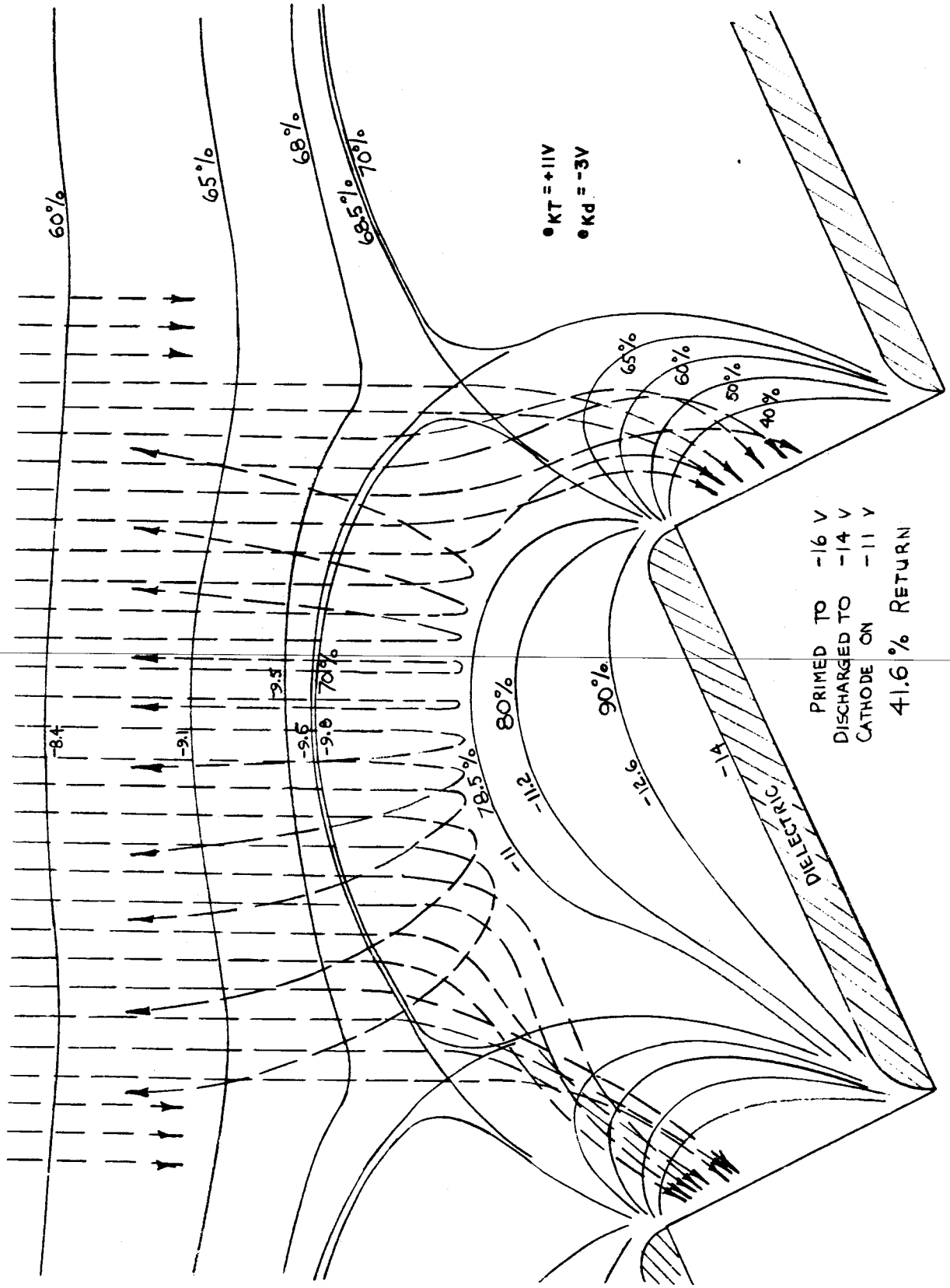

Figure 3.1.4 Equipotentials and Electron Trajectories at the Storage Target

a) Erasing

For the erasing mode of operation, the target is exposed to electrons having energies well past the first crossover. The secondaries thus generated will discharge the target dielectric surface until it is at an equilibrium with the target metallic surface. In normal operation, the cathode is set at ground potential and the target is raised past +175 volts. The electron beam is defocused slightly so that succeeding erasing scans will overlap and leave no structure in the target charge distribution. Figure 3.1.5 shows the plot of the dielectric equilibrium potential with respect to the metallic target as a function of the metallic target voltage with respect to the cathode.

It is seen from Figure 3.1.5 that the dielectric is fully discharged for voltages greater than +175 volts.

b) Priming

Here, the cathode is set at ground potential and the target is set to the positive priming potential, Vp, lower than first crossover. A sufficiently intense beam of electrons is directed toward the target and the dielectric surface charged until it is in equilibrium with the electron gun cathode. This is also shown in Figure 3.1.5. Here also, the electron beam must be defocused slightly to prevent depositing electrons in any line structure. The surface of the dielectric assumes a negative potential Vp, when the target is returned to ground.

c) Writing

The target is rotated so that it faces the photocathode. A negative voltage of 10 kV is applied to the photocathode with respect to the target and the photocathode is exposed to the optical signal for a given length of time by means of a mechanical shutter. The accelerating spiral lens in the image section will increase the velocity of the emitted photoelectrons to correspond to a kinetic energy of 10 keV. This will be sufficient to cause Electron Bombardment Induced Conductivity (EBIC) in the charged dielectric. A portion of the negative charge will leak off the dielectric surface, the amount in proportion to the number of energetic photoelectrons striking the dielectric. Since one energetic photoelectron falling on the magnesium fluoride dielectric can cause six to ten electrons, stored on the target surface by the priming operation, to be conducted to

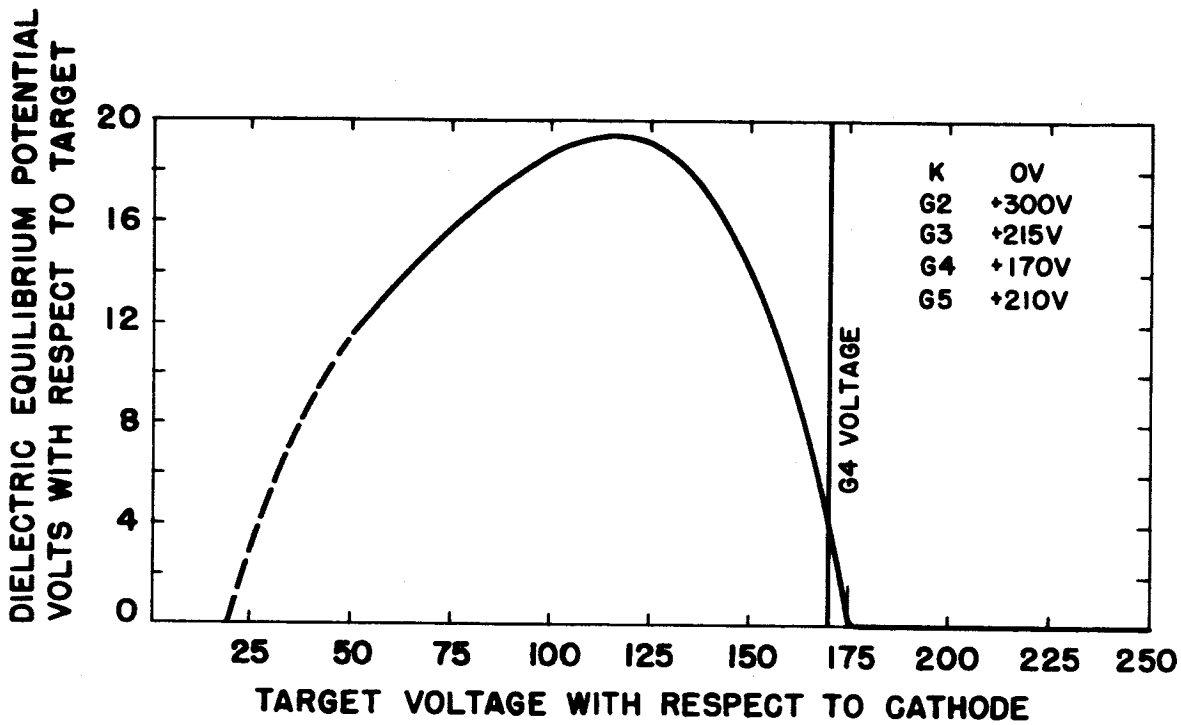

Figure 3.1.5. Plot of Dielectric Potential
Vs.
Target Voltage

the target, there is a gain associated with the writing process, called the EBIC gain. A conservative value for this gain is seven.

It was shown* that this tube also could be outfitted with an electronic shutter, consisting of an out-of-focus mesh in the image section. Shutter exposures of 100 microseconds were attained with a total voltage swing of 1 kV of the shutter mesh. No evidence of the presence of the shutter could be seen in a stored pattern of 500 lines per inch (shutter mesh was 250 mesh per inch).

The first tubes made were constructed so that the target could be rotated by gravity by a combination of rotation around and tilting of the longitudinal axis of the tube. Work presently being done on another contract† has shown the feasibility of rotating the target by means of a pulse of current through a coil of wire whose plane is parallel to the longitudinal axis of the tube.

d) Reading

The target is rotated so that it again faces the reading gun, and the target is raised to the proper potential for reading. This potential varies according to the potential to which the target surface was primed, and the signal level stored. Due to the coplanar structure of the target, the reading process is described by a series of reading transfer curves. These curves represent the percentage of the reading beam current that is collected by the exposed metallic strips of the target (and therefore the percentage not returned to the electron multiplier) as a function of the potential variation caused by the signal stored on the target, and the target to cathode voltage difference. Figure 3.1.6 shows the history of the target voltage and dielectric potential during the operation of the tube for a three-volt written signal, and Figure 3.1.7 shows the reading transfer curves (Figure 3.1.8a) operating on a three-volt written signal at various target reading potentials. Figure 3.1.8b is the percent modulation of the reading electron beam per volt of stored signal, called the mutual transconductance of the grating storage target. This is plotted for a particular value

*Ref. 29, pp 3-6, 3-8

†NAS5-9020, "Grating Storage Camera Tube Study"

Photo-Cathode Voltage	Target		Cathode Voltage	Target Facing	Function
	Metal Voltage	Dielectric Potential			
0.0	+ 300 V.	+ 300 V. (Equilibrium)	0	Read Gun	Erasing
0.0	+ 14 V.	0.0 V. (Equilibrium)	0	Read Gun	Printing
-10 KV	0.0 V.	-14 V. unwritten -11 V. written	0	Photo-cathode	Writing
* 0	+ 39 V.	+25 V. unwritten +22 V. written	0	Read Gun	ELID
0	+ 11 V.	- 3 V. unwritten 0 V. written	0	Read Gun	Reading

*For Signals Written $<<$ 3 Volts.

Figure 3.1.6

Chart Showing Electrode Voltages
for the Various Operating
Conditions of the Optechon

(A Typical Value of 3 Volts Written Signal Shown)

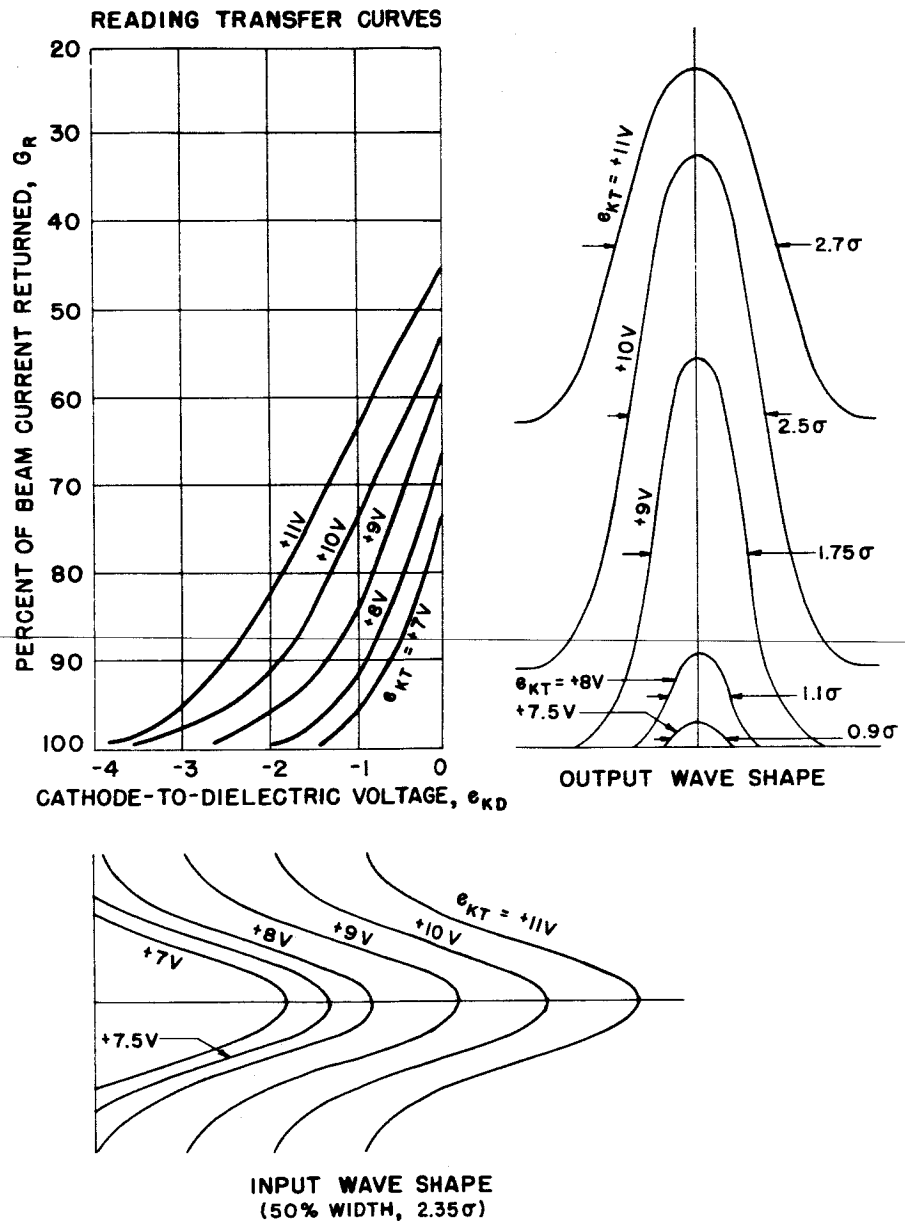

Figure 3.1.7. Effect of Varying Target Voltage Upon the Readout Signal

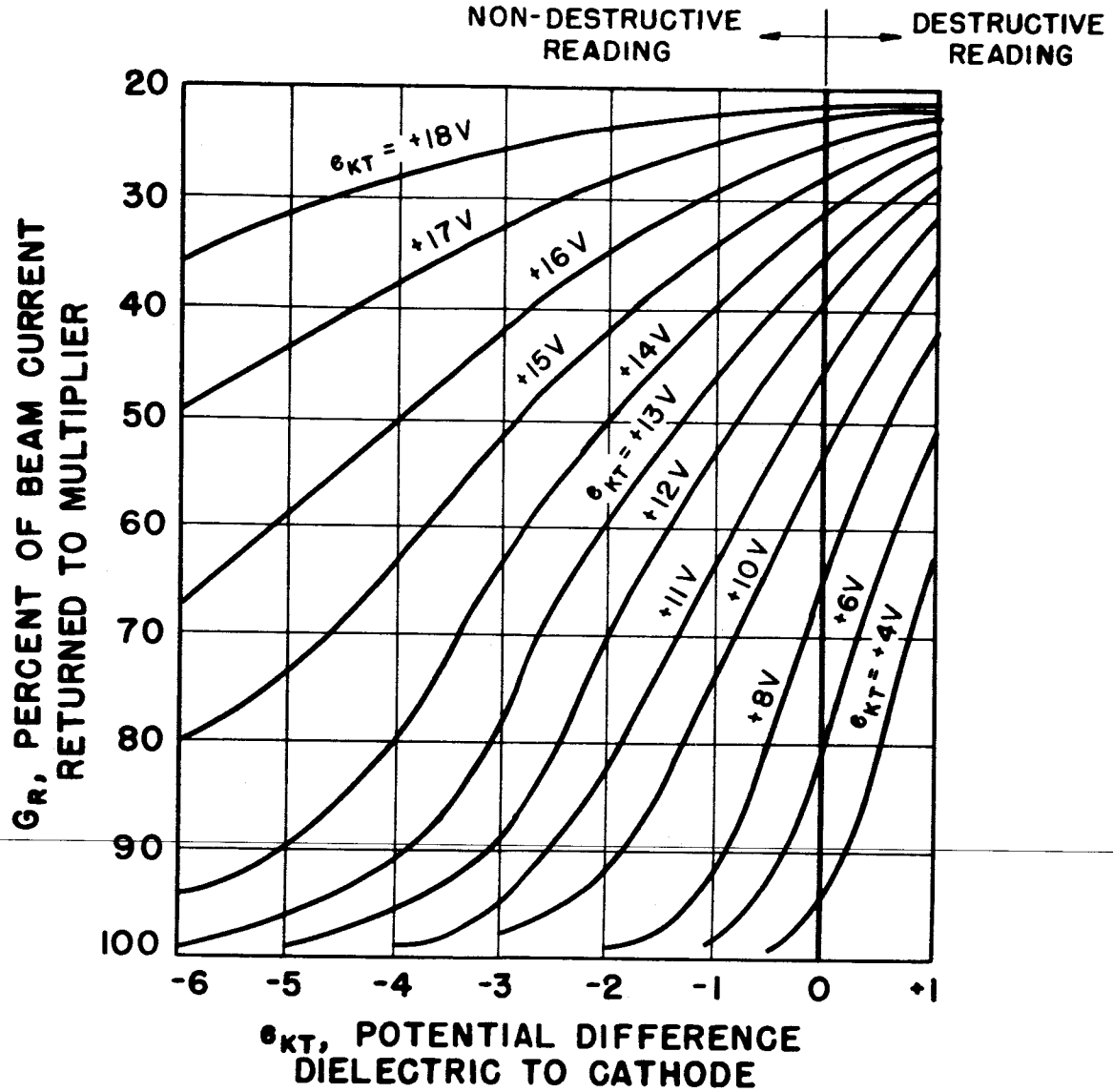

Figure 3.1.8 a) Reading Transfer Curves

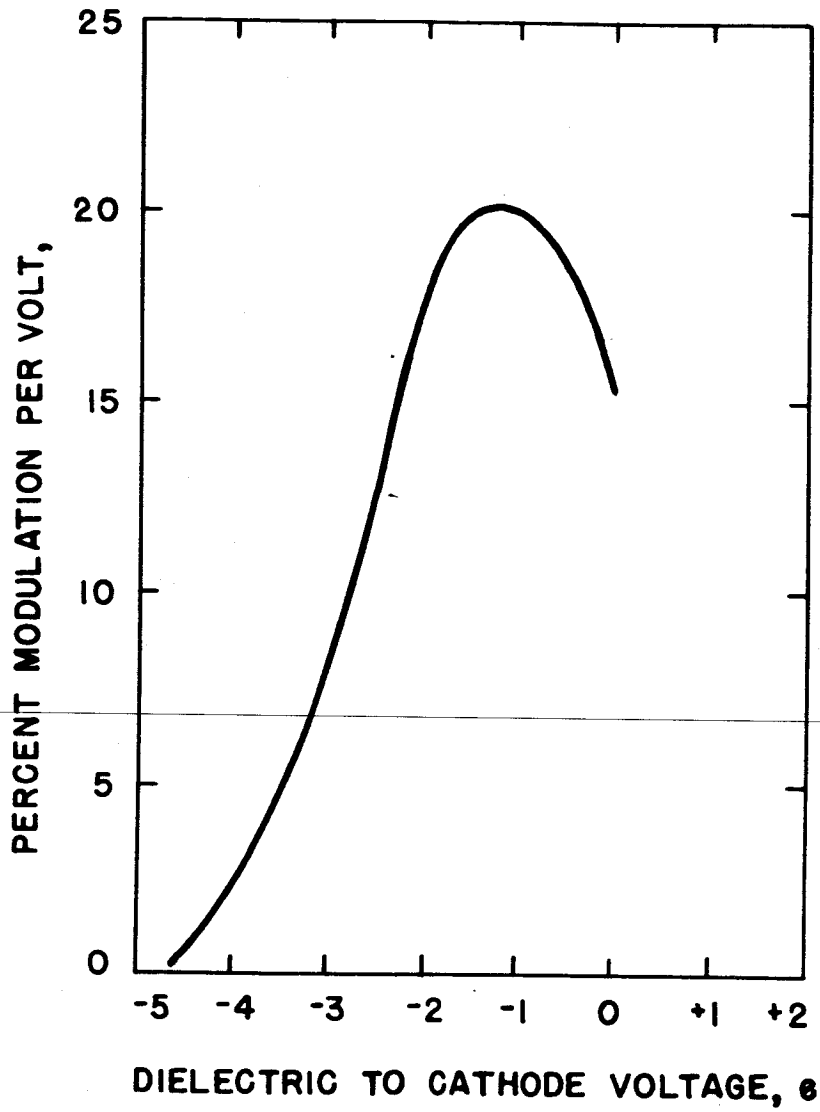

Figure 3.1.8 b) Percent Small-Signal Modulation per Volt
Versus
Dielectric to Cathode Voltage

of target base to cathode voltage, in this case +11 volts, and gives the small-signal modulating characteristics of the target. The reading transfer curves shown in Figure 3.1.7 give the large-signal modulating characteristics.

Using the figures given in Figures 3.1.6 and relating them to Figures 3.1.7 and 3.1.8:

Assuming that the target has been erased and primed to -12 volts dielectric surface to target voltage, and then written upon, so that a three-volt potential difference between written and unwritten portions will result: the written portion is positive with respect to the dielectric surface due to the EBIC writing process so that the peak of the written portion will be at -9 volts with respect to the target base.

If during the reading process the target is raised to +9 volts, the peak of the written signal will be at cathode potential, and the unwritten portion of the target will be at -3 volts relative to the cathode. Due to the nonlinearity of the reading transfer curves (Figure 3.1.7) any small signals will be suppressed, and the 50% width of the readout pulse will be 25% smaller.

If signals smaller than 3 volts are to be read for this priming condition, the target must be raised to +11 volts during reading. This will place the unwritten surface of the dielectric at -1 volt relative to the reading cathode, and therefore at the peak of the trans-conductance curve in Figure 3.1.8. While this will provide maximum reading beam modulation for weakly-written signals, any signal greater than 1 volt on the grating storage surface will be erased during the reading process.

Two modes of reading can be used: The output signal can be taken from the electron beam multiplier as the result of the reading beam electrons reflected from the surface of the target (orthicon mode); or

the output signal can be taken from the target directly as the result of the reading beam electrons collected by the target (vidicon mode). While the gain afforded by the five-stage electron multiplier may not be needed, it provides a low-capacitance output signal electrode (8 picofarads). The target, being a larger physical structure in the WX-5074, measures 50 picofarads in situ.

If the orthicon mode of reading is used, at least one stage of electron multiplication is recommended, so that the low gain of the first dynode (< 1) is overcome. The first dynode gain is purposely made low to prevent shading as the result of secondary emission variations as the return beam scans across it. Also, in the present structure, the first dynode is also G2 which has a sizeable direct current flowing through it and therefore is unusable as a signal electrode.

e) Electrostatic Latent Image Development (ELID)

This process may be applied before or between readings as a means of bringing up the contrast of the below-threshold signals stored on the target, since it does not operate upon the target disturbance noise. It is described further in Appendix D.

The voltage to which a particular target must be raised should be determined experimentally by priming the target, and then reading it to determine what percentage of the beam is returned for a given target to cathode potential. This can also be obtained from the reading transfer curves (Figure 3.1.6): for example; if the target is primed to -12 volts and read out at +11 volts, 63 percent of the beam should be returned. If the proper target potential is used during the ELID process (with no signal stored on the target) this percentage should remain constant for a wide range of development times.

After exposure, the target is raised to the proper potential for ELID and exposed to the reading beam of known beam current for a fixed amount of time. It can then be read out in the normal fashion. The gain of this process must be determined experimentally, since it will depend upon the secondary emission curve in the vicinity of the first crossover point, the time of development and the beam current. In practice, gains exceeding 10 have been achieved readily.

3.1.3 Signal-to-Noise Ratio Analysis

The Optechon, in comparison with the SEC Vidicon and Image Orthicon tubes, is somewhat difficult to analyze, since it has a gain associated with its nondestructive reading process and an additional prestorage gain that can be applied at will. To simplify the analysis, the method proposed by deHaan[25] was used, and this permitted the description of the signal-to-noise dependence in terms of the various gain processes occurring in the tube. The method is described in Appendix C; and a number of equations, derived in parametric form, are contained therein.

The standard form of the signal-to-noise versus photoelectrons per image element $\bar{\chi}$, equation is found to be

$$(S/N) = \frac{\bar{\chi}}{(\alpha \bar{\chi} + \beta)^{1/2}} ; \qquad (3.1)$$

where the α and β terms can be expressed parametrically in terms of tube or amplifier properties. The α term usually depends upon the gain terms attributable to the writing and reading processes as well as any loss terms associated with, say, aperture response, to name one. Reference to the figure in Appendix C shows that the value of α determines the approach of the tube signal-to-noise curve to the quantum limit at high values of photoelectrons per image element $\bar{\chi}$.

The β term determines the sensitivity of the tube, and incorporates such noise contributions as Johnson-Nyquist amplifier noise, beam shot noise, and electron multiplier noise. It determines the "roll-off" of the signal-to-noise curve at low values of $\bar{\chi}$.

By setting the equation equal to unity, the noise-equivalent sensitivity can be defined. At a signal-to-rms noise value of unity, the noise-equivalent signal $\bar{\chi}_{min}$ is

$$\bar{\chi}_{min} = \frac{\alpha + (\alpha^2 + 4\beta)^{1/2}}{2} \qquad (3.2)$$

$\bar{\chi}_{min}$ determines the intersection of the signal-to-noise curve with the S/N = 1 line.

The upper limit of the signal-to-noise curve is set by the storage capacity of the target and the prestorage gain. The storage capacity depends upon the electrical capacitance of an image element and the optimum voltage, V_o, to which the image element is charged for best reading characteristics, as determined by the reading transfer curves. Therefore

$$\bar{\gamma}_{max} = \frac{C_{e\ell}\, V_o}{e\, G_{ps}} \tag{3.3}$$

where G_{ps} is the prestorage gain which consists of the EBIC gain σ_1, and possibly the ELID gain σ_2, if it is used.

Figures 3.1.9 and 3.1.10 show the signal-to-noise curves for the Vidicon and Orthicon modes of reading, each with and without the additional prestorage ELID gain. Table 3.1.1 is a compilation of the computed equations and the conditions under which they were calculated.

Figures 3.1.11 and 3.1.12 show the same modes of reading, each with ELID gain, and at two different reading beam currents. The values for the tube and amplifier parameters (outlined in Table 3.1.1) were chosen partly from experimental data, and partly from experience obtained from a parametric study of the equations in Appendix C.

The parametric study showed the desirability of maximizing the aperture response of the tube A_y, of choosing the optimum value of image elements per cycle of bandwidth k, and of a reasonably high value of equalization ratio M. The effect of these changes was to improve the noise-equivalent sensitivity through increase of M, and decrease of k, and improve the signal-to-noise value at high $\bar{\gamma}$ through an increase in the aperture response A_y.

The resultant curves (3.1.9 through 3.1.12) in turn showed that for the Optechon, a high reading beam current leads to a better reading gain σ_3, and consequently better signal-to-noise characteristics.

Also, the curves showed (3.1.9 and 3.1.10) the importance of adding the ELID prestorage gain. At low values of $\bar{\gamma}$ the addition of ELID improves the signal-to-noise ratio by a factor of six.

The target capacity to ground being three times greater than the electron multiplier collector capacity to ground impairs the Vidicon

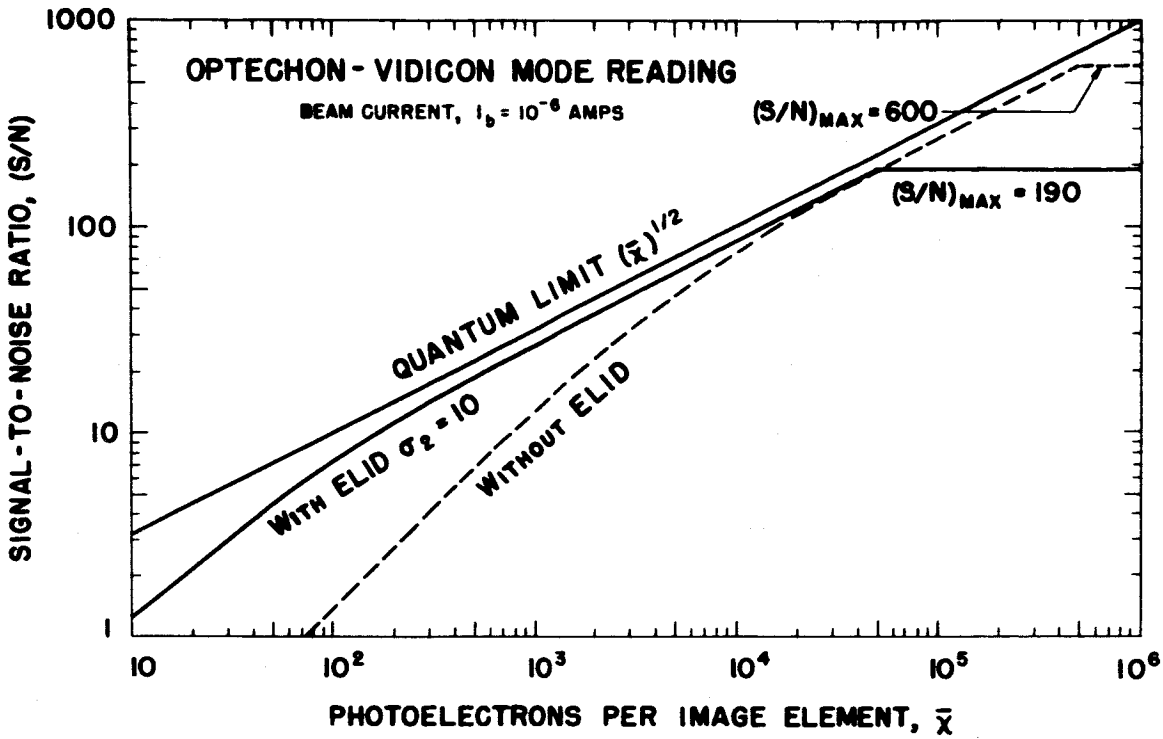

Figure 3.1.9. Optechon S/N Curves: Vidicon Mode Reading, Showing Effect of ELID

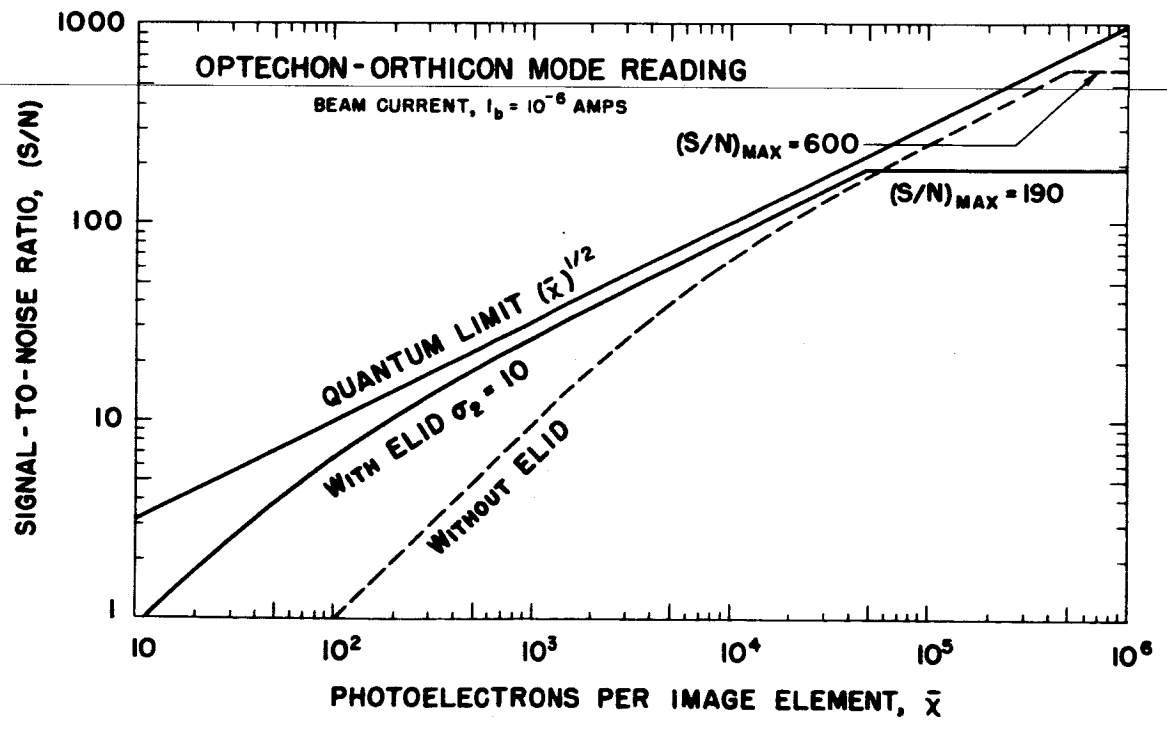

Figure 3.1.10. Optechon S/N Curves: Orthicon Mode Reading, Showing Effect of ELID

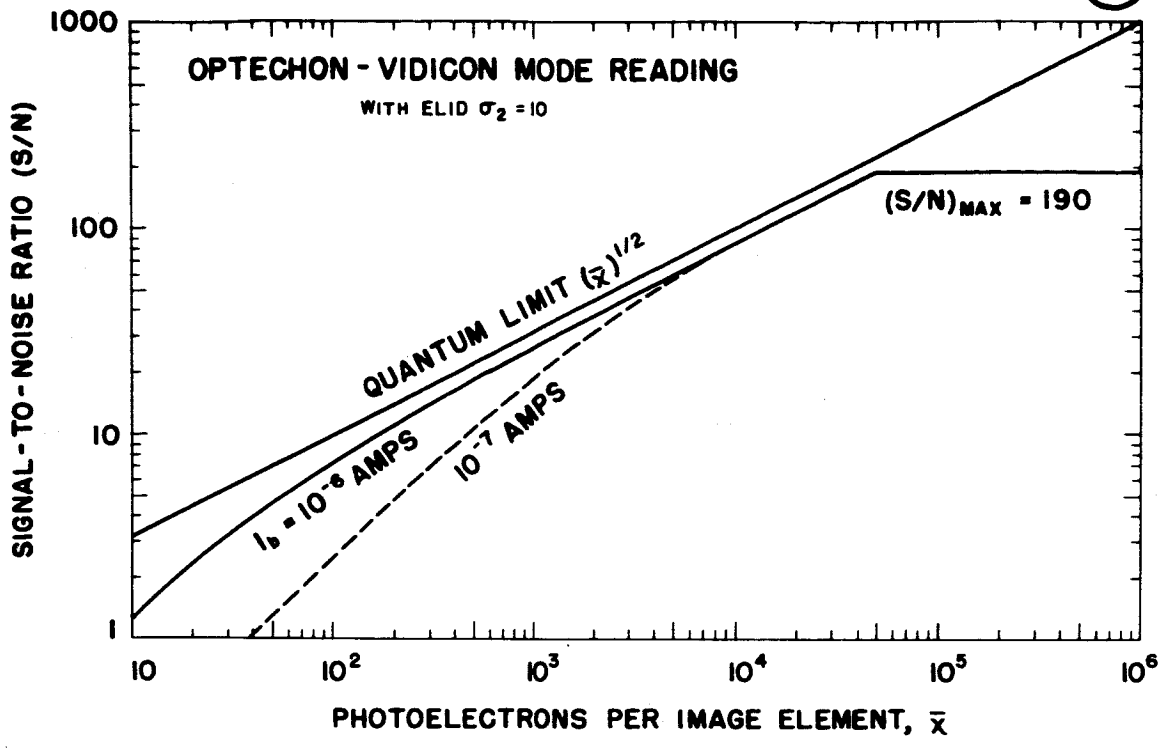

Figure 3.1.11. Optechon S/N Curves: Vidicon Mode Reading, Showing Effect of Beam Current

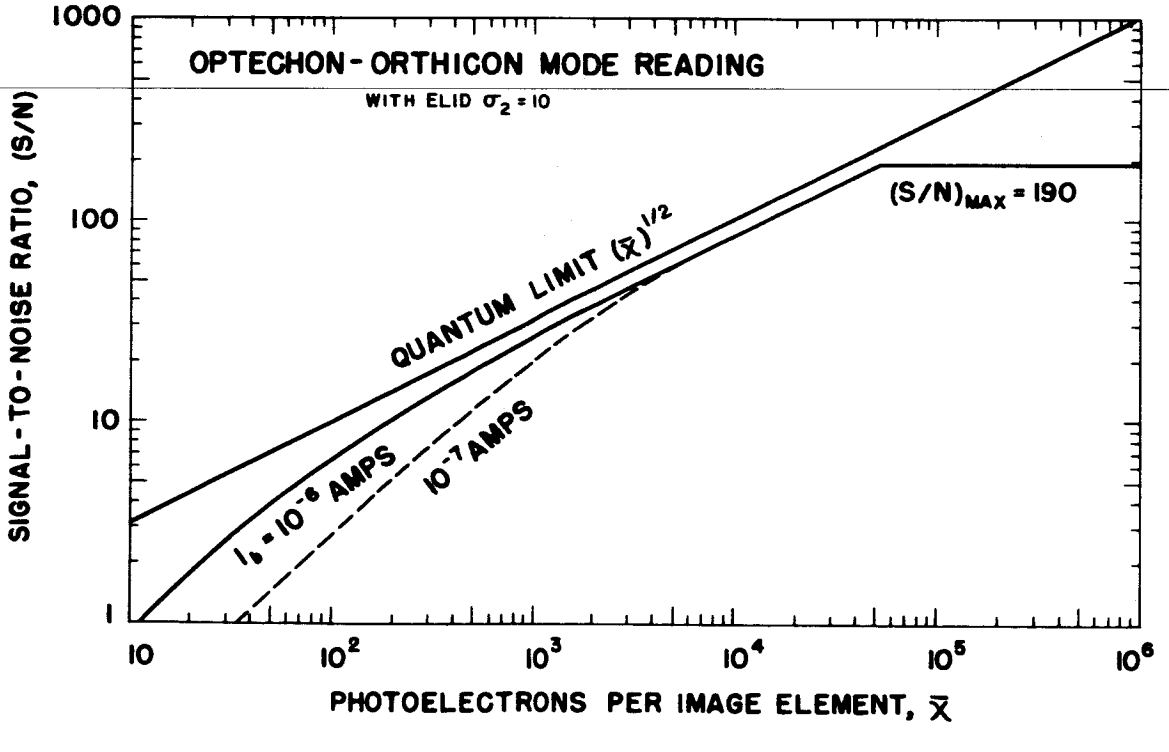

Figure 3.1.12. Optechon A/N Curves: Orthicon Mode Reading, Showing Effect of Beam Current

TABLE 3.1.1

SIGNAL-TO-NOISE RATIO

Optechon

Mode of Reading	Beam Current	
	$I_b = 10^{-6}$ A	$I_b = 10^{-7}$ A
Vidicon Mode	$\frac{\bar{\chi}}{(1.4\bar{\chi} + 5.1\times10^3)^{1/2}}$	$\frac{\bar{\chi}}{(1.5\bar{\chi} + 1.4\times10^5)^{1/2}}$
Vidicon Mode with ELID	$\frac{\bar{\chi}}{(1.4\bar{\chi} + 50)^{1/2}}$	$\frac{\bar{\chi}}{(1.4\bar{\chi} + 1.4\times10^3)^{1/2}}$
Orthicon Mode	$\frac{\bar{\chi}}{(1.4\bar{\chi} + 1\times10^4)^{1/2}}$	$\frac{\bar{\chi}}{(1.6\bar{\chi} + 1\times10^5)^{1/2}}$
Orthicon Mode with ELID	$\frac{\bar{\chi}}{(1.4\bar{\chi} + 1.1\times10^2)^{1/2}}$	$\frac{\bar{\chi}}{(1.4\bar{\chi} + 1.1\times10^3)^{1/2}}$

Conditions:

$A_v = 0.9$

$A_f = 1.0$

$\sigma_1 = 7$

$\sigma_2 = 10$

$\alpha = 1.74 \times 10^7 \frac{\text{elements}}{\text{amp-cycles}}$

$k = 1$ element/cycle

$f_c = 62.5$ Kc/S

$G_R = 0.64$

Image element: 50 micron diameter

Dielectric Constant, Storage Surface 5.3

$g_m = 0.2 \frac{1}{\text{volt}}$

$C_{el} = 1.84 \times 10^{-13}$ farad/element

$\overline{(\Delta i_n)^2} = 1.24 \times 10^{-21}$ (amp)^2 for Vidicon mode: $R_i = 1$ Meg, $C_i = 60$

$= 0.368 \times 10^{-21}$(amp)^2 for Orthicon mode $R_i = 3$ Meg, $C_i = 20$

$M = 24$

$R_t = 10^3$

reading mode operation somewhat, but it still is superior to the Orthicon mode of reading. A lower target capacity should be strived for in this tube.

The best operating condition for the Optechon at present is therefore represented by either curve 3.1.11 or 3.1.12. The ELID gain capability should be employed and the reading beam current should be maximized, but at a reading beam spot size corresponding to an aperture response of 0.9.

3.1.4 Experimental Results

The general program of experimental work on this study was limited to exploratory experiments designed to show in a quantitative manner, certain features of tube performance about which little or no information existed. Also, demonstrations of the performance of the tube at close to the OAO bandwidth conditions were sought.

To this end, the slow-scan unit, built to test the resolution capabilities of the grating storage target during prior investigatory programs, was employed. The optical conditions were carefully adjusted, and the target was underscanned so that the bandwidth of the signal derived from the storage target would be in the order of the 62.5 kc/s (OAO bandwidth). A description of the experimental setup is given in reference 31. Since the original slow-scan unit scanned a larger target area at high resolution, the amplifier was made capable of accepting up to 10 Mc/S signals. For the purposes of this study, a low-pass filter with a cutoff frequency of 83 kc/s was inserted after the amplifier. Figure 3.1.13a and b show the waveshapes of a single slit, and the edges of the mask used for calibration, as seen on an "A" scan oscilloscope. Figure 3.1.13c shows the monitor presentation and the direction and limits of scan. Figure 3.1.13a and b show the attenuation of the high frequency amplifier noise by the filter and the presence of the target disturbance noise. Figure 3.1.14 shows the "A" scope pattern for the two-stored slit experiment described in reference 31, and again shows the presence of the target disturbance.

An estimate of the maximum signal-to-noise ratio is given in Figure 3.1.15. Here a signal was overwritten and brought up to the proper reading potential in a. The readout signal-to-noise ratio is seen to be

a) Without Filter

b) With Filter

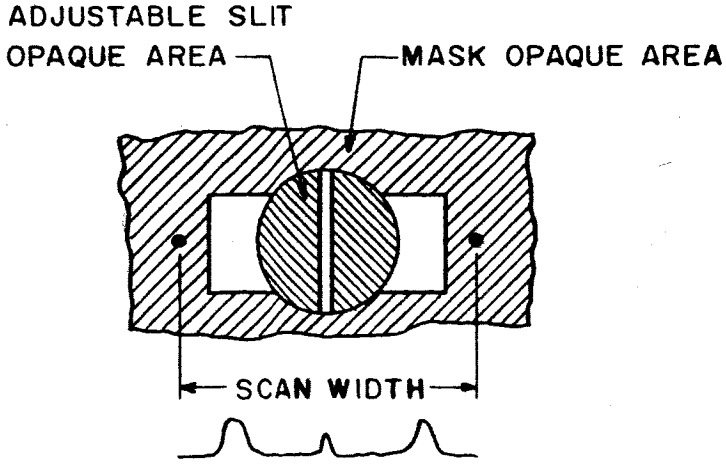

PHYSICAL ARRANGEMENT OF SLIT AND MASK

Figure 3.1.13. Effect of Low Pass Filter on Noise

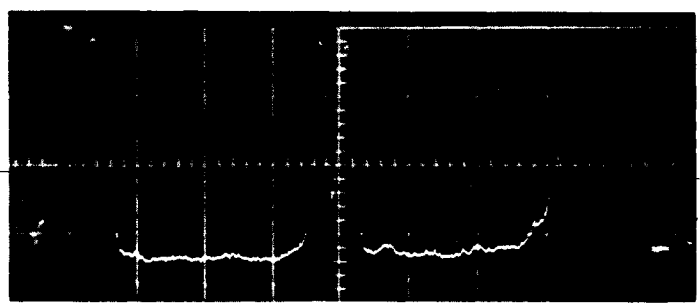

Figure 3.1.14. Stationary Target Disturbance Noise

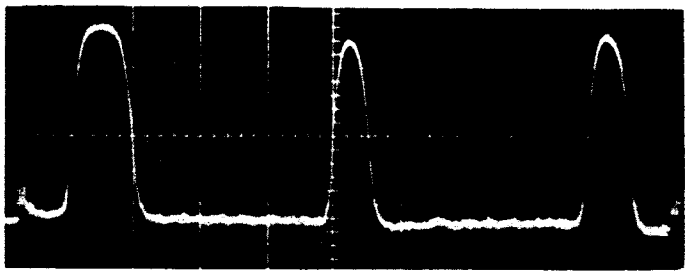

a) Normal Reading Voltage

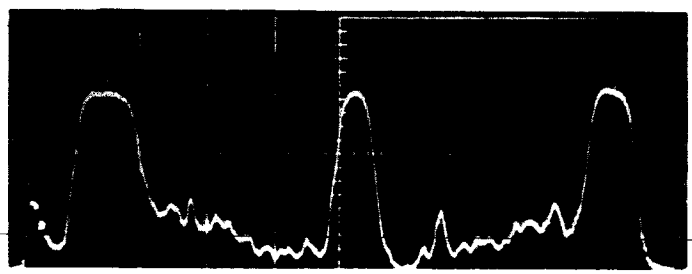

b) More Positive Target Reading Voltage

Figure 3.1.15. Effect of Reading Target Voltage Upon Target Disturbance Noise

about 80. When the target potential is raised so that the surface of the target is also read out (thereby bringing up the target disturbance noise), the signal-to-noise ratio drops to approximately 4. In other words, for small signals the target disturbance noise assumes a greater importance than for large signals. In the case of large signals, the nonlinear target transfer curves effectively suppress the amplitude of the noise on the baseline but the noise is still present on the top of the pulse. Since this is difficult to see on a small image element, a photographic step wedge was imaged and read out perpendicular to the direction of changing density (Figure 3.1.16). The intensity of the incident illumination is greatest for the lowest trace and least for the next to last top trace. The top trace represents the amplifier and Johnson-Nyquist noise. Note that the noise diminishes with increasing signal even though the reading gain is adjusted to be the same.*

The question of target disturbance noise requires some indication of its value. It was decided that the most meaningful description would be in terms of noise equivalent signal. The tube photocathode sensitivity was therefore measured, and signals were stored by varying the exposure to a calibrated light source until the amplitude of the signal approximated the target disturbance noise. The photoelectrons per 25 micron square image element were then computed for that exposure. In Figure 3.1.17a the "A" scope presentation can be observed, and the slit can be seen to be approximately equivalent to the maximum amplitude of the target disturbance. This would imply that the target disturbance noise is in the order of 10^5 photoelectrons per 25 micron square image element. Figure 3.1.17a is a measure of the minimum detectable signal for this particular tube if ELID is not used.

Figure 3.1.17b shows the same stored signal read out after Electrostatic Latent Image Development for three seconds. It may be seen that the gain introduced by the ELID process is approximately 5, and the signal-to-noise ratio has been increased from 1 to 15.

*For each level of illumination, the target voltage was raised until the same amplitude of signal was observed on the "A" scope. This, of course, would imply that the signals corresponding to the greatest illumination would be erased during the subsequent reading of the weaker signals.

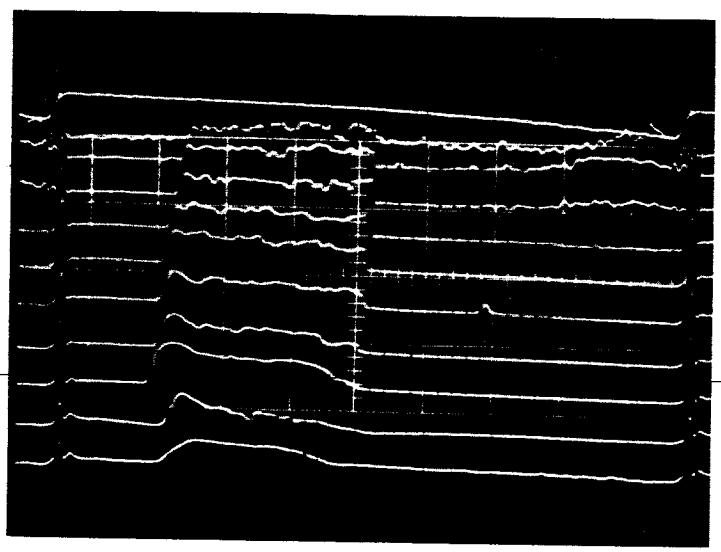

Figure 3.1.16. Target Disturbance for an Extended-Area Signal

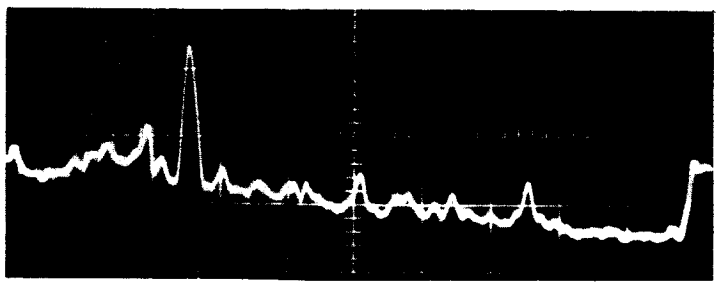

a) 9.6×10^4 Photoelectrons before ELID

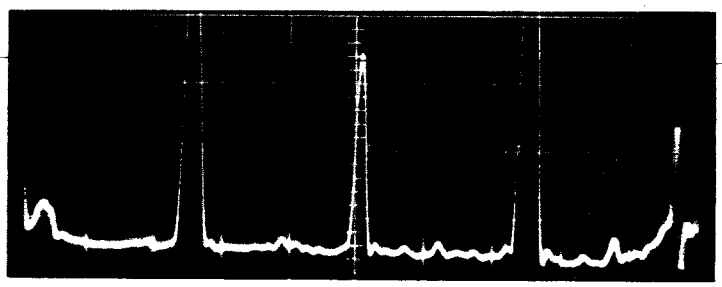

b) 9.6×10^4 Photoelectrons after ELID

Figure 3.1.17. Estimate of Target Disturbance Noise and Demonstration of ELID

Even more striking evidence of the efficacy of the ELID process is shown in Figure 3.1.18. An estimated 5×10^4 photoelectrons per 25 micron square resolution element was deposited upon the target, and read out giving the "A" scope trace shown in Figure 3.1.18a. After a four-second development, the trace shown in 3.1.18b resulted. The most important fact to be gleaned from Figure 3.1.18 is that the signal level can be raised out of the target disturbance noise without increasing the latter.

Evidently, the target disturbance can also effect the reproducibility of succeeding sets of data. Figure 3.1.19 shows two sets of readings taken in different directions along a grey scale, when the target voltage was varied to give a certain output signal on the "A" scope for each level. Estimated experimental error was 10 percent and most of the points agree within 20 percent. Figure 3.1.20, on the other hand, shows good agreement for all but three of the nine points taken. Figure was done with a slit source giving a 25 micron width stored bar on the target. The voltages were set very carefully with a Cubic V-70 digital voltmeter. The only uncontrolled variable was the portion of the target read out. Although probably optimistic, it is interesting to compare the deviation of the questionable points with the magnitude of the target disturbance.

Although integration longer than 10 minutes would not normally be necessary for a storage camera tube operating in the OAO series of experiments, ground-based equipment might require as much as a half-hour or more. The Optechon was therefore checked to determine if it could integrate for extended periods of time.

The conditions of this experiment were as follows: a small signal (derived from the illuminated slit shown in Figure 3.1.13) was stored with a short exposure on a target primed to 12 volts. It was read out immediately after exposure, and an "A" scope presentation is seen in Figure 3.1.21. The target reading voltage was +9 volts. This figure shows the amplitude of the signal without extended integration.

The target was then erased, primed and the signal restored at the same conditions, except with the image section high voltage applied and the focusing field on. Figure 3.1.22 shows the "A" scope presentation of the signal after one hour exposure to the image section with the high voltage on. It was read out at +6.3 target volts.

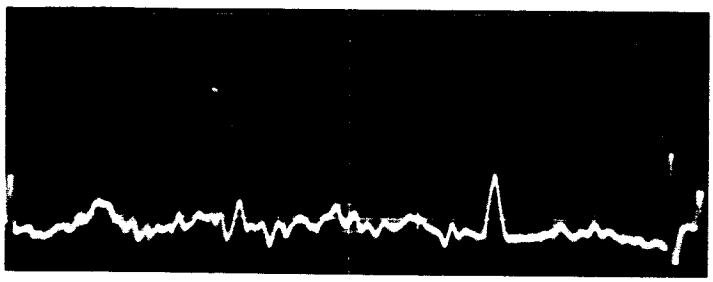

a) 4.8×10^4 Photoelectrons Before ELID

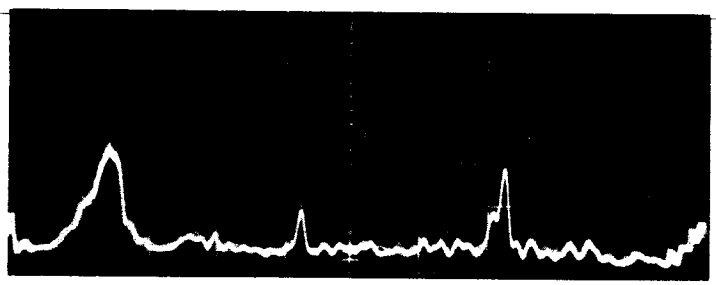

b) 4.8×10^4 Photoelectrons After ELID

Figure 3.1.18. Demonstration of ELID

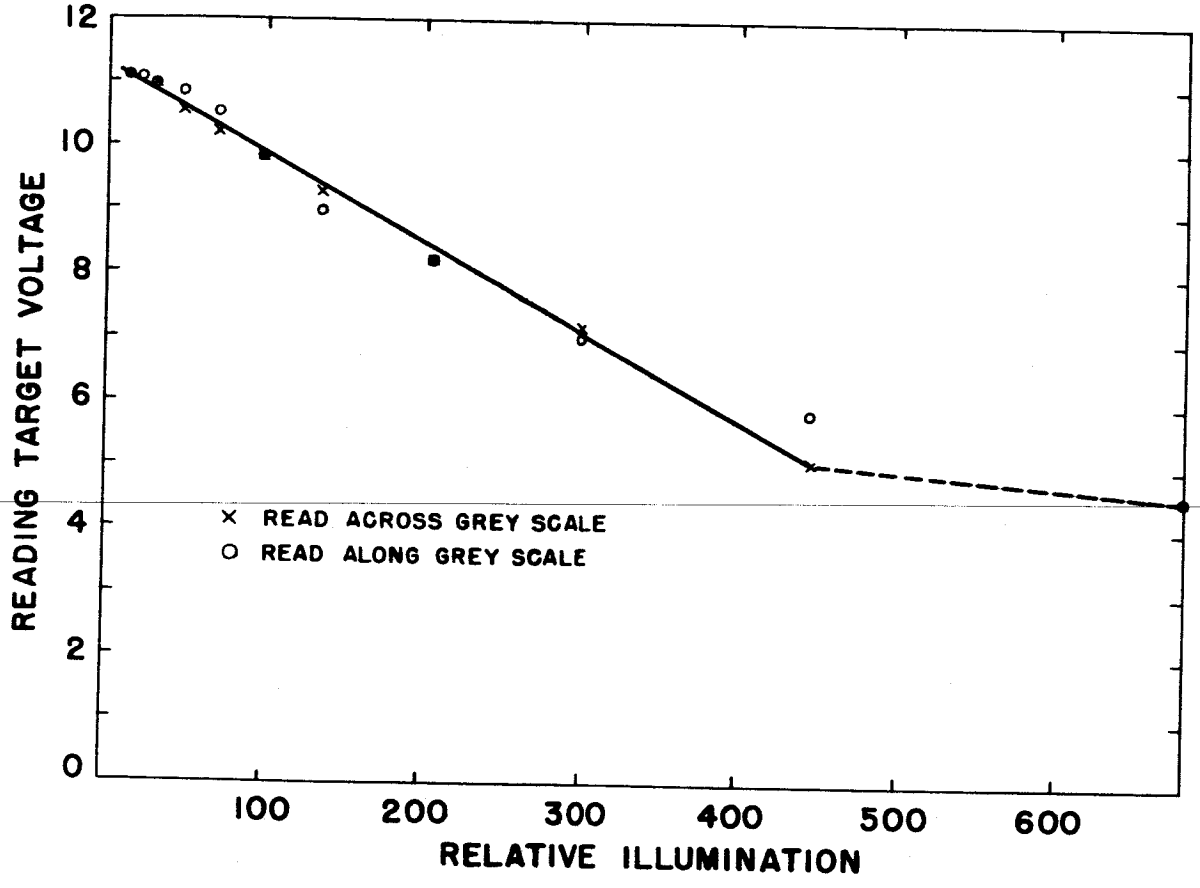

Figure 3.1.19. Reproducibility of Readout - Extended Area Source

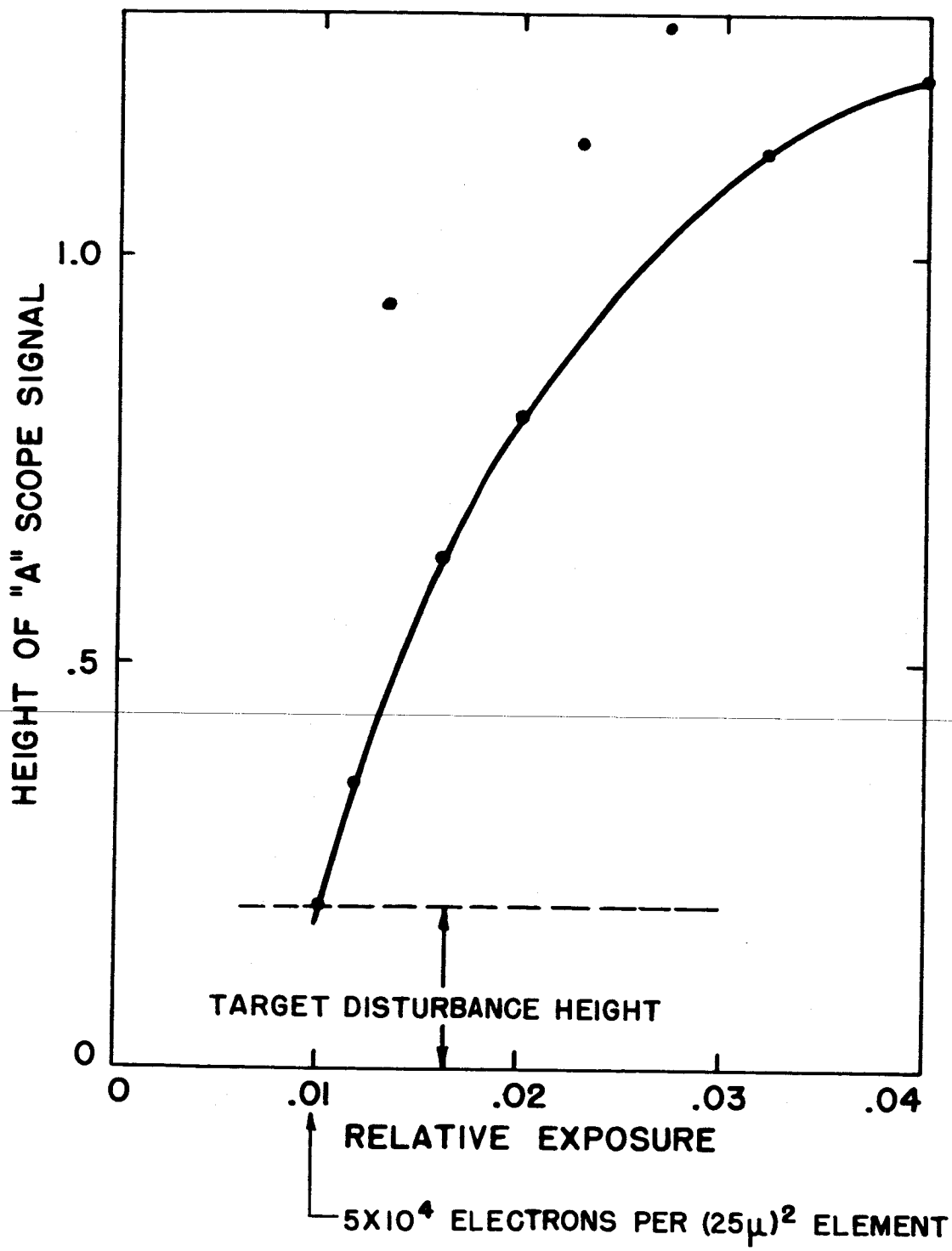

Figure 3.1.20. Reproducibility of Readout - Line Source

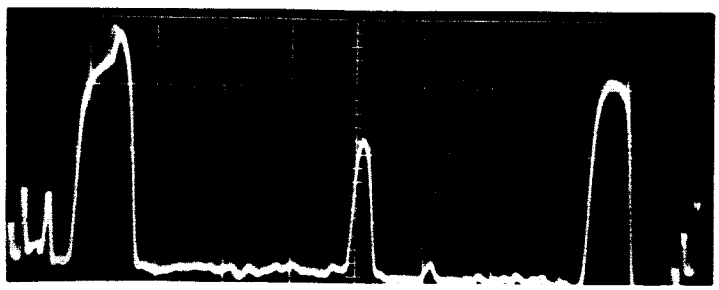

Figure 3.1.21. Integration Experiment -
Zero Integration Time Readout

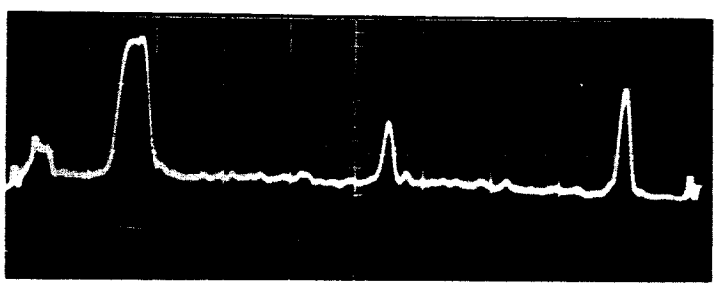

Figure 3.1.22. Integration Experiment -
1 Hour Exposure to Image Section at 10 KV

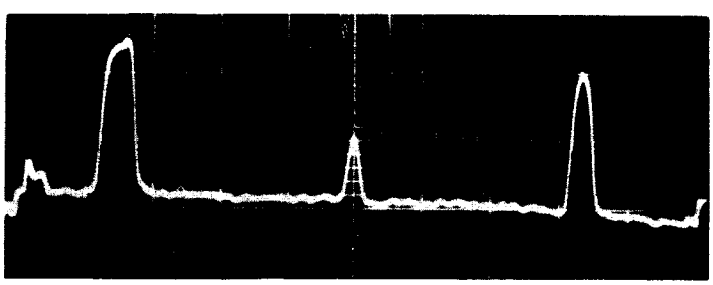

Figure 3.1.23. Integration Experiment -
1 Hour Wait Between Storage and Readout

In order to separate the effect produced by the image section, the same experiment was run, except the target was exposed to the image section with the 10 kV high voltage off. Figure 3.1.23 shows the trace readout at 8.4 volts, and indicates the amount of discharge of the target due to secondary causes, i.e., ion bombardment. It should be emphasized that this tube is nearly three years old, with many hours of use, and has shown evidence of gassiness.

It is seen therefore, that the target was discharged by 2 volts by dark current, which would correspond to 10^{12} electrons/cm^2-hr. removed from the target, or a dark current (taking EBIC gain into account) of 6 $\mu\mu A/cm^2$.

Figure 3.1.24 shows a plot of the results of several integration experiments with different exposure times to dark current. The main effect observed was a decrease in target reading voltage required for proper readout*, which was found to depend upon the presence or absence of high voltage during the exposure time.

Figure 3.1.25 shows a 1.0 ft. lambert brightness slit, integrated for 5 minutes at f/8, corresponding to 2 x 10^6 photoelectrons on a 25 micron square target element. A total of 2 x 10^6 photoelectrons were incident on a 25 micron square target element.

Two major experiments [30,31] were conducted to determine the interaction between two line images and the amount of image growth as the result of increasing exposure. It was found that interaction between two slit images was quite small, and less than the experimental error of three microns on the target. This corresponds to less than a grating line width for the 6000 line per inch grating used for the target.

Imaging spreading, what there was of it, was virtually absent. The small amount measured (1.4 times the input width, measured at 50 percent amplitude) was explainable by taking into account the reading transfer curve action during readout of the stored signal. This was found to be so, even though the storage target was overexposed by a factor of 6 to 1, which would imply that the written portions had been discharged to target potential.

*The reading voltage was determined by displaying the video signal on an "A" scope and increasing the target voltage until the target disturbance noise starts to appear on the baseline. Estimated error of this procedure is ±5%.

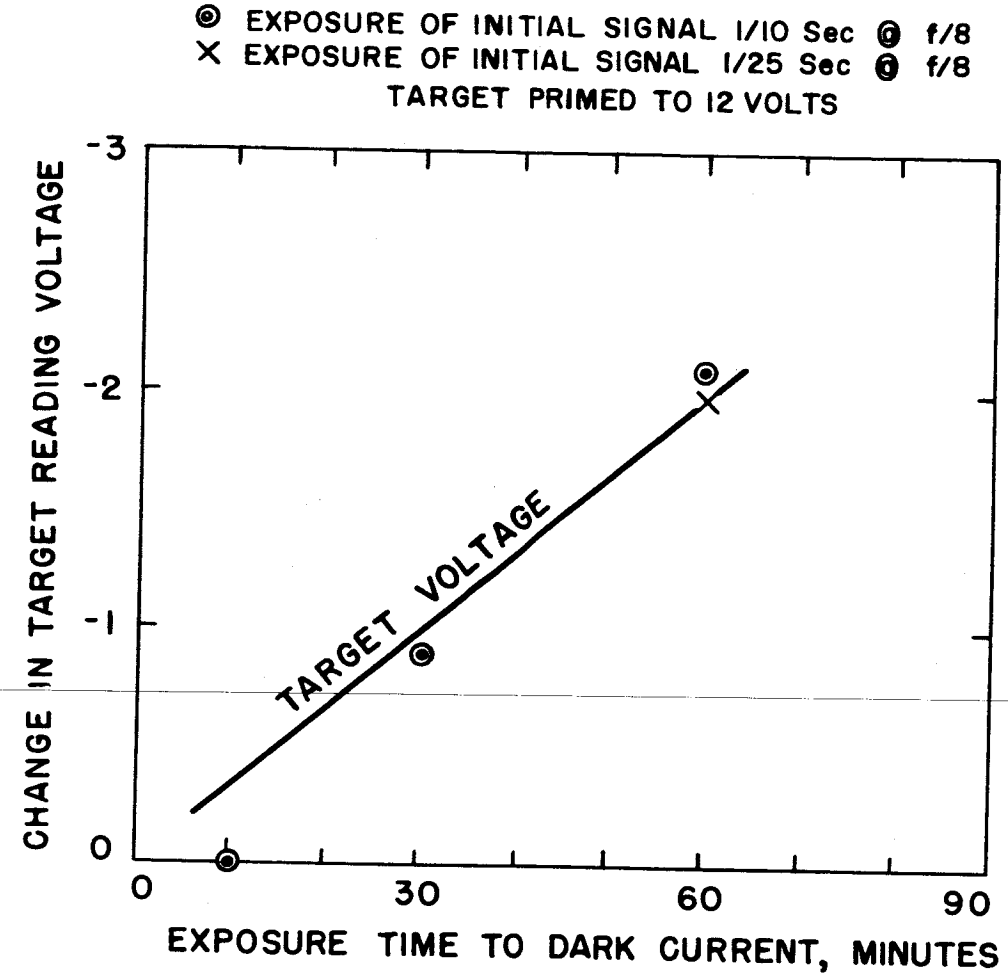

Figure 3.1.24. Variation in Reading Voltage with Exposure Time to Dark Current

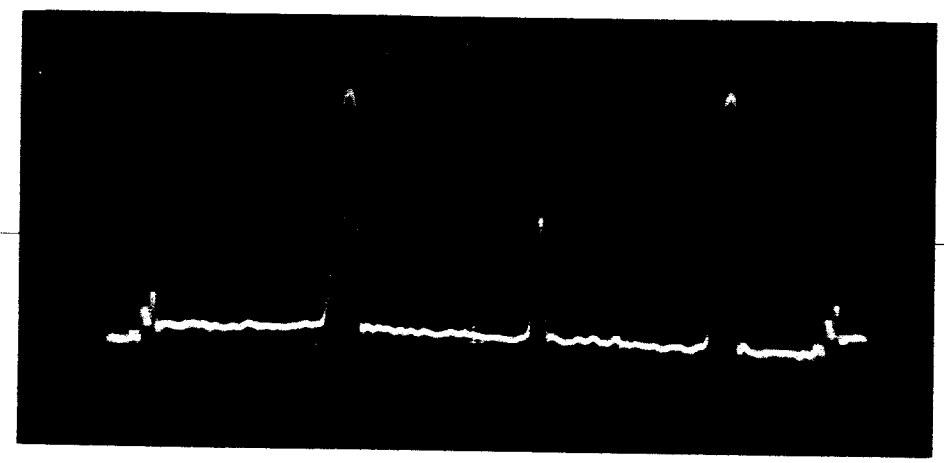

Figure 3.1.25. Integration Experiment 1 ft. Lambert Brightness at Object, Integrated for 5 Minutes. 2×10^6 Photoelectrons Incident on 25 Micron Square Target Element.

3.1.5 Applicable Properties - Optechon

3.1.5.1 Storage Capacity

The range of dielectric thickness S , for the Optechon grating storage target can be anywhere from 0.1 to 0.5 micron. For magnesium fluoride, the dielectric constant is 5.3. Consequently the range of capacitance per image element having a diameter of D is given in Table 3.1.2.

If the image element is discharged to a maximum of 3 volts, this would imply that $\bar{\gamma}_{max}$(3v.) electrons would be required. For a 15 volt discharging, $\bar{\gamma}_{max}$(15v.) electrons would be needed. These values are listed in Table 3.1.2.

In other terms, if the image element were discharged by 3 volts the storage capacity would be 1.8×10^{11} to 8.8×10^{11} electrons/cm^2. For 15 volts, the storage capacity would be 8.8×10^{11} to 4.5×10^{12} electrons/cm^2.

3.1.5.2 Spatial Resolution

The resolution of the Optechon is mainly determined by the reading beam spot size, which can be as small as 10 microns for a 1 microampere beam current. The reading beam spot size is measured at half-current amplitudes as the beam is scanned past a slit. This corresponds to a limiting resolution (5 percent response) of 75 line pairs per millimeter for the tube. The resolution of the image section alone has been measured[29] to be 220 line pairs per millimeter limiting resolution at the center. The above data is for an all-magnetic (magnetic focus, magnetic deflection) tube.

It is interesting to note in Figure 3.1.26 that there is no appreciable change in the aperture response curve after 41 hours of storage, indicating no leakage of charge across the surface.

3.1.5.3 Readout Mode

In its normal mode of target readout, the Optechon reading beam probes the potential distribution above the target surface, and the

TABLE 3.1.2

ELECTRICAL AND STORAGE CAPACITIES PER IMAGE ELEMENT

Optechon

D	C_{el}	$\overline{\chi}_{max}$(3v.)	$\overline{\chi}_{max}$(15v.)
10 micron	$7.4\text{-}37 \times 10^{-15}$F	$1.4 \times 10^5 - 6.9 \times 10^5$	$6.0 \times 10^5 - 3.4 \times 10^6$
25 micron	$46\text{-}230 \times 10^{-15}$F	$8.6 \times 10^5 - 4.3 \times 10^6$	$4.3 \times 10^6 - 2.2 \times 10^7$
50 micron	$184\text{-}920 \times 10^{-15}$F	$3.4 \times 10^6 - 1.7 \times 10^7$	$1.7 \times 10^7 - 8.5 \times 10^7$
100 micron	$736\text{-}3680 \times 10^{-15}$F	$1.4 \times 10^7 - 6.9 \times 10^7$	$6.9 \times 10^7 - 3.5 \times 10^8$

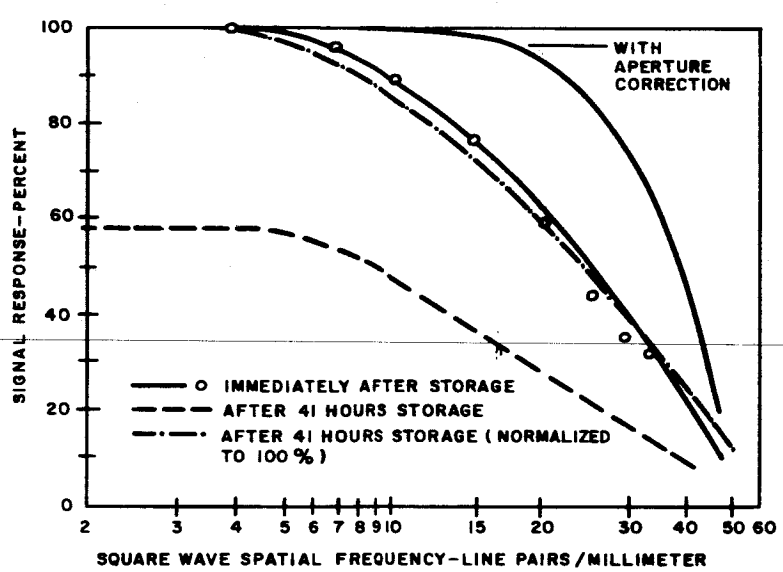

Figure 3.1.26. Square Wave Response Before and After 41 Hour Storage

percentage of beam electrons returned to the electron multiplier as the result of reflection from the target constitutes the signal from the tube. This is the orthicon (return beam) mode of reading. The vidicon mode is essentially the same, insofar as the target-gun-dielectric potentials are concerned except that the signal is obtained from the target itself. Both modes can be read out destructively or non-destructively, but the latter is the usual case. The destructive mode implies that the reading beam electrons have sufficient energies to land upon the dielectric and charge the written (positive) portions of the target.

For non-destructive reading, a measure of gain is obtained through the triode characteristics of the grating target. A relatively small amount of charge deposited on the target can control the reflection of a relatively large beam current, and the gain can be expressed as

$$\sigma_3 = \frac{g_m I_b}{C_{el} k f_c}$$

For f_c = 62.5 kc/s, k = 1 element per cycle of bandwidth, a 25 micron image element giving C_{el} = 46 x 10^{-15} farad, and a target mutual transconductance of g_m = 0.2 volt; the gain is

$$\sigma_3 = 70 \times 10^6 I_b .$$

Therefore for reading beam currents higher than 1.4 x 10^{-8} Amp, the reading gain exceeds unity.

Destructive reading implies that for each electron removed by the writing process, the reading beam will replace an electron, and this replacement process gives rise to the signal current output from the tube. This destructive mode of reading process therefore has a gain no greater than unity.

Another consideration in the readout mode is the electrical capacitance of the signal electrode to ground, whether it be the electron multiplier collector or the target. The capacitance of the image orthicon anode terminal to ground is 12 picofarads, while the target to ground capacitance of the three-inch Optechon (WX-5074) is 49 picofarads measured in situ. It can be expected therefore that the vidicon mode of reading,

where the signal is taken from the target, might be inherently noisier than normal.

3.1.5.4 Positional and Size Accuracy

In applications where the position at the object must bear a 1:1 relation to its position as read out by the sensor, the Optechon has a definite advantage. Errors in readout position can result from the optics and the stability and linearity of the ancillary electronic equipment: assuming that these effects are minimized, positional accuracy can also be affected by the sensor.[27,2,1,34]

Electron-optical aberrations in the sensor can cause errors in position and image size, but in general these are reproducible from measurement to measurement and do not depend upon the input signal amplitude.

The errors introduced by the nature of the storage target are more difficult to resolve since they often depend upon the amount of stored charge, mode of reading and writing, sweep speeds, etc. Often, it is necessary to change the nature of the target at the expense of some other parameters, for example, resolution.

Position and size accuracy are affected by two major phenomena: "beam bending" and secondary electron redistribution. Both are present in the garden-variety image orthicon; both are absent in the Optechon.

The reason for their absence in the Optechon stems from two causes: EBIC writing is used rather than secondary emission writing; the Optechon has a unique coplanar structure, limiting the extent of the field above it. In all fairness to the Optechon, even if secondary emission writing were used, the voltage between the target structure and a collector electrode would minimize the effect of secondary electron redistribution.

Figure 3.1.27 shows the electrostatic field distribution above the surface of a grating storage target, and the paths of the reading beam electrons during non-destructive reading. The "guarding" provided by the bare metallic diffraction grating slopes is readily seen to limit the extent of the potential distribution due to stored charges not only perpendicular to the grooves, but also along the grooves and above the target surface. This "guarding" also provides a readily-accessible path for secondary

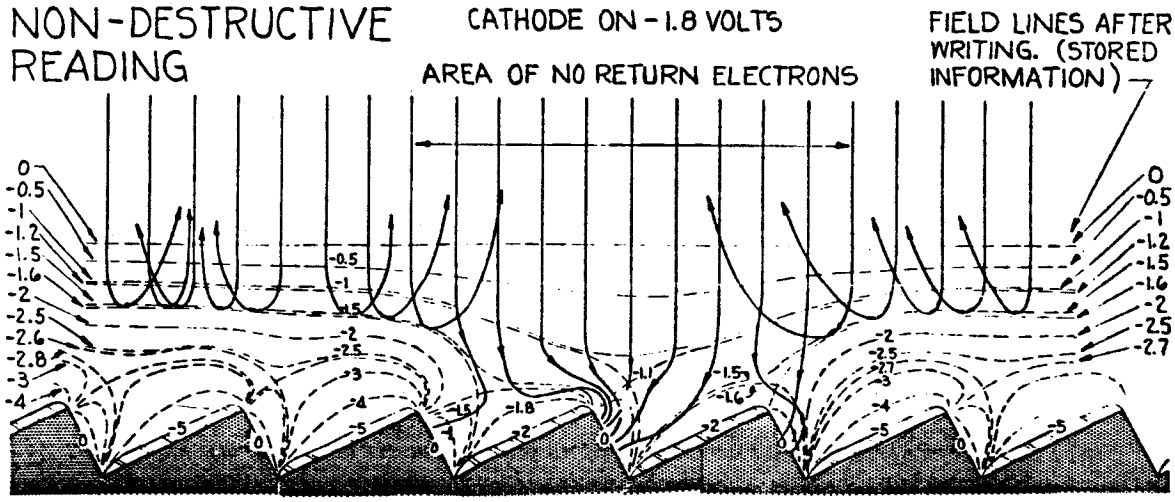

Figure 3.1.27. Field Distribution Above Grating Storage Target

electrons released from the dielectric surface, thereby preventing secondary electron redistribution. More important, it provides an "escape path" for energetic electrons that have insufficient energy to land upon the charged dielectric surface, and thereby effectively increases the reading beam modulation provided by the target.

The constraint of the fields above the target surface by the "guarding" feature of the grating storage target not only allows high resolution imaging (limited not by the target, but by the width of the reading beam), but also restricts to one groove width the effect of spot spreading and beam bending, which are found to be much more extensive in smooth-surface targets.

Spot spreading is the condition observed in some imaging tubes where an increase in exposure upon an image element will cause an increase in the size of the readout image. While it can be caused by secondary electron redistribution, most often it is the result of beam bending; i.e. the false positional indication of a stored image by a scanned reading beam as the result of the deflection of the beam by the potential field produced by the stored image.

References 30 and 31 report on measurements made with the WX-5074 Optechon on beam pulling and spot spreading. It was found that the beam pulling with a 6000 line per inch grating storage target was less than the experimental error, or less than 3 microns. Spot spreading observed with the WX-5074 was explainable in terms of the effect of the reading transfer curves upon the readout signal. Over a 6 to 1 over-exposure there was no significant spot spreading at all.

3.1.5.5 Target Configuration

Present WX-5074 and WX-5023 Optechons are being made with plane, rigid targets rotated with the aid of gravity by a combination of rotation around the longitudinal tube axis and tilting around a transverse axis through the target bearing axis. Under another contract* the feasibility of

*Contract No. NAS 5-9020 with National Aeronautics and Space Administration, Goddard Space Flight Center, Greenbelt, Maryland, "Grating Storage Camera Tube Study".

rotating the target, by passing a pulse of current through a coil attached to the target, is being studied. Results of this study are encouraging, and may result in an electrically rotatable Optechon early in 1965.

While this target structure may have some disadvantages with respect to the ruggedness and mechanical vibration sensitivity of the tube it is conceivable that these could be overcome by a suitable mechanical redesign of the tube. One advantage stemming from the opaque target is the light shielding it provides: the light from the thermionic cathode is prevented from falling on the photocathode during the integration time by the target. This limitation shortens the integration time possible with the image orthicon[6], and can be expected to affect the integration time of any tube combining a photoconductor and insulator in the same sensitive surface, unless special means are taken to shield these sensitive surfaces from the cathode light output.

3.1.5.6 Signal-to-Noise Characteristics

From the analysis of the Optechon given in Section 3.1.3, it is seen that for this tube it is desirable to maximize the aperture response, and the filter response (through a suitable choice of k), and to increase the value of equalization ratio M to a practical limit (Appendix A). Also, the beam current I_b should be increased to the highest value that does not compromise the aperture response through the increase in beam diameter.

Finally, an added measure of prestorage gain is highly desirable (as may be seen in Figures 3.1.9 to 3.1.12) by the use of Electrostatic Latent Image Development. If this is done, 13 percent accuracy (S/N = 7) is possible at 10^2 photoelectrons per image element and 1.2 percent accuracy (S/N = 83) at 10^4 photoelectrons per image element.

It should be made clear that the signal-to-noise ratio obtained here is a theoretical value depending only on the gain (and attenuation) processes in the tube. It does not take into account such sources of noise as the target disturbance noise which will limit the sensitivity of the Optechon, even with the use of ELID prestorage gain (see Section 3.1.5.10).

3.1.5.7 Production Status

The Optechon is still in a laboratory experimental tube category. Not over 20 tubes will be made by mid-1965, and all will be, or have been, used in improving its performance, and measuring characteristics of the grating storage target heretofore unmeasured. Tubes made prior to this contract were used as a test vehicle for first resolution measurements made on the grating storage target, and have served to verify the absence of beam pulling, image spreading, influence of ELID, and other measurements made on this program. Further work and additional experimental evidence is required on such problems as the influence of beam current on signal to noise reduction of grating disturbance, ELID conditions, effect of grating parameters upon the mutual transconductance factor, to name a few. These will enable a specification to be drawn up for this tube, this specification having sufficient information to guide the systems designer in its use.

3.1.5.8 Ruggedization

This specification sheet would also indicate that the tube was capable of withstanding certain mechanical and other environmental conditions. For the present state-of-the-art Optechon no substantiating data has been taken that could be applied to evaluating the ruggedness of this tube or to suggesting means by which the tube could be made more rugged.

Ruggedization is generally the last step in a tube development program, since it depends greatly upon the configuration of the tube to that point, which in turn would depend upon the electrical characteristics desired. Often, wise choices can be made during a tube development program that can simplify the task of ruggedization. In most cases, environmental tests are run after the electrical design of a tube is complete, and this usually implies that the use of the tube has already been determined. Since the Optechon is a relatively "young" tube in terms of development time, it has not been seriously considered for many applications; consequently there has been no need to ready it for any specific environmental condition as against another.

3.1.5.9 Reproducibility of Charge Readout

The Optechon does not normally read information out by replacing the positive charge stored upon it, electron by electron, as do the vidicon, orthicon, or SEC Vidicion. Instead, it samples the potential distribution above the target surface in a non-destructive manner, and the signal derived from this sampling is a function of the stored charge resident upon the target. This mode of non-destructive reading has the important advantage of providing a gain mechanism, but the disadvantage of introducing several parameters having an influence on the relation between the input stored charge and the output signal.

The expression for the reading gain is

$$\sigma_3 = \frac{g_m I_b}{C_{el} k f_c}$$

The mutual transconductance of the target g_m, is a slow function of the target potential and the priming voltage. Also, with careful processing, the elemental target capacitance, C_{el}, can be held to one percent or better over the target surface. The remaining factor, reading beam current, I_b, must also be kept quite stable.

Not included in the assessment of the parameters capable of introducing errors in the reading gain, are the parameters associated with the spatial frequency or aperture response of the tube A_γ, the filter response of the amplifier A_f, and the hidden electron-optical aberrations such as "shading" due to first dynode secondary emission variations, or "shading" due to non-orthogonal landing.

This is not to imply that a functional relationship between the output and input cannot be established, but that care will be necessary to insure that circuit stability and tube design is adequate, and predictable enough to maintain calibration.

As yet there has not been enough experimental information on the reproducibility of readout for the Optechon to enable a firm estimate based upon actual experience to be given. It is believed to be better than 5% but requires further study for verification.

3.1.5.10 Target Disturbance Noise

It has been established that the present limit to the resolution of the grating storage target is the half-amplitude width of the reading electron beam. The grating itself is not resolved unless periodic errors in ruling change the mutual transconductance of the target locally. However, target disturbance does exist and is believed to be caused by work function variations, artifacts, dust, pinholes, all classified under the appellation of "blemishes". Sometimes the blemishes can be seen with the unaided eye, while at other times only the electron beam can sense them.

Work performed on Westinghouse funding disclosed that a special processing would improve the appearance of the target, suppressing the majority of the blemishes normally seen with a virgin target. This work has been relatively recent and no quantitative comparison has been made between the old and new processing methods. The target disturbance of the new targets is believed to be at least an order of magnitude smaller than that measured* on an old tube as the result of the present study.

It has been found that signals buried in target disturbance noise can be enhanced by ELID while the target disturbance noise is not increased significantly.

It is believed that further work can effect greater improvement of the target disturbance noise. At present it is the greatest limitation upon the sensitivity of the Optechon at reasonable signal to noise ratios.

3.1.5.11 Focusing

The present design for the WX-5074 and WX-5023 is for magnetic deflection and magnetic focusing in order to realize the full resolution capabilities of the grating storage target. While no immediate plans are being made to "hybridize" this tube; i.e., to have magnetic deflection and electrostatic focusing, some thought has been given the consequences of such design changes. Reference 32 considers the possibility of having

*10^5 electrons per 25 micron square image element, measured on an early model tube.

electrostatic focusing in an imaging tube which would be the equivalent of the Optechon image section and concludes that unless a spherical geometry target were used the resolution degradation is excessive at the edges, and suggests a spherical geometry for the target.

Since the Optechon has a rigid rotatable target it is conceivable that it could be made in a spherical form: from the electron-optical standpoint this would be most convenient, since it would present the appropriate concavity to both an electrostagic image section and an electrostatic reading section. It is therefore believed that a high resolution, completely electrostatic Optechon with a rotatable grating target might be possible. Some additional target disturbance may have to be tolerated, however, so that a decelerator or field mesh can be used during reading to maintain a small reading beam spot for low energy reading.

3.2 The SEC Vidicon

3.2.1 Historical Background

The SEC Vidicon represents a new type of television camera tube that combines the ability to store large amounts of charge with a pre-storage electron multiplication in the storage surface itself. The tube was developed at the Westinghouse Research Laboratories by G. W. Goetze and A. H. Boerio[35] in the course of studies on high gain transmission secondary electron emission layers consisting of low density, smoke-type insulator targets.[36,37] This work in turn grew out of the studies of transmission secondary emission from vacuum evaporated, solid KCl films[40,41] used in the Astracon type of image-intensifier.[42]

The first application of this new type of storage-target was made as a replacement of the electron-bombardment-induced conductivity (EBIC) target in the uv sensitive camera tube (UVICON) developed for the Smithsonian Astrophysical Observatory as the sensor for the Smithsonian experimental package of the first Orbiting Astronomical Observatory (OAO).[16] Tubes with similar targets, but with photo-cathodes sensitive in the visible, were developed for the U.S. Air Force Aeronautical Systems Division, and are commonly referred to as SEC-Vidicons, where SEC stands for "secondary

electron conduction" in the open spaces of the porous targets, as will be described briefly below.

3.2.2 Theory of Operation

The SEC-Vidicon or Uvicon operation can be briefly summarized with the aid of Figures 3.2.1 and 3.2.2, showing a schematic diagram of the Uvicon tube and the storage target.

Photo-electrons released from the photo-cathode on the inside surface of the window are accelerated by a potential of the order of 8 - 10 kilovolts and strike the target. The incident primary electrons I_p penetrate the thin supporting foil consisting typically of an aluminum oxide film about 1000 Å thick, followed by a conducting layer of aluminum 300 - 500 Å thick. The electrons then enter a porous layer consisting of KCl "smoke" approximately 25 μ thick, formed by evaporating KCl in an inert gas atmosphere,[36,37] where they dissipate most of their energy in the formation of secondary electrons. These secondary electrons escape from the fibers of the smoke particles and are collected in part by the wall-screen and in part by the aluminum conducting layer. This is achieved by maintaining the back-plate positive relative to the surface of the target, the potential of which was previously fixed at ground potential by scanning with a low velocity electron beam produced by an ordinary Vidicon-type of gun.

As a result, a positive, or rather reduced negative, charge remains behind in the insulating layer wherever primary electrons have ejected secondaries. The scanning beam I_b is used to neutralize this charge, leading to a pulse of electrons flowing away from the target through the load resistor whenever the scanning beam passes across a charged picture element. Since, in effect, the scanning beam acts just like a switch discharging a condenser on which a charge has accumulated during integration, the total charge ΔQ passing through the load resistor in the scanning time per element $\Delta\tau$ is a direct measure of the number of photoelectrons integrated between scans, multiplied by the secondary electron gain G.

This secondary electron gain consists in general of two parts,

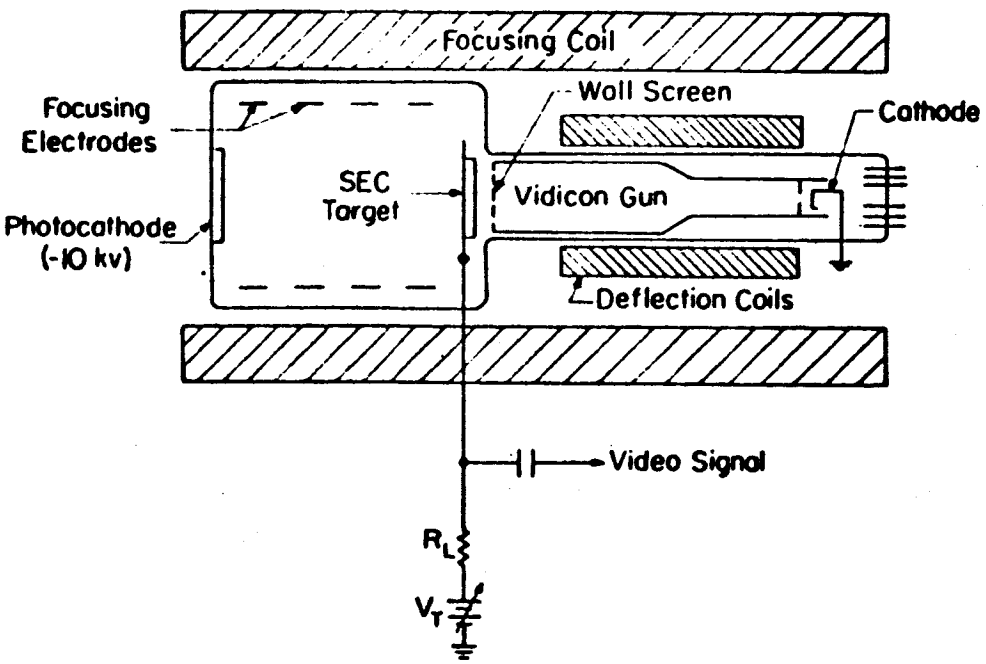

Figure 3.2.1. SEC Vidicion Schematic

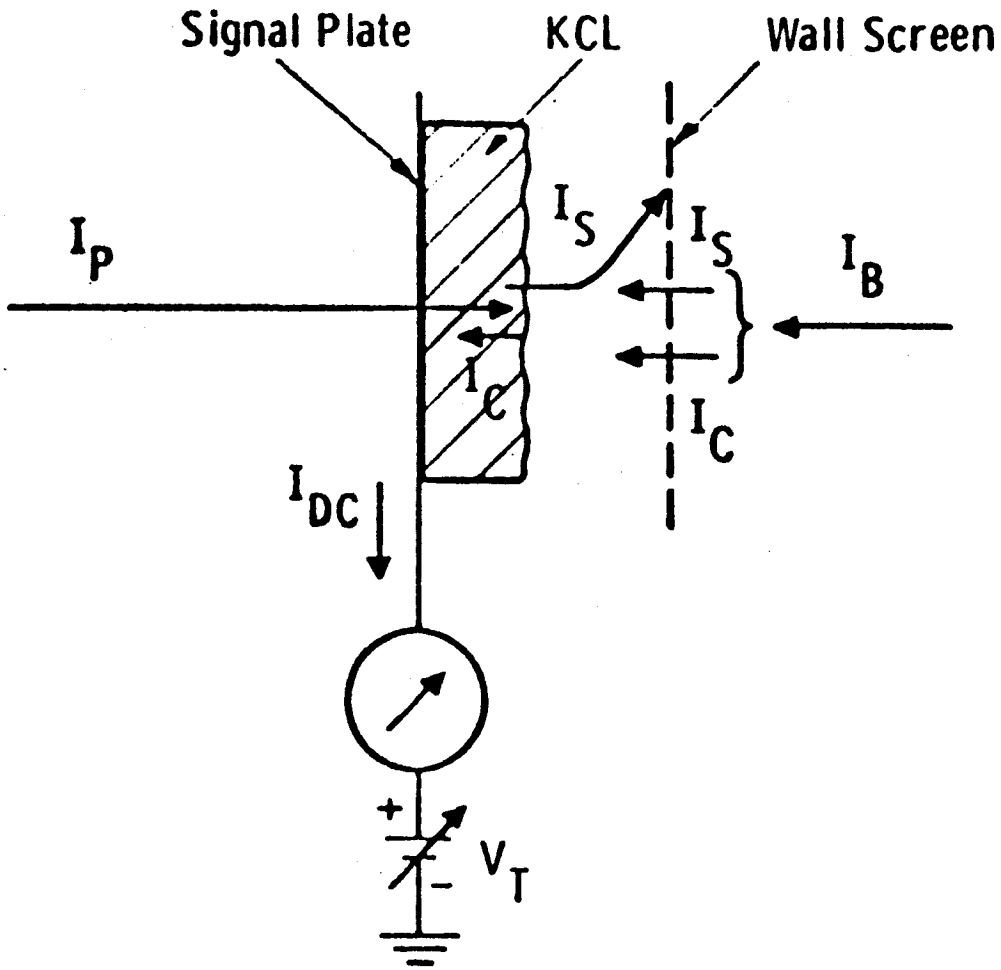

Figure 3.2.2. Schematic Diagram of Currents Involved in SEC Target Operation

a portion due to secondaries collected by the target back-plate by conduction through the open pores of the smoke film, G_C, and a portion due to the secondaries that escape from the surface as ordinary, external secondaries, G_{SE}. In the usual mode of operation, the internal field acting to pull the secondaries liberated in the smoke layer to the metallic target backing is very strong, and nearly all the gain is due to "conduction" within the target. Only when the surface has charged up significantly towards the back-plate potential, thereby reducing the internal field, does the escape of secondaries from the surface become the more significant contribution.

The relation between the two types of processes controlling the gain is shown in Figure 3.2.3, plotted for a constant field between target surface and field mesh. As the potential difference across the target is decreased in the course of charging, the conduction gain, G_C, decreases relative to the transmission secondary emission gain, G_{SE}, and the combined gain decreases towards G_{SE} alone. Note that the typical gains have the large values of 60 to 200 in the range from target surface to back-plate potentials V_T between 0 and 200 volts. Such large gains are realized because nearly all the secondaries formed are collected, in contrast with secondary emission from solid layers, where only a small fraction of all secondaries can escape. Since it is known that approximately 30 ev are required to form a secondary,[44,45] if the primaries dissipate some 6-9 kev in the smoke-layer, maximum yields of 200 to 300 are to be expected. Such high escape probabilities follow from the fact that the smoke consists of small fibers less than a few hundred angstroms thick, a distance small compared with the measured mean free path of secondary electrons in KCl.[46]

Figure 3.2.3 shows gain as a function of surface potential V_S for a given fixed backplate potential V_T and for a field mesh potential that rises with V_S to maintain a constant external field. Actually, the external TSE gain does not vary appreciably with change of this external field so long as the field mesh potential is always more positive. From this standpoint, the field mesh may be set at some conveniently high positive potential. From another standpoint, however, the field mesh potential must be kept low enough to prevent the target from charging more positive relative to the cathode than the first-crossover potential

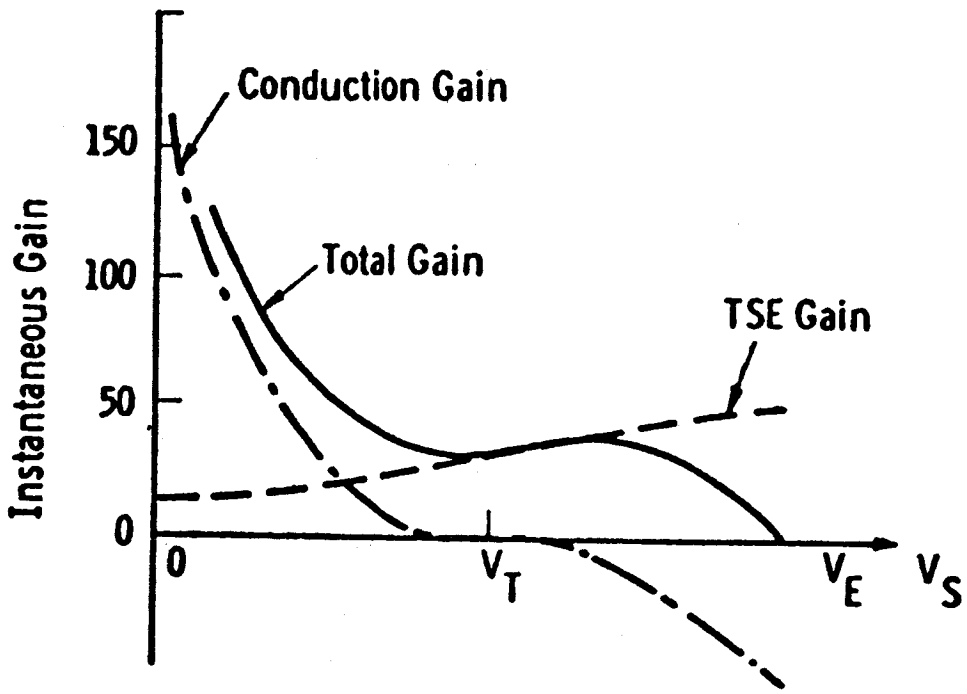

Figure 3.2.3. Conduction Gain, Secondary Gain, and Total Gain as a Function of Target Surface Potential, V_s

of the secondary emission curve. If the target surface potential rises higher, the reading beam will charge the surface more and more positively, instead of discharging it, and destructive breakdown of the target can occur. Since resolution is improved by having the field mesh at higher potential during readout, it can be advantageous to switch this potential from a typical value of +15 volts during storage to as high as +400 volts during readout. There has also been success with introducing an intervening suppressor grid at about +15 volts, with the field mesh potential then left high.

Figure 3.2.4 shows gain as a function of varying target backplate potential V_T, where the target surface potential V_S is held nearly constant near zero by the readout of the beam. The internal conduction secondary emission gain rises with increase of V_T as the electric field within the SEC layer becomes proportionally higher. Meanwhile, the external TSE gain decreases because the secondaries are drawn instead to the backplate.

The total gain of the target will vary from its initially high value towards increasingly lower values as the surface charges up towards both the back-plate and the field-mesh, in a manner indicated schematically in Figure 3.2.5. This variation of gain will accordingly determine the shape of the transfer characteristic, defined as the dependence of charge stored and read-out on the the charge of primary electrons (photoelectrons) accumulated.

The shape of such transfer characteristics is indicated schematically in Figure 3.2.6 as obtained from typical Uvicons. The slopes of these curves are analogous to the gamma of photographic plates, so that it is clear that the choice of initial target potential, mesh potential, and primary energy permit some control over the gamma of the tube. When the highest sensitivity to small signals is desired, the initial gain should be high, resulting in a large initial gamma. When it is desired to accumulate a large signal with high accuracy, the initial gain can be reduced to get a more constant slope of the transfer curve.

The ultimate limit to the amount of charge that can be stored is dictated by the total voltage drop across the target that can be tolerated and the effective capacity of the surface per unit area. The voltage across the target for astronomical spectroscopy will probably be

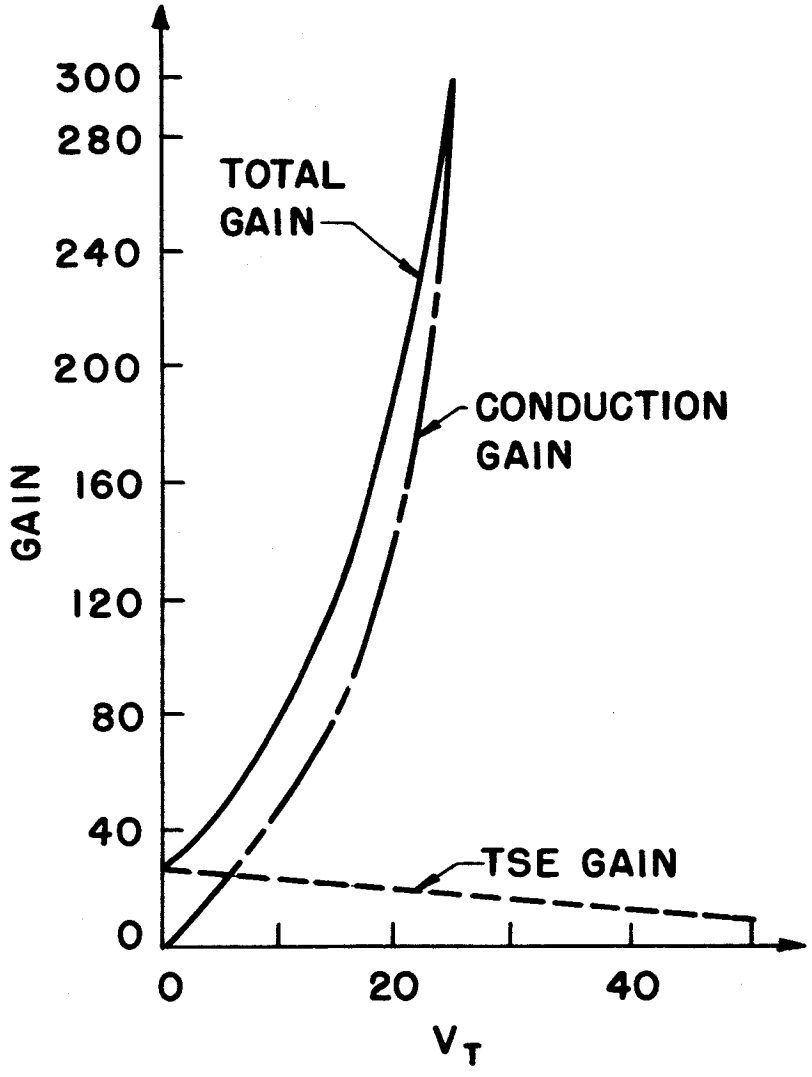

Figure 3.2.4. Contribution of Conduction Gain and Secondary Gain to Total Gain as a Function of Target Backplate Potential.

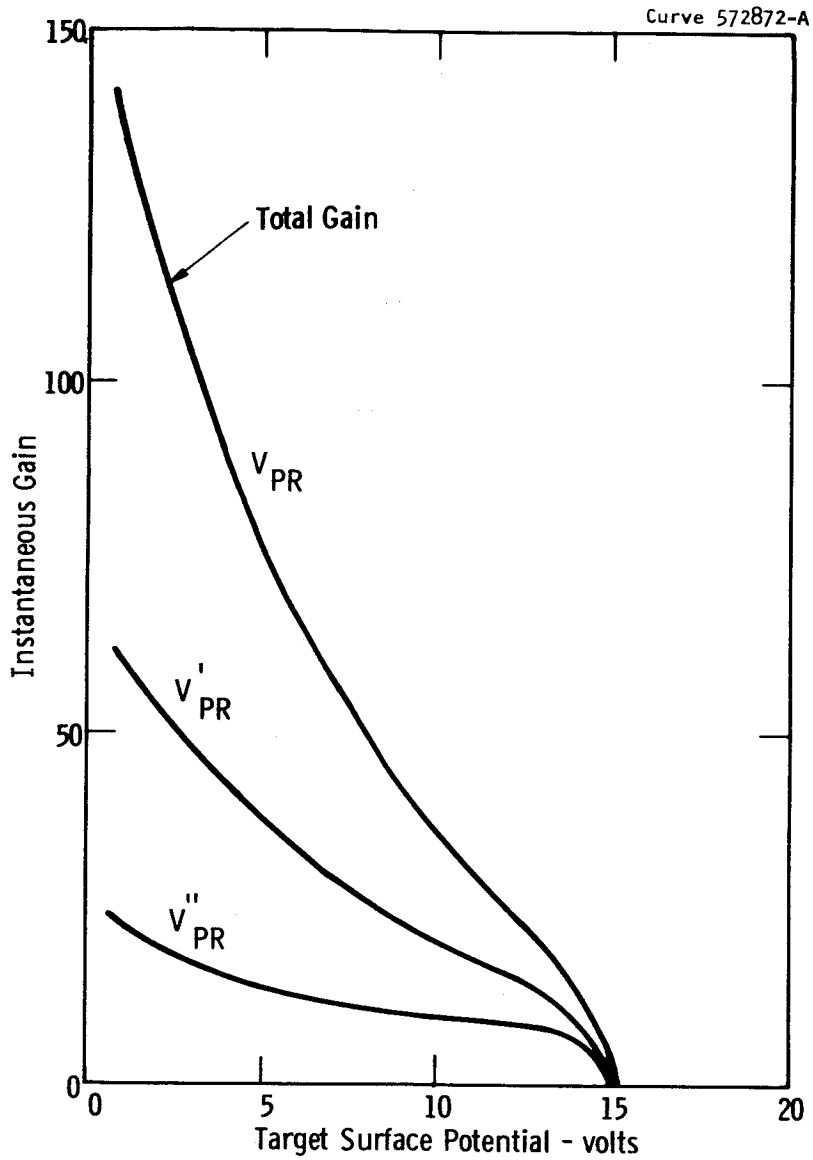

Figure 3.2.5. Schematic Diagram Illustrating the Variation of Total Target Gain with Increasing Charge Accumulated on the Target. Curves are Drawn for a Typical Fixed Field-Mesh Potential of 15 Volts and Three Different Primary Electron Energies V_{PR}.

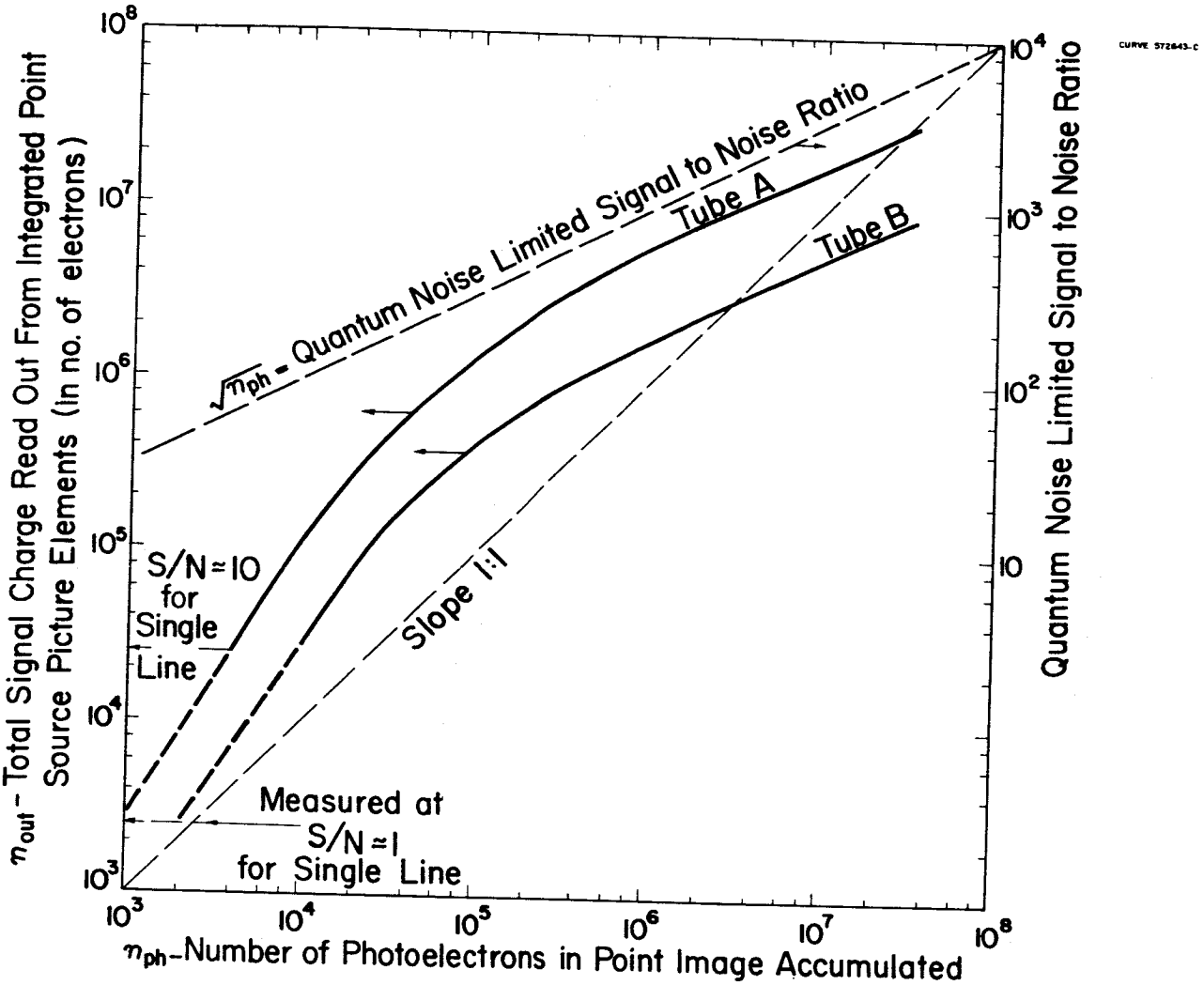

Figure 3.2.6. Typical Transfer Characteristics of SEC-type Storage Targets as Measured for Two Different UVicons. The effective charge read-out per point image is determined both by target gain and by circuit characteristics. For purposes of photometry, a signal-to-noise ratio of 10 sets the lower limit of operation. For high charge input, the output signal is limited by quantum noise of the incident flux.

limited to values of the order of 15 to 20 volts by the onset of target graininess with high total light exposure and a slow mode of discharge similar to that encountered in EBIC or Vidicon type of surfaces. At low voltages, the discharge process is extremely fast,[47] since it is primarily due to free secondary electrons in the vacuum between the smoke fibers. The action stops completely when exposure stops, and the image is completely removed in a single readout. At high voltage, ordinary solid-state conduction begins to play a significant part, and this process leads to internal polarization which relaxes only slowly. Although lag of response might seem unimportant for long astronomical exposures, residual image building up after readout can appear in a later picture and is therefore unacceptable.

The target capacity is determined by the exact distribution of the charge within the storage layer, and can therefore not be calculated from the known thickness. The actual capacity turns out to be many times larger than the value of $35 \mu f/cm^2$ calculated if the charge is assumed to reside on the surface only. In fact, since typical layers have been about two percent of the bulk density of KCl, and the individual particles are less than 1μ in size, fiber thickness must be still less and therefore very small compared with the 25μ thickness for the whole layer. As will be discussed in more detail below, the actual capacity is considerably larger than this. In the extreme, the very large amounts of charge actually observed to be stored for point images, namely, close to 10^{11} electrons per cm^2, suggest effective capacities more than 10 times the ideal plane-parallel value calculated above.

The loose fiber structure leads to a very high resistivity measured to be in excess of 10^{17} ohm-cm. The RC time constant is very large. Charge images may be stored on the target without detectable loss of resolution for many days at a time.

Thus, by combining a large storage capacity with a very long time-constant, this type of target represents in effect an electrostatic photographic plate with controllable gamma and rapid, quantitative charge-readout. Compared with a photographic plate, the storage capacity is many orders of magnitude larger. Thus, even with an average gain of 100, this type of target can store 10^9 photoelectrons or independent events per cm^2,

3.2.2.1 SEC Vidicons Data

		WX-5419	Uvicon	WX-30150
1.	Res. (cntr.) limiting, in TV lines/im.ht.	500-600 (20 lp/mm)	300-350 (18 lp/mm)	600 (20 lp/mm)
2.	Image Height	0.6 inch	0.375 inch	0.6 inch
3.	Focus/Def.	M/M	E/E;E/M; M/M	M/M
4.	Image Sec. Dia.	3 inches	2 1/4 inches	2 inches
5.	Gun Dia.	2 inches	1 inch	1 1/2 inches
6.	Length	18 inches	8 1/2 inches	10 1/2 inches
7.	Geometric Distortion	None	Dep. on 3	None
8.	Availability	Present	Present	January 1966
9.	Projected Use		Smithsonian Expt.	Comm.

Notes: All electrostatic focus tubes have curves photocathodes.

In general, electrostatic focus tibes are down 30% in resolution at the edges.

compared with a storage capacity of 10^6 - 10^7 grains per cm^2 for typical astronomical plates.

3.2.3 Signal-to-Noise Ratio Analysis

In order to allow a measure of comparison between the SEC Vidicon and the Optechon, the same analysis technique was applied, namely that outlined in Appendix C. The different reading mechanism of the SEC Vidicon enabled some simplification, resulting in four equations, bracketing the operating ranges of the tube with respect to gain and aperture response. These equations are tabulated in Table 3.2.1, plotted in Figure 3.2.7 and show the desirability of high gain and a large value of aperture response. Although not explicitly stated, these curves also imply that the target capacitance relative to the other electrodes should be as low as possible. The curves are based upon a target and amplifier stray capacitance of $60\mu\mu f$, and an equalization ratio of 24. It may be possible to decrease the target capacitance by half to $30\mu\mu f$, which would have the effect of increasing the sensitivity of the tube. Lacking this, it is possible (Appendix B) to increase the equalization ratio to a higher value, say 200 - 300, and still stay within the practical limits of tube and circuit operation. This condition is shown as the dotted curve in Figure 3.2.7 for an equalization ratio of M = 200, corresponding to a load resistance Ri of 8.5 megohms.

Figure 3.2.7 shows the theoretical signal-to-noise ratio dependence upon the photoelectrons incident upon the target, but does not take into account extraneous noise generated outside of the normal gain (or loss) mechanisms in the tube. One such noise is believed to be due to the statistical nature of the target structure itself, resulting in a microscopic variation in gain across the surface of the target, and a fixed-pattern target noise. While merely conjecture at the present state of knowledge of the mechanism of the SEC target operation, it seems to have substantiation, since the noise amplitude increases in proportion to the stored signal. The pattern noise on low level signals is well below the amplifier noise, however.

It should be pointed out that the analysis assumes that an image element is discharged in a single scan. If it is necessary to integrate the

TABLE 3.2.1

SEC VIDICON SIGNAL-TO-NOISE RATIO

	Target Gain = 50	Target Gain = 150
Aperture Response $A_y = 0.5$	$\frac{\bar{\chi}}{(4.1\bar{\chi} + 2\times10^4)^{1/2}}$	$\frac{\bar{\chi}}{(4\bar{\chi} + 2.2\times10^3)^{1/2}}$
Aperture Response $A_y = 0.9$	$\frac{\bar{\chi}}{(1.3\bar{\chi} + 6.1\times10^3)^{1/2}}$	$\frac{\bar{\chi}}{(1.2\bar{\chi} + 680)^{1/2}}$

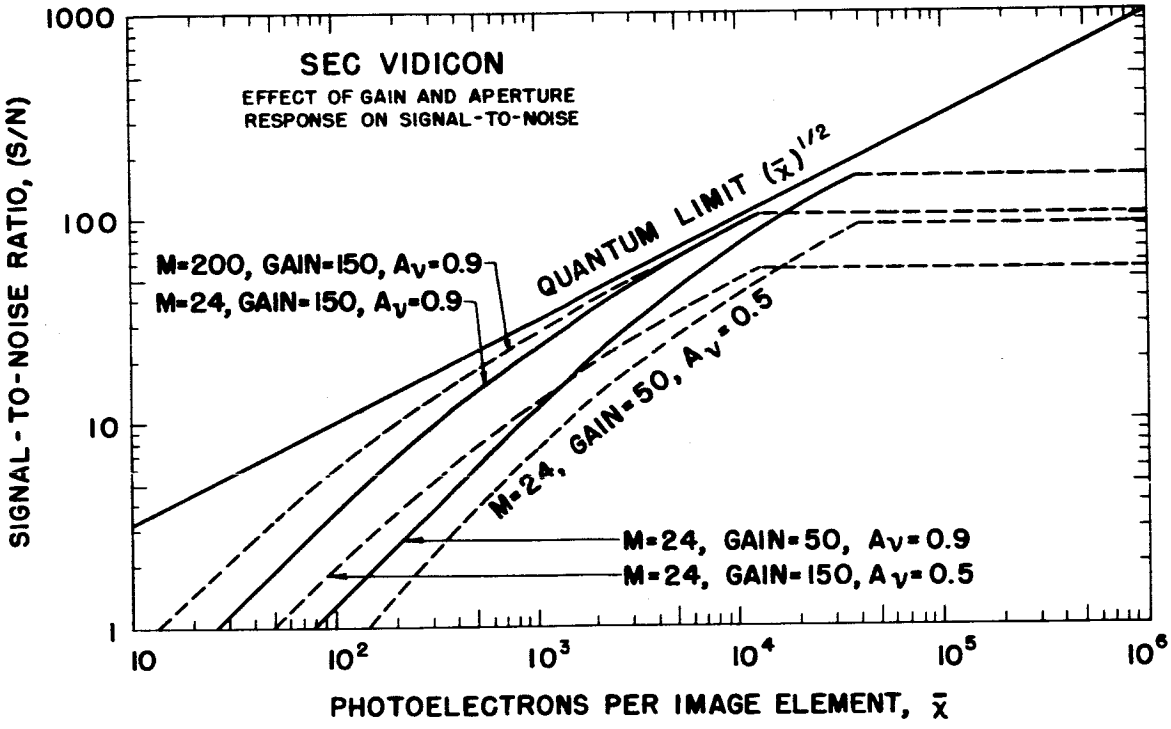

Figure 3.2.7. Effect of Gain and Aperture Response on Signal-to-Noise Ratio

output signal over several scans, it can be expected that the increase in noise contribution will be of the order of the square root of the number of scans.

3.2.4 Applicable Properties and Experimental Results

Summary of Inherent Advantages and Limitations of the SEC Vidicon

Before proceeding with a detailed analysis of the performance characteristics of the SEC Vidicon as they apply particularly to the astronomical application of interest here, it seems desirable to list briefly the main advantages of the SEC principle over presently existing camera tubes.

1. Large storage capacity of dynamic range equal to more than four orders of magnitude for point-sources.
2. High storage surface resistivity of $> 10^{17}$ ohm-cm.
3. Large prestorage gain capability (up to 200).
4. Essentially complete readout in a single scan.
5. Relatively high target uniformity.
6. Absence of halation and redistribution effects.
7. Good recording statistics of each photoelectron due to high target gain.
8. Accurate and reproducible charge readout to within better than 2 percent about 10^4 photoelectrons per point-source.
9. The absence of readout beam and multiplier noise.

The principal limitations of this type of camera tube are believed to be:

1. The presence of some degree of readout beam-bending.
2. Possible resolution limitation resulting from smoke particle size.
3. Point-image spreading at high light intensity.

Operating Characteristics of SEC Vidicon Studied in Detail

In the course of the present study, the following points were investigated experimentally with specific reference to the astronomical integration application of this tube:

1. The degree of reproducibility of the charge read-out for a given light input.
2. The physical process responsible for the growth of a point source image on the monitor with accumulated charge, and its relation to beam-bending.
3. The effective capacity for a point image, and its relation to the charge-distribution in the target layer.
4. The ability to integrate over extended periods of time in the presence of residual gas ionization, thermal emission, field emission, and light emitted by the gun-cathode.
5. The effect of neighboring point images on each other.
6. The performance of the target in distinguishing shades of grey in extended areas.
7. The actual target fixed pattern noise in present tubes under various operating conditions.

The detailed accounts of these studies follow below.

3.2.4.1 Reproducibility of Charge Readout

In order to replace a photomultiplier as a sensing element in photometry or quantitative spectroscopy, it is essential that an integrating camera tube must give a highly reproducible read-out each time a given number of photons are recorded. Ideally, the reproducibility should be limited only by the inherent statistical fluctuations of the photons incident, a situation closely approached by present photon-counting techniques using photomultipliers. This is, in fact, reflected by the specifications for the present study, in which the error in an accumulated 6×10^4 photons is to be at most 5% and preferably less than 2%, compared with the quantum noise limit of 0.4%.

Early data obtained by R. J. Davis of the Smithsonian Observatory using a Uvicon suggested a considerable scatter of the integrated charge amounting to more than 10%.[48] However, these data reflected the early operating difficulties of the digital television system and computing circuits then under development for the Smithsonian experimental package.

In order to provide an independent check of these results, data on the integrated charge for a point-source of known intensity recently obtained on Uvicons at our laboratory by R. R. Beyer, G. W. Goetze and

D. D. Doughty to check the effect of field mesh potential[49] were examined for charge-reproducibility at a fixed point on the target. The technique involved integration of the light from a uv source illuminating a 1 mil diameter aperture for various periods of time from 3 to 100 seconds, and comparison of the areas under the A-scope traces of the single frame readout in successive pictures. Two typical photographs of these traces are shown in Figure 3.2.8. A photograph of cardboard cut-out models of such traces is shown in Figure 3.2.9. The two in the foreground are those for the traces of Figure 3.2.8.

Two different methods for measuring the areas were employed. The first technique involved approximating each pulse by a triangle, and comparing the areas calculated from the height and width of all pulses associated with the point-source. The second technique employed as a check on the first used a planimeter to measure the area under enlarged photographs of the traces. Both these graphical techniques are limited by the amplitude of the amplifier noise, the width of the traces and the errors in area measurement to an estimated 2 - 3 percent, depending upon the total area of the pulses.

The data obtained are summarized in Table 3.2.2 for the eight pictures taken under identical conditions except for variations of light exposure as shown. Inspection shows that the inherent charge reproducibility in separate readouts is about 2 percent and is probably limited mostly by the technique employed. In fact, in some cases, the accuracy comes within a factor of 4 of the theoretical limit set by quantum noise. Thus, it would require a more sophisticated technique of readout than was available here to set smaller limits on the charge reproducibility.

It should be added that recent experience with the Uvicon as reported by R. J. Davis[48] indicates that the integrated charge from a point-source is also substantially independent of a small change in focus when the charge is measured by adding the signal amplitudes of all the elemental areas associated with a given point image. Thus, it appears that the SEC-type of target is particularly well suited for the absolute photometry of individual stars or spectral lines over a large dynamic range, even when the resolution varies across the cathode diameter.

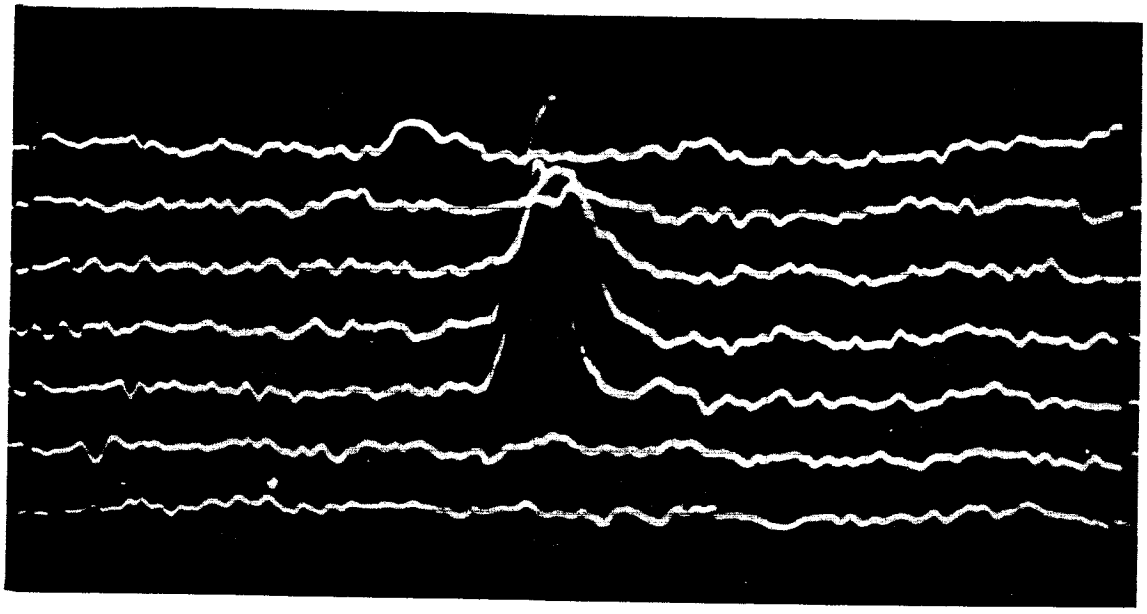

a) 1.5×10^5 Photoelectrons

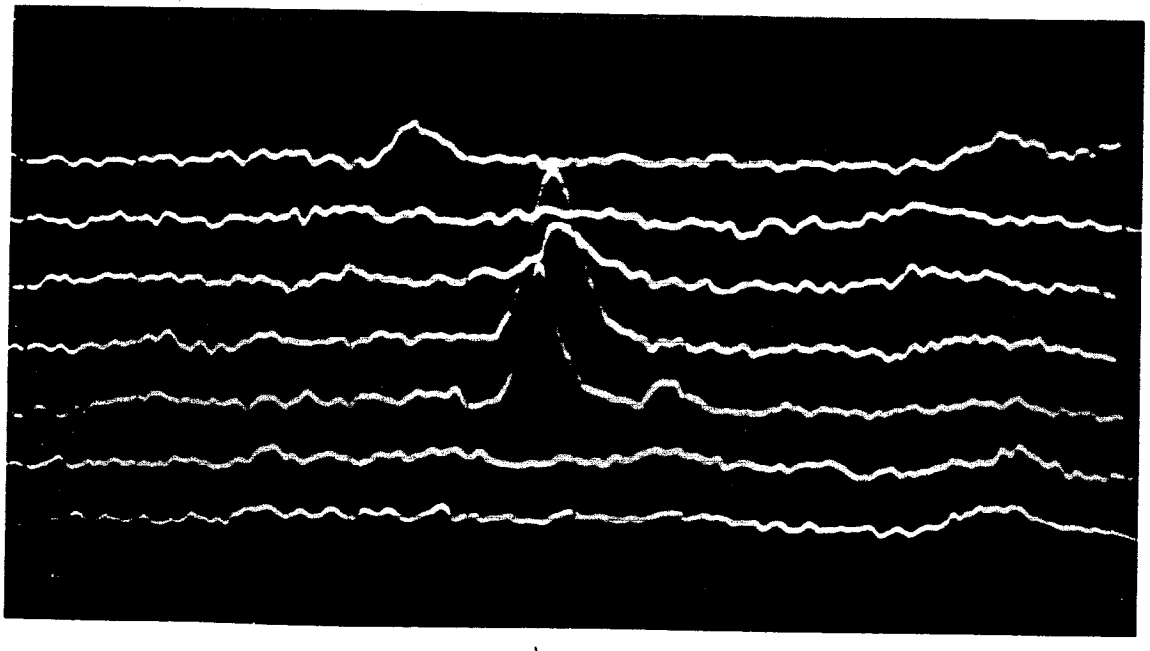

b) 3×10^4 Photoelectrons

Figure 3.2.8. Multiple A-Scope Trace Photographs of a Point Image

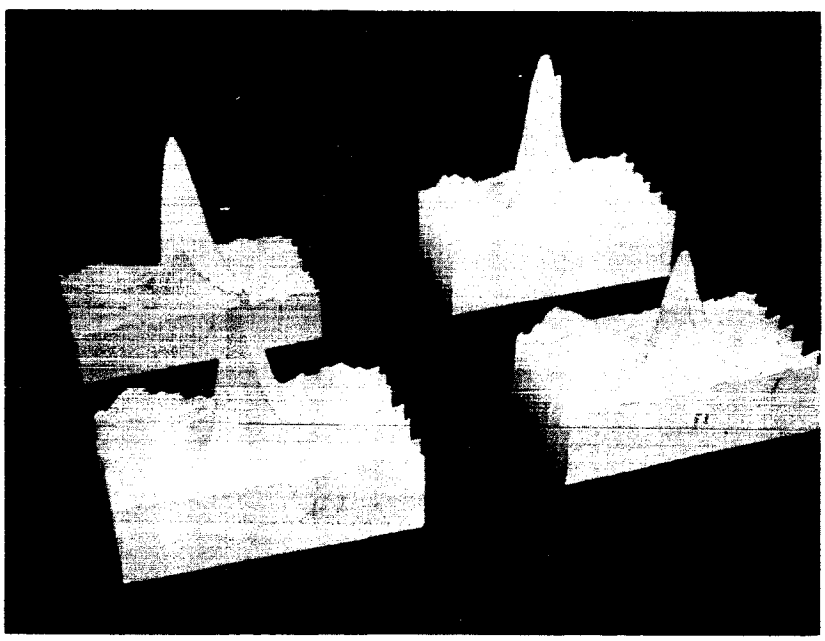

Figure 3.2.9. Cut-Out Model of Point Pulses like Those Shown in 3.2.8

TABLE 3.2.2

REPRODUCIBILITY OF CHARGE READ-OUT IN REPEATED INTEGRATIONS FOR SEC TARGET IN TYPICAL UVICON

(a) By Triangle Approximation

Picture No.	# of Photo-Electrons	Area under Pulses-Orbit Units	% Deviation from Mean	Estim. Error of Method	Estimated True Error	Quantum Noise Limit
1	3×10^4	118	± 3.5%	± 3%	± 1.5%	0.58%
2	3×10^4	110				
3	1.5×10^5	288	± 1.5%	± 2%	< ± 1 %	0.26%
4	1.5×10^5	297				
5	1.5×10^6	941	± 1.0%	± 2%	< ± 1%	0.08%
6	1.5×10^6	961				
7	3.0×10^6	1809	± 2.3%	± 2%	± 1.1%	0.06%
8	3.0×10^6	1731				

(b) By Planimetry

3	1.5×10^5	130	± 3.3%	± 3%	± 1.5%	0.26%
4	1.5×10^5	139				
5	1.5×10^6	420	± 2.3%	± 2%	± 1.2%	0.08%
6	1.5×10^6	440				

The capability of the SEC-Vidicon for storing charge through a large dynamic range is seen to be superior to that of the image orthicon for several reasons. First, the image orthicon target has a considerably smaller electrical capability, ranging from about $1 \mu\mu f/cm^2$ for thin-film orthicons to $40 \mu\mu f/cm^2$ for glass target tubes. Next, the useful voltage excursion of the target surface is about 15 volts, as compared with only 2 volts for orthicon operation. Further, the SEC-vidicon approaches saturation asymptotically, with a transfer curve somewhat resembling that of a standard vidicon. The saturation limit is not reached abruptly with great change of the character of the image (e.g., dark halo effects) as in the orthicon. It is evident that the thin-film orthicons best able to store charge without loss by lateral conduction are inherently unable to integrate as well for attaining the large number of independent events necessary to make quantum noise small compared to all other sources of noise in the system. Another pertinent factor is that it has not been possible to develop orthicon targets that permit nearly complete read-out in a single frame scan, so that further loss of information results.

3.2.4.2 Point-source Image Diameter and Beam-Bending

One of the most serious limitations noted by other investigators for the image orthicon is the rapid growth of a stellar-image with increasing brightness.[1,18,20] This imposes a severe restriction on the ability to resolve faint objects close to bright ones, and applies equally to spectroscopy where faint satellite lines near bright emission lines would be lost.

In the image-orthicon, Livingston found this to be due to at least two factors, electron redistribution in the image section and deflection of the scanning beam during readout, the so-called beam-bending effect.[1,50] To this must be added the possibility of actual spreading of the stored image on the target due to the scattering of the incident primary electrons, the finite electrical resistivity, and light-scattering due to optical imperfections.

In the SEC-Vidicon, the redistribution effect is absent since the photoelectrons penetrate to the scanning side of the target, and the dominant number of secondary electrons formed are not emitted but instead

collected by the conductive backing. Only when the target elements have charged close to the field-mesh potential and therefore also close to the target back-plate in potential an appreciable fraction of the secondaries emitted from the surface. Thus, as long as the target remains well below full saturation, corresponding to 10^{11} electrons/cm^2, ordinary redistribution remains a small effect.

Some possibility of sideways spreading of the charge within the layer thickness of 25μ does exist. If the diffusion were Lambertian at the entrance side of a 25μ layer, the resolution limit would be about 1 lp/25μ , equivalent to 40 lp/mm. However, the effective thickness is less, and resolutions twice this have been observed, with a possibility of still higher resolution to come. Nevertheless, one expects to find an increase of the image diameter relating to the layer thickness due to scattering of the incident photoelectrons by the accumulated positive charge, as well as a certain amount of broadening associated with the scattering and diffusion of the slow scanning beam electrons within the smoke-layer. This sideways diffusion of electrons in the target should be a function of the internal field created by the charge already present, so that an increase of apparent diameter to a few times the target thickness of 25μ might be expected at high point intensity as a result of this cause alone, as indicated schematically in Figure 3.2.10.

As to the effect of beam-bending produced by the charge on the target, this should be present to the extent expected from the known field-mesh spacing and the velocity of the scanning beam electrons at the field-mesh before they are slowed down. It was therefore of interest to determine how large a beam-bending effect was to be expected theoretically, and to compare it with the observed growth of point-source diameter as determined on the monitor in the experiments carried out by Beyer.[49]

The observed dependence of apparent point-source diameter on the total number of photoelectrons producing the image is plotted in Figure 3.2.11. It is seen that when plotted on semi-log paper, this apparent diameter grows approximately in proportion to the logarithm of the integrated photon flux or charge over the range from 10^3 to 10^6 photo-electrons per image. Since the gain of this particular tube was set at approximately 20, this corresponds to a range of 2 x 10^4 to 2 x 10^7

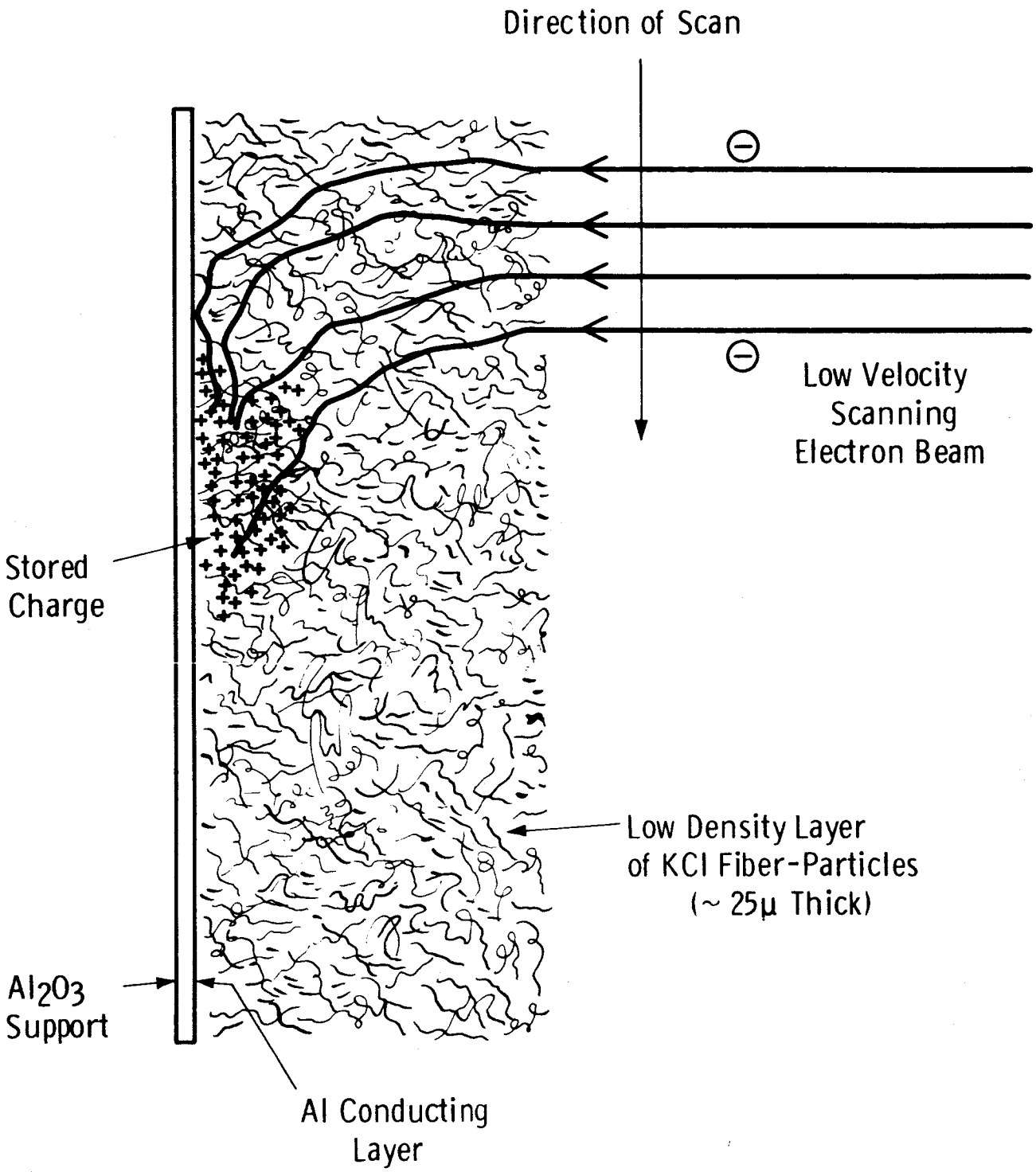

Figure 3.2.10. Schematic diagram illustrating the side-ways diffusion of the scanning-beam electrons believed to take place in the porous layers of an SEC target.

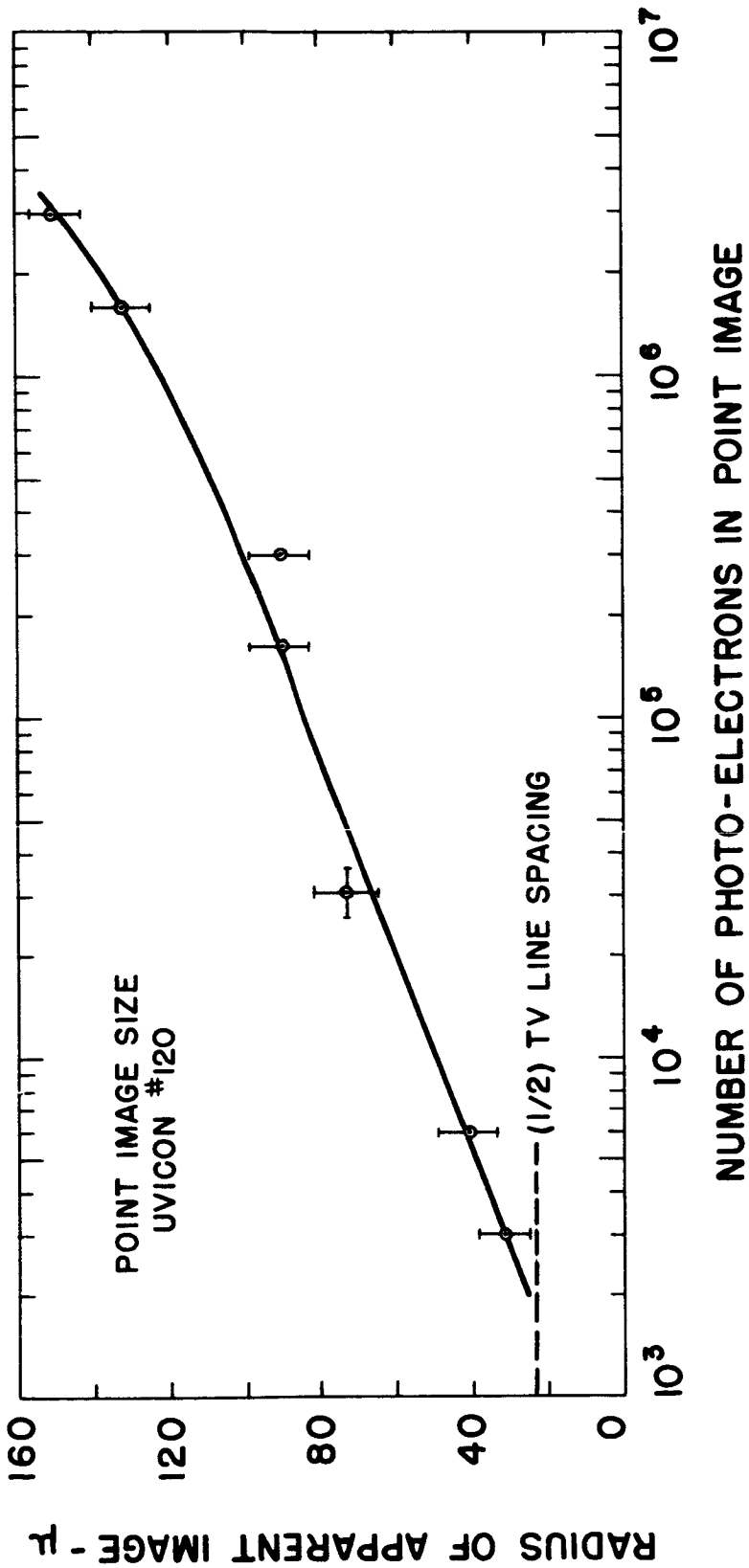

3.2.11. Plot of Radius of Image Vs. Photoelectron Number

electrons per point source. Beyond 10^6 photo-electrons, the image size is seen to grow more rapidly, corresponding to the fact that the surface potential reaches and even exceeds that of the field-mesh and redistribution becomes important. A similar logarithmic dependence of image size on brightness exists in the photographic plate, where it is in fact used to measure stellar magnitudes. Likewise, Livingston has shown a similar dependence of image-size on magnitude in the image-orthicon.[1] However, under the conditions used, the absolute sizes were much larger and the dynamic range available was only a factor of 40 to 4 stellar magnitudes as shown in Figure 3.2.12 for tubes of different field-mesh spacing.

From the dependence on field-mesh spacing on the scanning beam size, Livingston concluded that beam-bending is the dominant effect in the image-orthicon. To see whether this is the case in the SEC-Vidicon, it was decided to calculate the expected beam-bending by means of a computer ray-tracing program recently developed at our laboratories by A. K. Rigler. In order to obtain a potential for which a simple analytical solution could be found, it was decided to examine the more severe case of a single linear charge distribution on an infinite target plane, with dimensions to fit the Uvicon grid spacing and operating potentials. This situation would be encountered for a bright spectral line on a uniform background, and by using the potential to which the strip is charged relative to the target-field mesh potential difference, a series of conditions as might be encountered in spectroscopy could be simulated.

The actual spacings and potentials are shown in Figure 3.2.13 together with the notation used. Electron-beam trajectories were traced for a series of starting positions a distance R_o from the position of the charge-strip, and the deflection ΔR calculated at the target plane, which was assumed to have a small potential approximately twice that of the thermal velocity of the scanning beam. The resulting ΔR for a series of assumed strip potentials and scanning beam energies of field-mesh potentials are tabulated in Table 3.2.3, with distances given in microns.

A plot of the deviation ΔR against the log of the target strip potential is shown in Figure 3.2.14. The curves are seen to have the same general character as the plot of image diameter versus the log of the number of photo-electrons stored. However, the absolute magnitude of the

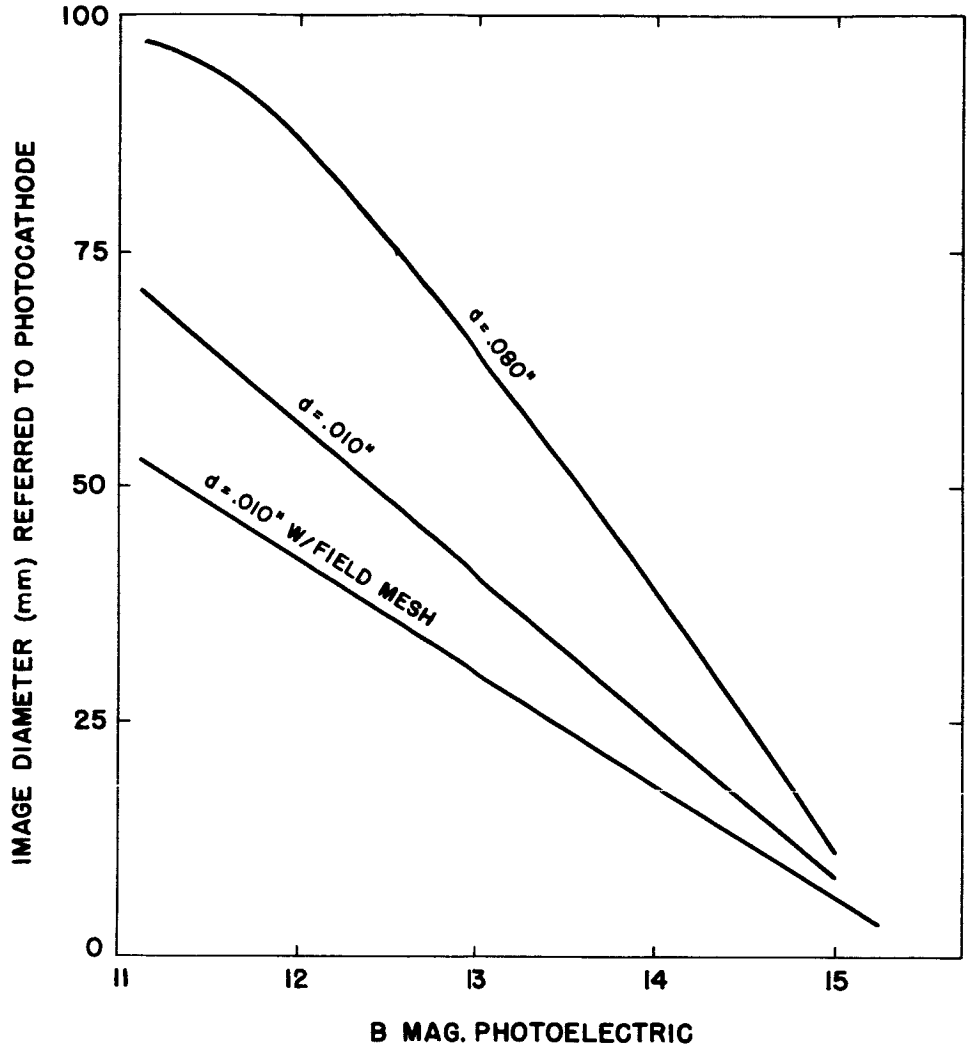

Figure 3.2.12. Diameter of a Televised Star Image as a Function of Star Magnitude (Reference 1, Livingston)

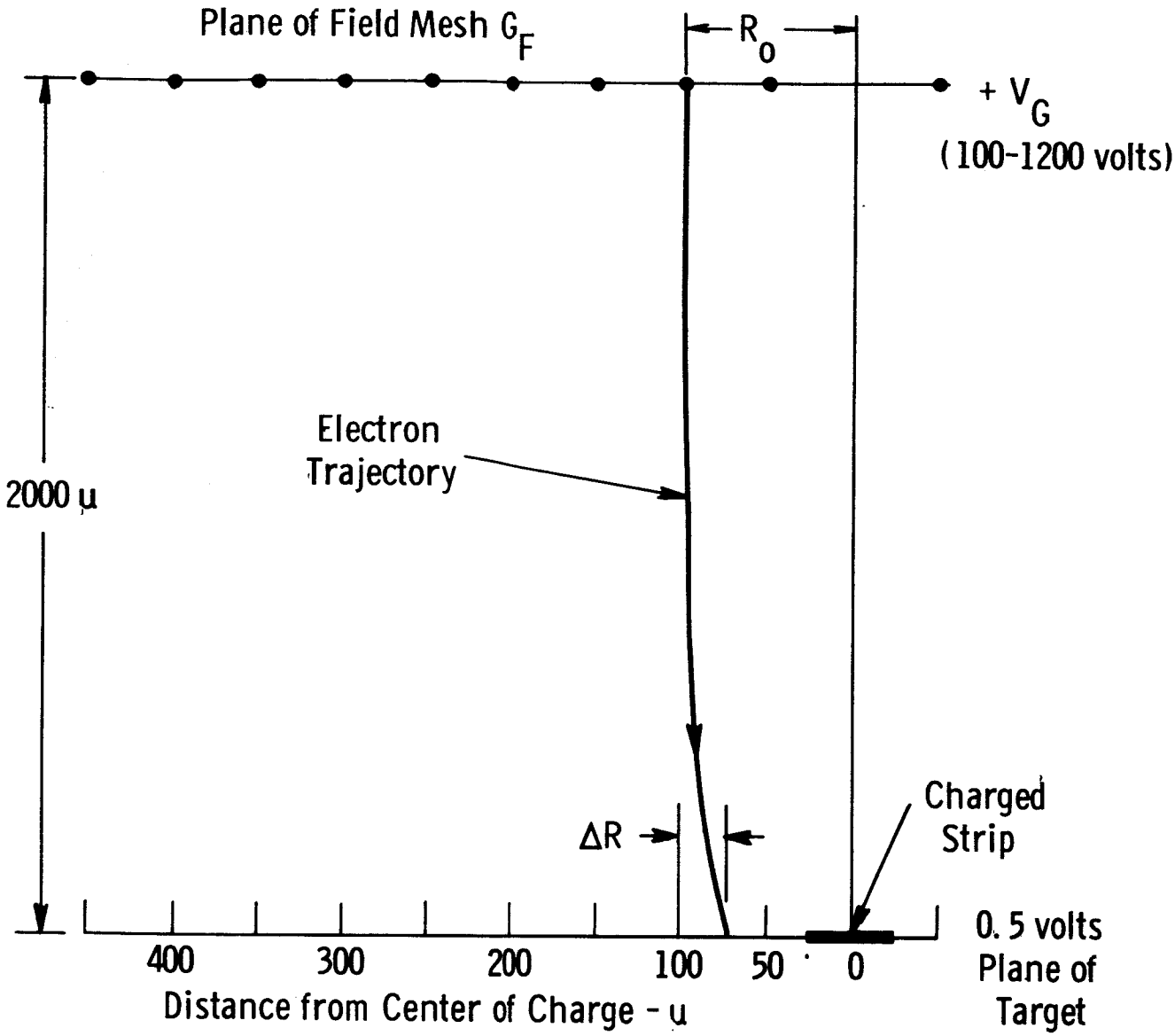

Figure 3.2.13. Diagram illustrating the electrode spacing and applied potentials used for the computer calculation of scanning-beam deflection ΔR due to a target strip charged to a positive potential relative to the remaining target. R_o represents the distance from the center of the strip to the point of entrance of the beam.

TABLE 3.2.3

Strip Potential	Dist. from Center R_o	DECELERATING POTENTIAL 100 ΔR	200 ΔR	400 ΔR	800 ΔR	1200 ΔR
1.88	50 μ	11.50	6.20	3.35	1.81	1.27
	75	6.24	3.48	1.90	1.02	0.72
	100	4.56	2.53	1.37	0.73	0.51
	150	3.07	1.68	0.90	0.48	0.33
	200	2.34	1.27	0.67	0.35	0.24
	250	1.90	1.02	0.54	0.28	0.19
3.75	50 μ		14.38	7.17	3.74	2.60
	75	13.53	7.25	3.87	2.06	1.43
	100	9.47	5.16	2.76	1.47	1.02
	150	6.22	3.38	1.80	0.95	0.65
	200	4.71	2.54	1.34	0.71	0.48
	250	3.80	2.04	1.08	0.56	0.38
7.50	50 μ			16.77	7.97	5.38
	75	33.09	15.85	8.09	4.20	2.90
	100	20.64	10.76	5.64	2.96	2.04
	150	12.84	6.86	3.63	1.90	1.31
	200	9.57	5.12	2.70	1.41	0.97
	250	7.67	4.09	2.15	1.12	0.77
15.0	50 μ				18.39	11.54
	75		39.49	17.62	8.73	5.90
	100	50.78	23.46	11.75	6.03	4.11
	150	27.41	14.15	7.35	3.82	2.61
	200	19.72	10.38	5.42	2.82	1.93
	250	15.59	8.24	4.31	2.24	1.53
30.0	50 μ					
	75			43.98		
	100	75.14	58.21	25.43	12.40	8.34
	150	63.36	30.08	15.11	7.71	5.23
	200	42.00	21.31	10.96	5.65	3.84
	250	32.20	16.68	8.64	4.47	3.04

Potential in Volts
Distance in Microns

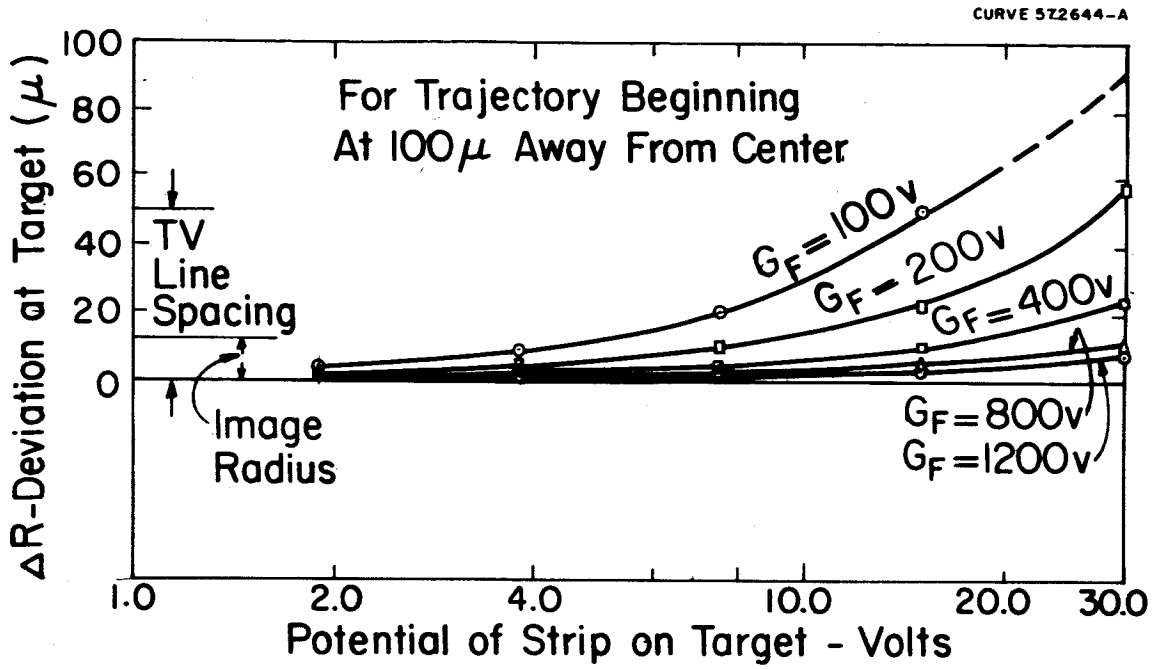

Figure 3.2.14. Result of beam-bending calculation for the deflection at the target ΔR as a function of the potential of the charged strip on the target of a UVicon. Curves are shown for a series of field-mesh potentials. The curve for a mesh-potential of 400 volts represents the calculation for the actual experimental conditions used in present tubes.

deflection at a target potential of 15 volts and a field-mesh potential of 400 volts corresponding to operating conditions in the Uvicon is considerably less than the observed value for target saturation between 10^6 and 10^7 photoelectrons. For a ray starting 100 μ away, the calculated deflection is only 11.8 μ, compared with the point-source half-width of 12.5 μ and an observed broadening to a half-width of some 150 μ. With a TV line spacing estimated to be approximately 50 μ, the beam would have had to be deflected by about three TV scan lines to account for the observed broadening in terms of beam-bending alone.

Since the calculated case would lead to stronger beam-bending than the actual case of a circular source, it would seem that in the range of operation below saturation at least, beam-bending is not the limiting factor on image size. Instead, it would appear that diffusion and scattering of the scanning beam electrons within the porous target layer under the influence of the field of the charge stored accounts for most of the image widening. In a sense, this is another form of beam-bending, but the mechanism is different from the straightforward beam-bending calculated. The difference of the further diffusion mechanism is that beam electrons that penetrate into the interspaces of the target layer may find themselves at near-zero velocity and within the field inside the layer from whence diffusion wandering inside the layer can occur.

If this is right, it follows that only marginal improvement could be expected from efforts to reduce point-image width by using higher beam voltages and closer field-mesh spacing. However, it might be possible to achieve somewhat smaller images by reducing the target thickness.

3.2.4.3 The Effective Capacity for a Point Image

Data concerning the capacity of the target layer for extended-area images will be discussed later. The subject here will be the effective capacity for a point image. During the course of the present study, evidence accumulated to indicate that the point-image capacity may effectively be higher by powers of ten than might be expected from the area associated with the resolution element area and the capacitance of the order of 25 to 40 $\mu\mu f/cm^2$ computable from the typical layer thickness. A final answer is not yet known with confidence, but some of the points

considered are of interest. It now seems likely that the point-image capacity is high, though perhaps not by the very large factors originally considered.

As Figure 3.2.11 shows, the number of photoelectrons to a point image may be as high as 3×10^6. The number of stored electrons is still larger, increased as it is by the gain of the target layer. If all of this charge, as actually measured, were contained within the diameter of a spot resolvable at low intensity, and if the capacity per area is that computable as above, then the potential of the target surface at the point-image peak would be many hundreds of volts, or even thousands. Now the obvious explanation is that the charge spreads. However, the resistivity of the material is so high that images may be stored for days. This leads to the thought that the charge may not spread sidewise. Since it seems impossible for the point image or any part of the surface to rise significantly above the nominal +15 volts at which the suppressor grid is operated, one is led to the thought that the capacity of the point may rise in some way to meet the occasion of the large electrical charge, without large positive potential excursion.

The theory of the mechanism of charging of the layer by secondary electron emission does actually suggest that an action of this sort may occur. Briefly, the target material is highly porous, and the charge would be expected to reside at some significant depth below the surface. Further, as a result of the field distribution within the layer, later portions of the charge contributed during the exposure would be expected to reside at increasing depths from the surface, or closer to the target backplate. The condenser thus formed is, so to speak, increasingly thinner as the exposure progresses, and thus the capacity is increasingly large.

As a further separate likely effect, Livingston has pointed out[1] that even for a regularly behaving dielectric layer, an isolated picture element has approximately four times the capacity calculated from the parallel-plate formula, which may be further increased by the presence of excess negative charge in the surrounding area.

It is therefore likely, due to either or both of these effects, that the point-image capacity is quite large, probably at least ten times the plane-parallel value. Attempts to measure this effect directly have, however, proved inconclusive to the present time, although the results

suggest high point-image capacity. The visualization is that the actual electrical point image is significantly smaller than that apparent on the monitor and that the excess apparent dimension is due to beam bending and sidewise diffusion of scanning electrons as previously discussed.

3.2.4.4 Long Term Integration

Although integration with full voltage on the tube have been demonstrated in the Uvicon over periods of many hours, no such data was available on the SEC-vidicon with a photocathode sensitive to visible light. Accordingly, two different tubes of the type presently available (WX-5419) were studied in this respect.

A demonstration model used over a period of a year and a half (Tube #6) was operated with all normal potentials on (except for the beam, which was cut off by a negative control grid potential). It was operated for three minutes before a visible ion-spot became noticeable during integration. This tube was found to be relatively gassy, and could not be pumped down further by the attached ion gage. It was also found that the filament in the thermionic cathode contributed to the background when it was left on at its full voltage during integration. No evidence of background due to the thermal or field emission was found.

A second tube of this type also showed no effect of any thermal or field emission during 10 minutes of integration, which was again limited by an ion spot developing, which became a limiting factor after 15 minutes.

Since there was no requirement to build tubes capable of such long integration under the Air Force contract for which these tubes were originally designed, the actual performance in this respect was better than expected. There appears to be no reason why SEC-vidicons cannot be built that will be as free from gas as Uvicons, once sufficient care in bakeout and tube processing is used.

3.2.4.5 The Effect of Neighboring Point Images

A series of A-scope studies and photographs were made in order to determine the effect of image broadening and beam-bending on the shape of point images and the mean position of neighboring point images. In particular, efforts were made to observe any charge-dependent image asymmetry or displacement of the type noted by Livingston for the image orthicon.

Early A-scope photographs like those in Figure 3.2.8 seemed to show an asymmetry or tilt of the pulse into the monitor quadrant from which the beam approaches in its scan pattern. This proved to be incorrect, with the tilt originally observed dependent upon the detailed beam focus adjustment. The three photographs shown in Figure 3.2.15 were made under improved instrumentation and widely different adjustments of the A-scope and of the vertical interval between scan lines. All are output images of sub-aperture input point images. They show no tilt of the output pulse at an angle into the direction of the upper left corner, as suggested by the earlier photographs. It is now established that no asymmetry develops in the direction of the scan lines. However, as the point intensity increases, the output image does tilt vertically into the direction from which the scan lines approach, and the centroid of the output image shifts into this direction. This is shown best by observing the comparative positions of neighboring points.

The effect is shown in Figure 3.2.16 (a) and (b). In the first photograph, three nearby point images are seen at low intensity. It was found that the relative positions of these images remained unchanged as long as the intensities remained small, even for intensities differing by a factor of 2 or 3. However, when the intensity of the central image was increased to a high level, as shown in the second photograph, its mean position shifted upward perpendicular to the scan direction, or toward the direction from which the successive scanning lines advanced during the field scan.

The effect is a type of "beam bending". Since a number of scans are required to read off the full image, the amount of discharge during a single scan is not a large fraction of the total charge present. During the course of a single line scan, the beam is pulled about as much

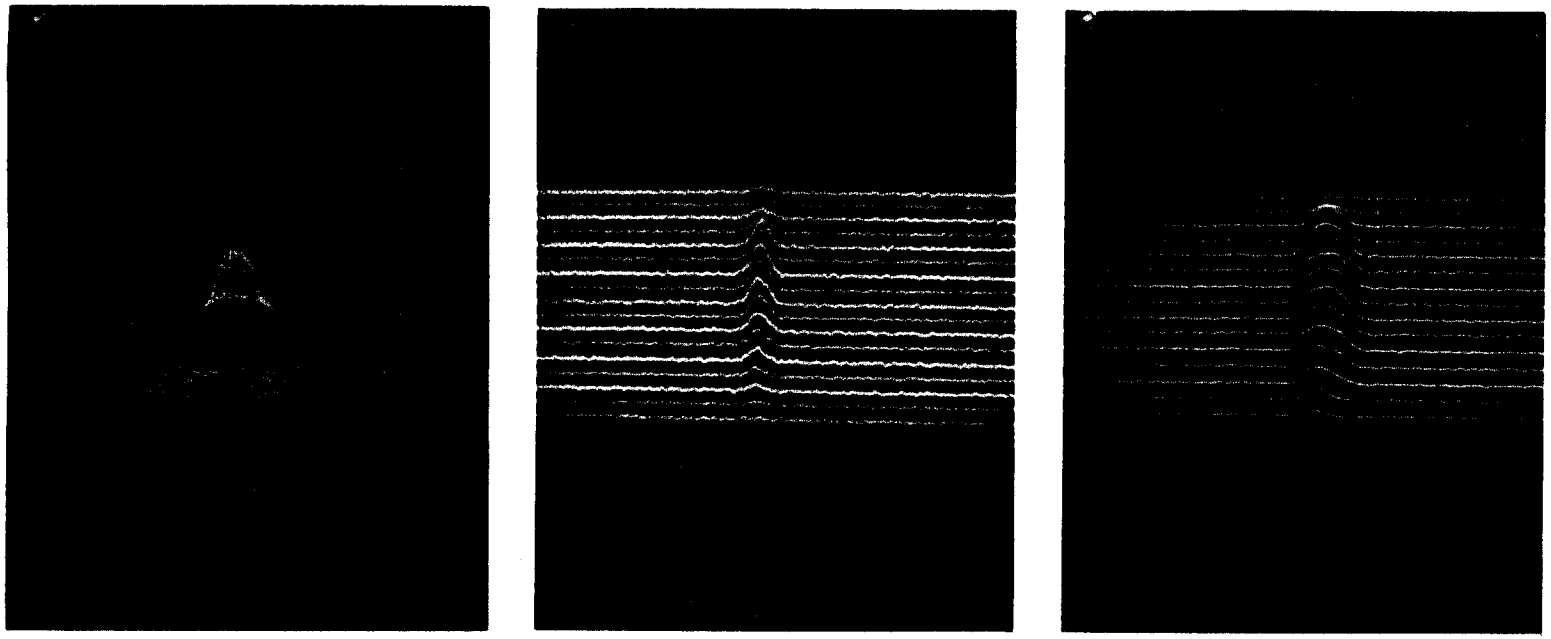

(a)

9/11, T15 VIII. Source: 19.5fc, , f/1.9, .45mm.
SEC: I_b .5, V_t 15v, G_4 20, G_3 145, G_2 280, 2:1.
PHOTO: f/1.9, 1/100, .5v/cm, 1mcs/cm.

(b)

#T5VIA, 9/11. SOURCE: 19.5fc, f/.87, .45mm.
SEC: I_b .5, V_t 5v, G_4 20, G_3 150, G_2 280, 2:1.
PHOTO: f/1.9, 1/100, .5v/cm, 2mcs/cm.

(c)

9/11, T15 V. SOURCE: 19.5fc, f/1.4, .45mm.
SEC: I_b .5, V_t 15v, G_4 20, G_3 145, G_2 280, 2:1.
PHOTO: f/1.9, 1/100, 1v/cm, 1mcs/cm.

Figure 3.2.15. Maintenance of Left-Right Symmetry of Point Images.

(b)

(a)

Figure 3.2.16. Position Shift of Point Image Position with Intensity Increase

on approach and recession from the point, and no right-left asymmetry develops. However, in the vertical direction the approaching beam is pulled by the full point charge, whereas the receding beam is not pulled upwards since the point has by that time been discharged. It should be noted, however, that for wider spacing between the scan lines, as in the earlier photographs of Figure 3.2.8, some displacement to the left might be detectable.

The effect is similar to the "beam bending" observed by Theile[50] and by Livingston[1] in the image orthicon, although none of the rather complicated secondary oddities of shape observed by Livingston appear to be present. The upward shift of the point image position at high intensity seems to be a bit larger than expected from the computer program calculations. Therefore, it is believed to involve diffusion of the scanning electrons in the smoke layer as well as regular beam bending. Further studies would have to be carried out to see whether this explanation is correct and, if so, whether the effect can be reduced by the use of thinner target deposits. Although the shape of the circular image is distorted, Beyer's measurements show that the total amount of light or charge associated with the bright central source can be determined accurately independent of this distortion.

The absence of any unusual influence or distortion of two neighboring point sources as they approach each other is illustrated by the pictures of two crossed filaments in Figure 3.2.17.

These pictures were obtained with a special light source constructed in the course of the present study, designed to provide a convenient means of simulating two point sources of arbitrary brightness and continuously-varying separation.[51] Figure 3.2.17 shows the two filaments, equivalent effectively to a series of point sources of equal intensity, approaching each other. A detailed examination shows that neither the width nor the positions are distorted as the two sources merge and their amplitudes add. Since the input images of the filaments are much smaller than the resolution elements, the brightness adds at the point where they cross. It is hoped that this type of test-device can be used in future measurements of the performance of electronic image tubes for astronomy.

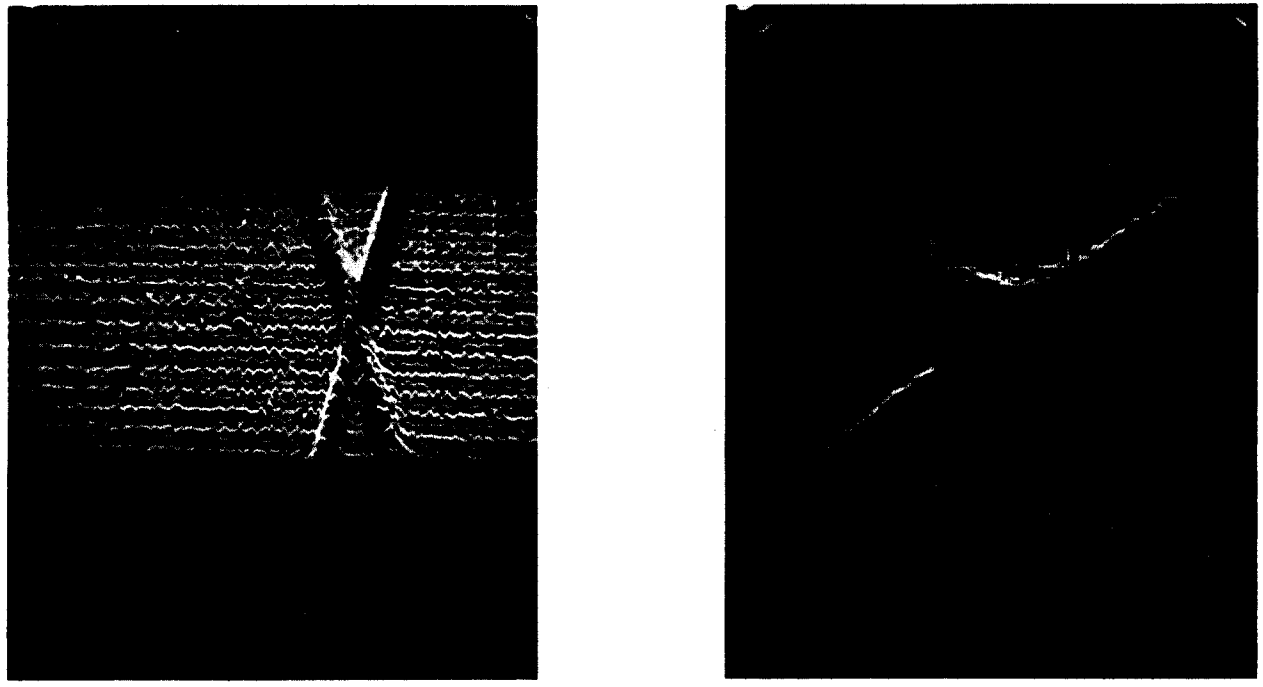

(a) (b)

Figure 3.2.17. Multiple A-Scope Trace Presentation of Crossed Filaments

3.2.4.6 Target Performance in the Photometry of Extended Areas

A series of measurements were carried out at the Aerospace Division laboratories to determine the performance of the SEC-Vidicon in the accurate measurement of the brightness for extended area sources, and to check for a possible variation of effective target capacity with charge density stored. These tests involved a measurement of the integrated charge on a limited central area of the target, with a sumultaneous measurement of the voltage to which the surface of the target had risen.

The charge was measured by photographing the video signal for successive scanning fields scanned in interlaced lines every 1/60th of a second, and adding the charge determined from the current amplitudes in the successive fields. A complete frame is scanned in two successive fields, so that two fields are required to reach every part of the target. As shown from a typical photograph of the video signal in Figure 3.2.18 and the plot of Figure 3.2.19, more than 92% of the total charge stored is read out in a complete frame consisting of two interlaced fields, even when the target surface is charged close to voltage saturation.

The target surface potential after the exposure to light, was measured by "feeling" with the reading beam, until the potential difference between cathode and target was increased (from a negative value) to the point at which a threshold image flash on the monitor was just perceivable. The accuracy of this method seemed to be about 0.2 volt at the higher target surface potentials in the region of +15 volts, but the uncertainty became a volt or two at low surface potentials in the region of 2 to 3 volts. The reason is attributable to the effective reduction of contrast in the monitor display: at +15 volts, the edge of the illuminated image area was a high-contrast, sheer drop-off of 15 volts potential difference, whereas at +2 volts, the edge was less contrasty.

This method of measurement involved integrating the image of a small area 0.2 inch by 0.15 inch on the photocathode with a known scene brightness of 0.88 ft-candles for an exposure of 0.5 second, followed by triggering the succession of fields for recording on the A-scope. The broad horizontal line in each of the photographs of Figure 3.2.18 is a

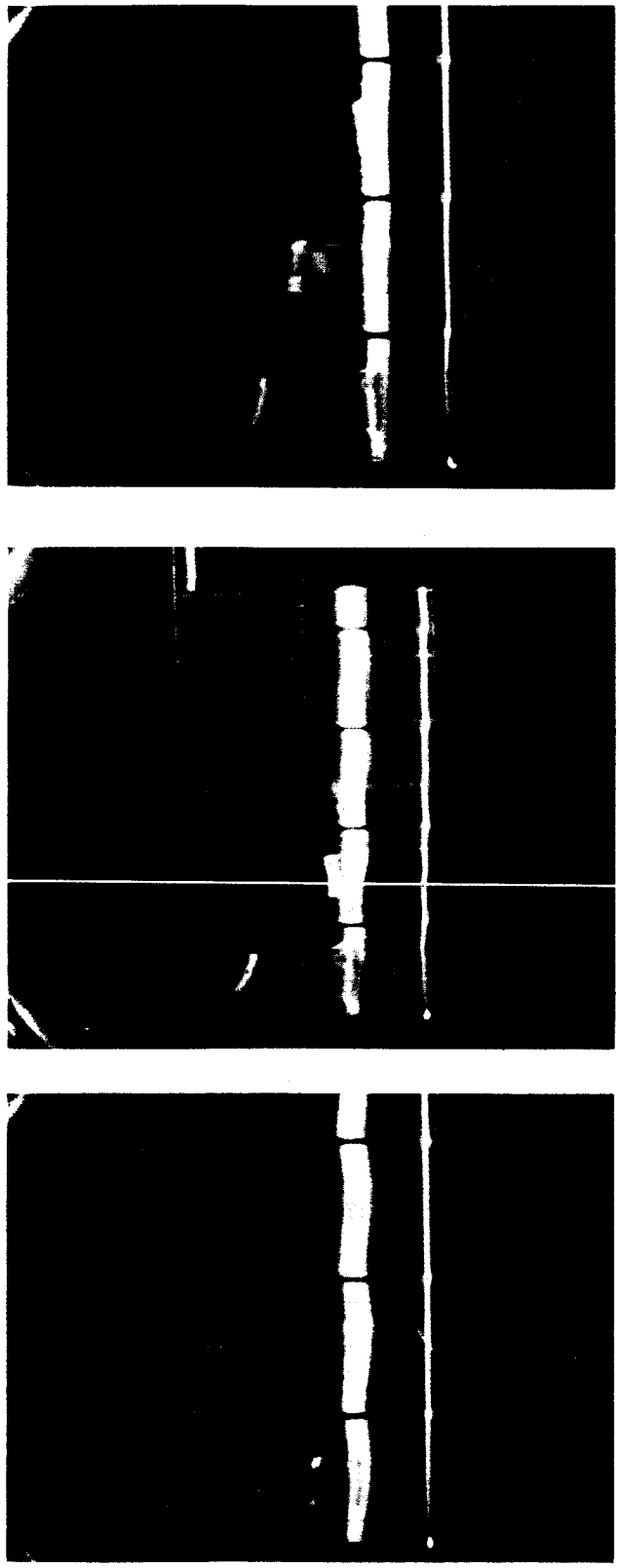

Figure 3.2.18. Charge Readout by TV Fields

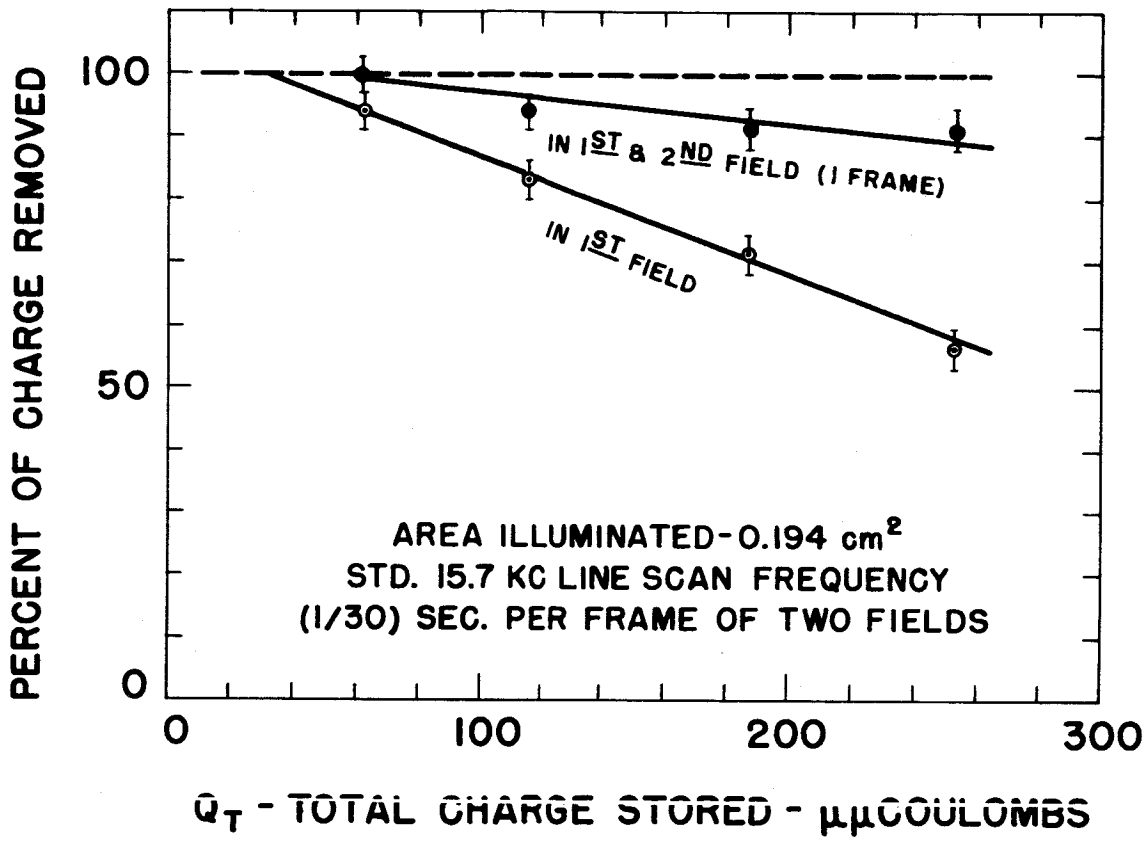

Figure 3.2.19. Completeness of Readout

base line, interrupted by short dark intervals corresponding to the blank between fields. The fainter lifted portions correspond to the readout trace for the electric image of the pattern.

The photocathode illumination was varied by changing the lens opening, keeping the exposure time constant. The three photographs of Figure 3.2.18 are the field readout records respectively for the target surface charged to 4.6, 10.0, and 14.3 volts, always with the suppressor grid at 25 volts. Readout is very complete in one field at 4.6 volts, but three fields are required for completion at 14.3 volts, since this potential approaches the first-crossover potential closely. A plot of target surface potential V_s and total charge stored, as a function of light exposure is shown in Figure 3.2.20. The target back-plate potential V_t was at 10 volts, and the suppressor mesh was at 25 volts, as noted above.

It is seen that the surface potential V_s increases from the low-exposure value at the left somewhat less rapidly with exposure than the charge Q_t stored on the target. This suggests that the effective target capacity, proportional to the ratio of Q_t/V_s increases with increasing total charge. The same indication is obtained from a plot of V_s vs. Q_t in Figure 3.2.21 where the points would fall on a straight line for increasing Q_s, if the capacity were constant. The effective large-area capacity is plotted against Q_t in Figure 3.2.22, and it shows a consistent gradual increase with Q_t from a minimum of $22 \pm 10 \mu\mu f/cm^2$, expected if the charge is near the top surface of the layer, to $94 \mu\mu f/cm^2$ corresponding to a reduced mean distance from the back-plate. The probable error of the measurements is indicated on the plot, and is distinctly poorer for the two lower points. It is felt, however, that the accuracy is sufficient to establish the non-constancy of the capacity.

It should be noted that even the maximum value of $94 \mu\mu f/cm^2$ for a large area is considerably smaller than the capacity estimated from other measurements for a point source. The point image value may well be 10 times as great.

From the measured charge density of 1.6×10^{-9} coul/cm^2 at a surface potential of 17.5 volts, one finds that 10^{10} electrons/cm^2 can be stored on this particular target before saturation is reached, and that, as judged from Figure 3.2.20, probably 10 times this charge

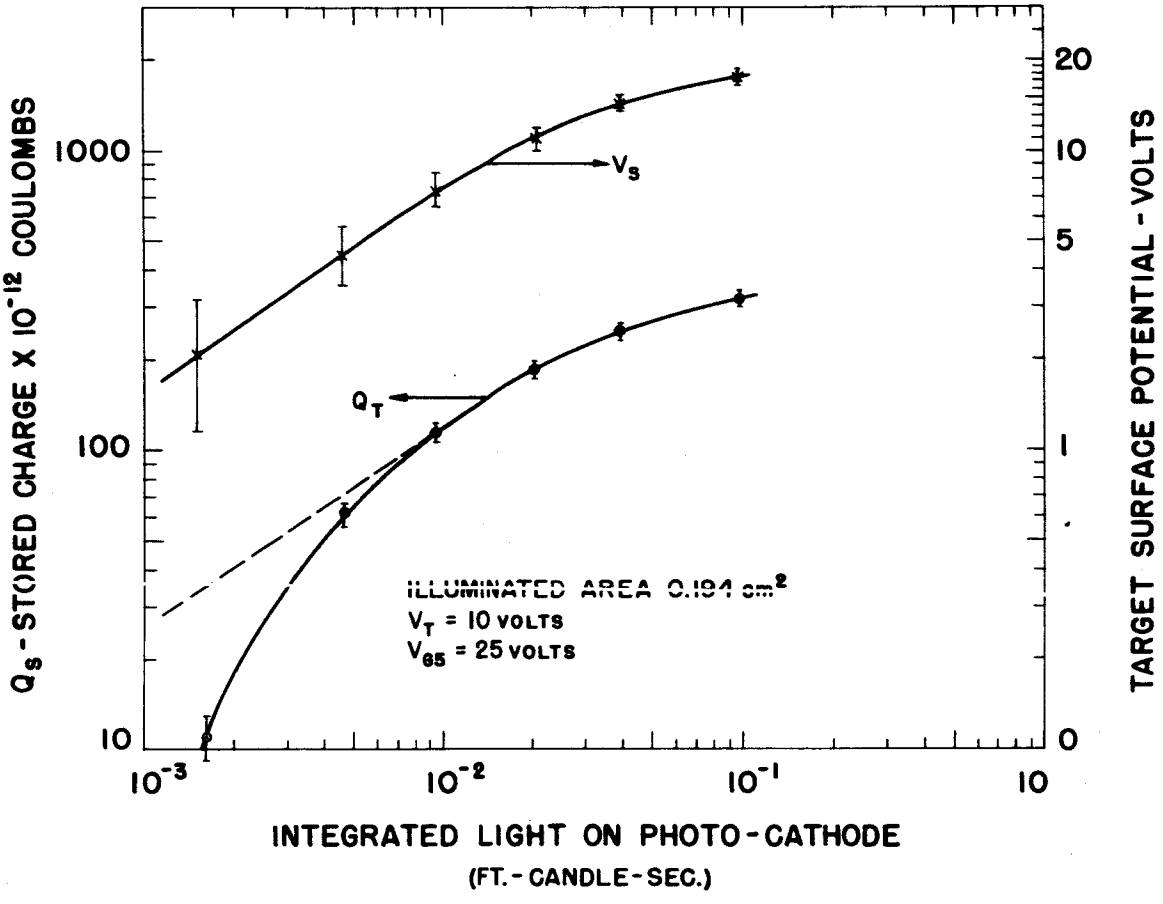

Figure 3.2.20. Surface Potential V_s and Stored Charge Q_t as a Function of Exposure

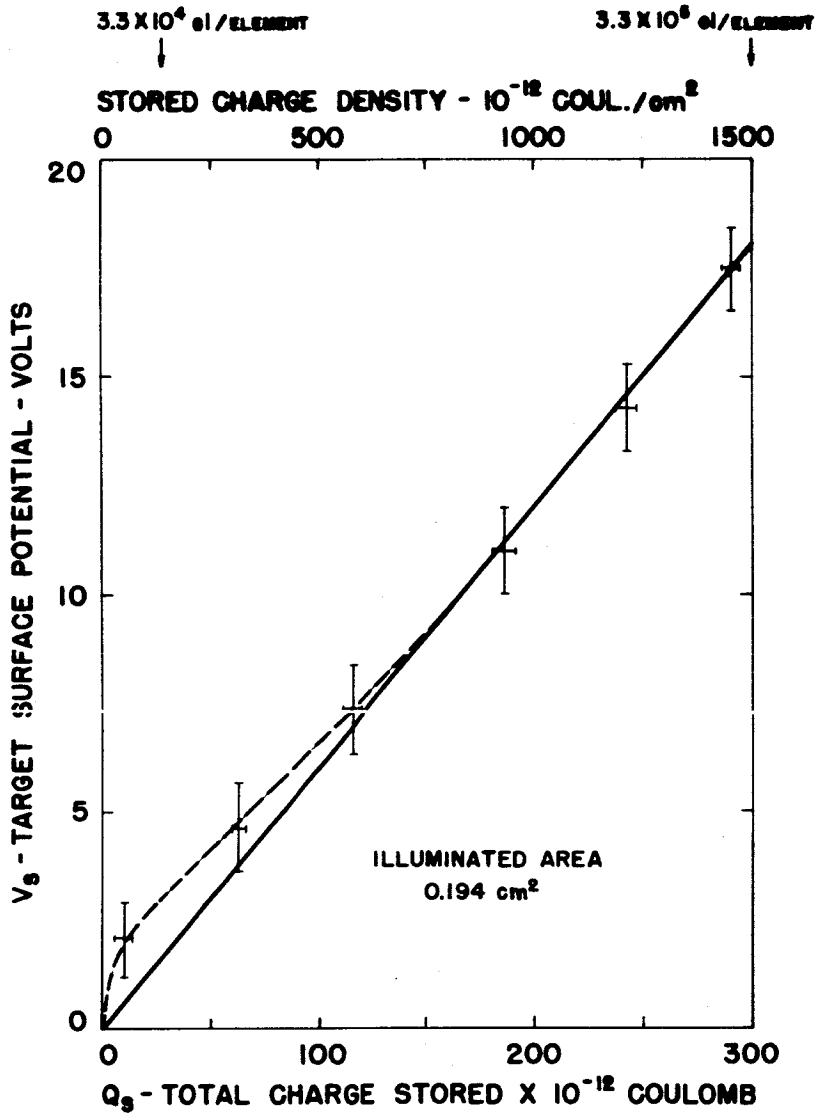

Figure 3.2.21. Surface Potential and Charge

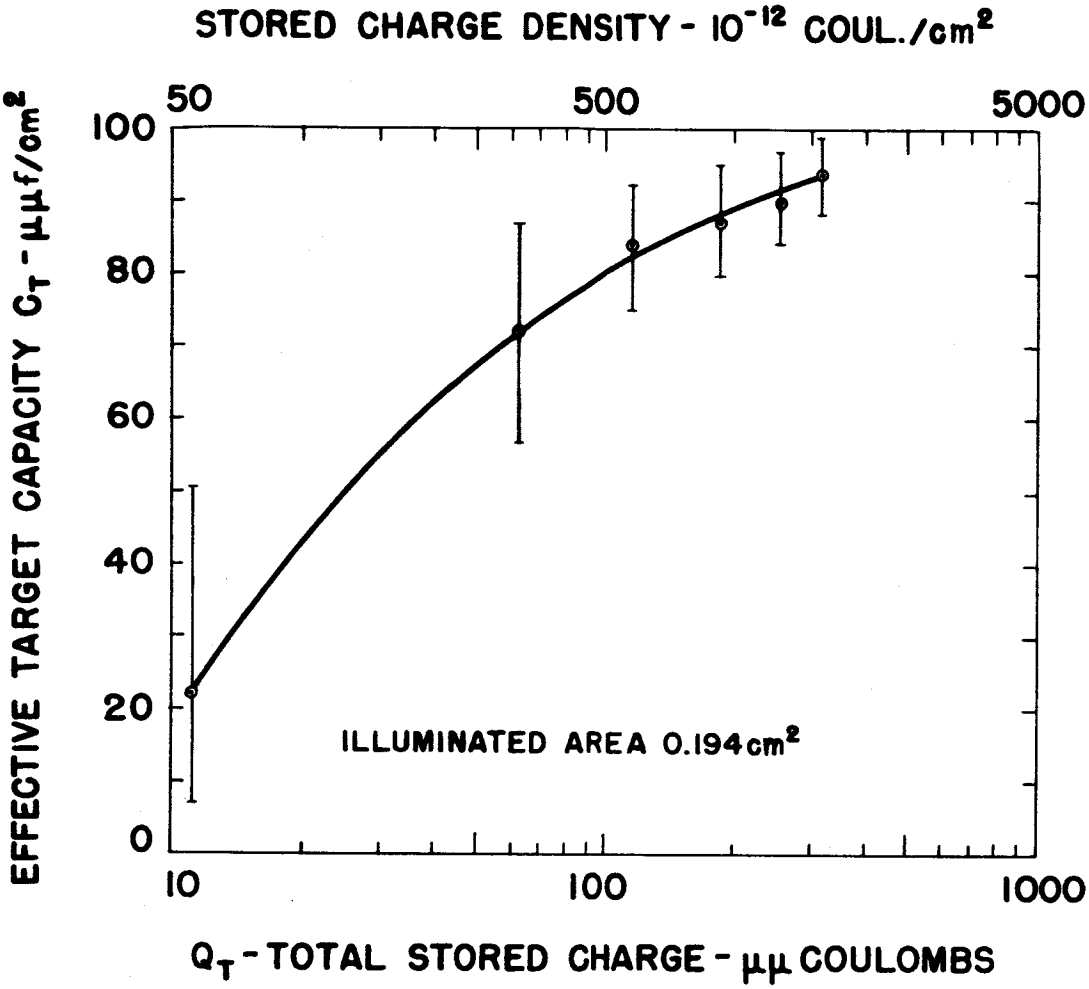

Figure 3.2.22. Variation of Extended Area Capacity with Stored Charge

could have been stored before V_t attains the limit set by V_{G5} at 25 volts. The area of the resolution element corresponding to a pair of TV lines is 33.5×10^{-6} cm^2, leading to a stored charge of 3.35×10^5 electrons per element at 17.5 volts for V_s. It follows that the inherent quantum noise limited accuracy of determining the charge, is 0.17% at this total charge, or 0.54% at 3.35×10^4 electrons per element. This is well-within the desired accuracy of two percent.

For the wideband amplifier used and the high scan rate of standard TV, the target used for most of these studies gives a measured dynamic range (maximum signal divided by noise) for area sources, of about 66, or 1.5% accuracy, using the noise amplitude as 1/6 of the peak-to-peak noise signal. This is illustrated by the photograph of a step grey scale reproduced in Figure 3.2.23, where the difference between the two areas of lowest transmission represents 2.5% of full transmission. The filter transmission steps are listed in Table 3.2.4. A plot of signal amplitude vs. light transmitted is shown in Figure 3.2.24.

TABLE 3.2.4

Filter Transmission for Figure 3.2.23

Step No.	Transmission
1	0.015
2	0.028
3	0.035
4	0.054
5	0.075
6	0.135
7	0.180
8	0.250
9	0.340
10	0.530

3.2.4.7 Fixed-Pattern Noise in the SEC-Vidicon

Although experience with the UVicon has shown that the image defects that stand out as bright "stars" can be held to less than 2 to 4, even after the violent shaking experienced on the shock-test table, there

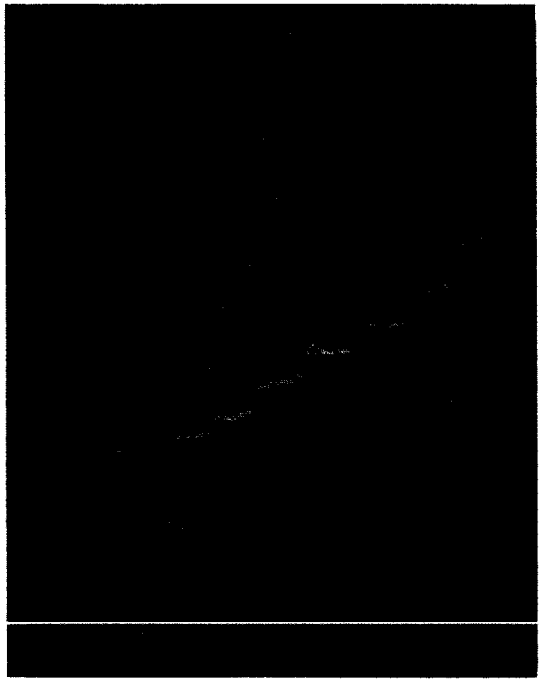

Figure 3.2.23. Grey Scale Rendition

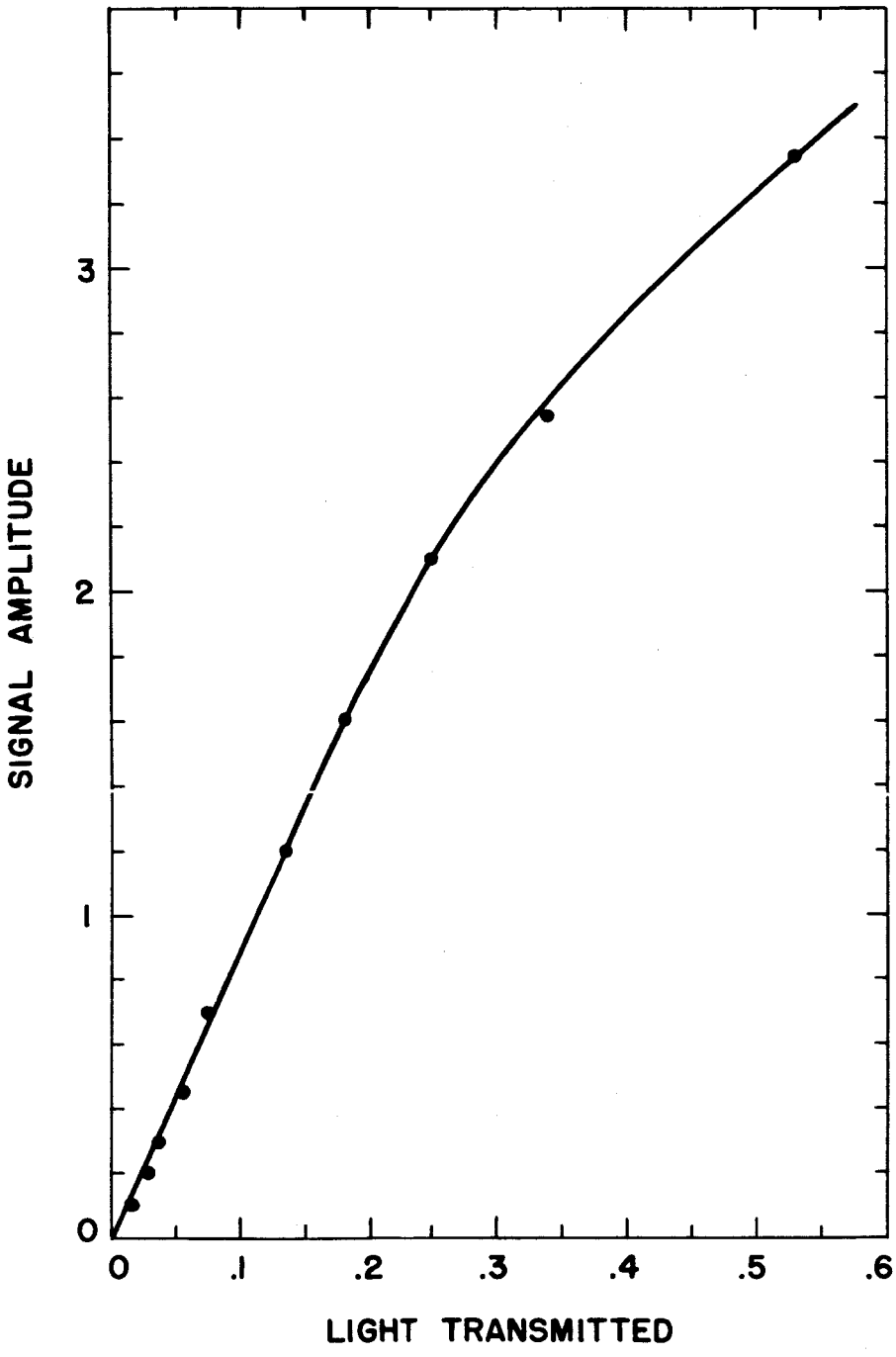

Figure 3.2.24. Filter Transmission

does exist some low-level fixed noise on SEC targets under certain conditions. This is, for instance, indicated in Figure 3.2.25, where the grey scale is shown as recorded at another portion of the target and at higher brightness than used to produce Figure 3.2.23. It is seen that at high states of charge, some fixed noise appears, the origin of which is not understood at present. In this tube the pattern noise was not originally present, and increased with the age of the tube. Other tubes have not shown this increase of pattern noise with age, and in general, the degree of this effect will vary from tube to tube.

It is found that when targets have been carefully prepared, and when they are operated at low target voltages or gains, such noise does not appear. Studies with a scanning electron microscope of the local variation of secondary electron emission from smoke films, carried out by M. Green[52] under another contract, have shown that for areas 10 microns on an edge, the secondary electron emission varies by less than 1%. However, this variation is greatly increased in amplitude if target processing control is lost.

It is hoped that further work now in progress will allow a better understanding of the fixed pattern noise. However, on the scale of resolutions presently contemplated (25 to 50 microns), it is believed that targets can be made whose sensitivity does not vary by more than 2% from element to element.

3.3 Common Properties

3.3.1 Size, Weight, and Power

Eventually, the Optechon and SEC-Vidicon will be considered for use in the OAO experiment. In fact, the Uvicon has already been slated for the Smithsonian Series of OAO experiments, and some of the results quoted on the reproducibility of charge readout were performed as the result of work performed on this contract.[53]

The two tubes are generally alike in physical configuration and operation, so that it is possible to estimate the size, weight, and power requirements for a sensor-system package for either. Based on our work

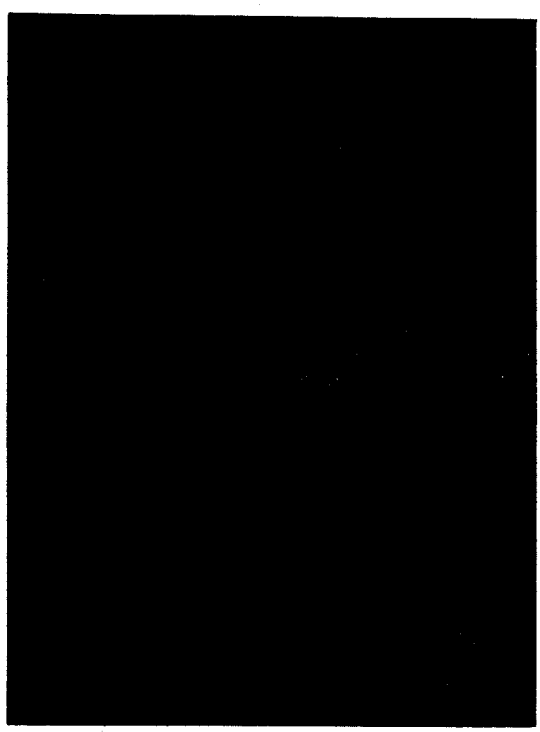

Figure 3.2.25. Fixed Pattern Noise

with the Manned Spacecraft Center at NASA, Houston, under Contract NAS 9-3548 (Development and Fabrication of Lunar Low Light Level Television Camera for LEM), we are in a position to make a realistic estimate for a spaceborne star spectra camera for the OAO.

This estimate is based upon a hybrid type of SEC-Vidicon or Optechon being used, with the lowered resolution resulting from this mode of operation, and would apply to space qualified, highly reliable equipment:

Size	120 in^3 (Typically 10 in. x 3 in. x 4 in.)
Weight	7 lbs (Less primary power supply)
Power	7 watts

This equipment would represent a state-of-the art slow scan camera modified for the more complex scan and synchronization scheme envisaged for the OAO application.

In order to provide higher resolution, the above figures would need to be increased to provide for an all magnetic system, using either an electromagnet or permanent magnet for the focusing field, and the added size, weight, and power necessary to stabilize the tube and circuit operating potentials.

3.3.2 Compatability of Substrate and Photosurface

In order to realize high quantum efficiencies, photocathodes having cesium as a constituent must be deposited under carefully controlled, if not ideal, conditions. In addition to its utility as a semiconductor type of photoemitter, cesium is a highly-reactive metal: consequently it will react with any and all foreign materials within the tube envelope if these materials are not compatible with it.

The formation of the semiconductor photosurface takes place at an elevated temperature with a particular partial pressure of the alkali metal above the base metal, usually antimony. For a multialkali photosurface, the process of formation is carried out in several stages, the deposition of the cesium usually being the last. If the partial pressure of the cesium is not correct, due to "gettering" of this metal by impurities, the quantum efficiency of the photosurface will suffer. Consequently, the establishment of maximum quantum efficiency within a

tube structure that has undergone certain processing operations is largely a matter of cut and try. Once it is established however, it can be kept under control by proper control of the prior processing history of the tubes. The suitability of the substrate material for the photosurface is also of great importance in the preparation of high quantum efficiency photoemission coatings. In normal image orthicon production, the code number of the glass has been found to influence the sensitivity. Certain cleaning procedures, rather than cleaning the surface of contaminants, replace them with a material more harmful than the contaminant they remove. Ammonium bifluoride is an example.

Early in the program, the suitability of the Lithium Fluoride window as a substrate for the S-20 multialkali photosurface was questioned. While successfully used in the Uvicon, the Cesium Iodide photosurface used in this tube was deposited as a compound rather than formed on the window substrate, as must be done with the S-20 surface. This is further complicated by the fact that lithium fluoride is a hygroscopic material* and must be thoroughly baked out before photocathode processing.

It has been hoped that several photodiodes could be made to check the compatability of the S-20 photosurface with the lithium fluoride window material. Consultation with Westinghouse Electronic Tube Division engineers showed that unless a sufficient number of samples were made, the results would tend to confuse rather than clarily the issue. Failure in making high quantum efficiency photocathodes in the first few tries would not necessarily indicate noncompatability, but more probably lack of process control.

This problem is therefore unresolved, and requires further effort, mainly of an experimental and possibly of a developmental nature.

*D. D. Doughty, and G. Skorinko, "Cesium Iodide Photodiode," Final Report for Contract NAS 5-961, (NASA Goddard) dated 1961-1962 Research Report 63-912-255-R3.

3.3.3 Magnetic Focusing

Depending upon the relative importance assigned spatial resolution in astronomical applications, it may be mandatory to use magnetic focusing for image tube sensors in space. Experience with the Astracon has shown that the resolution drops by an order of magnitude if a confining magnetic field is not used.

The problem implicit in magnetic focusing is twofold if an electromagnet is used: first, the weight of the focusing coil; and second, the weight, volume, and power consumption of the power supply. Depending upon the resolution required, the latter may vitiate any advantages that may be gained.

A patent[39] was assigned to Westinghouse Electric Corporation by Dr. G. W. Goetze describing a method of providing an axial magnetic field, that can be varied over a range, for imaging tubes (Figure 3.3.1). It has already been successfully used with the Astracon and shows excellent promise for space application. No power supply or cooling is required, and ceramic magnetic materials can be employed to permit weight reduction. The field configuration can be confined within a permeable magnetic shield, thereby decreasing the stray magnetic stray field that may interact with the earth's magnetic field in space, producing a perturbing torque.

Before a fair weight-volume comparison can be made, further work is required in order to design a permanent magnet focusing system for an imaging tube, and measure its long- and short-time stability, preferably under actual operating conditions with a high-resolution system. It can then be compared with an electromagnetic focus coil and supply of comparable stability characteristics with respect to weight and volume. Both electromagnetic and permanent magnet system would require special effort to determine the optimum magnetic shield configuration (thought to be spherical) in order that the torque of this system is minimized.

Nov. 3, 1964 G. W. GOETZE 3,155,860
CONTINUOUSLY VARIABLE PERMANENT MAGNET FOR IMAGING PURPOSES
Filed Oct. 7, 1960 2 Sheets-Sheet 1

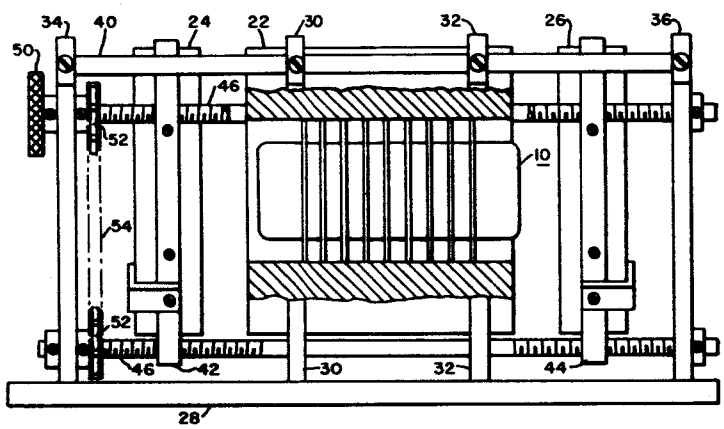

Fig. 1

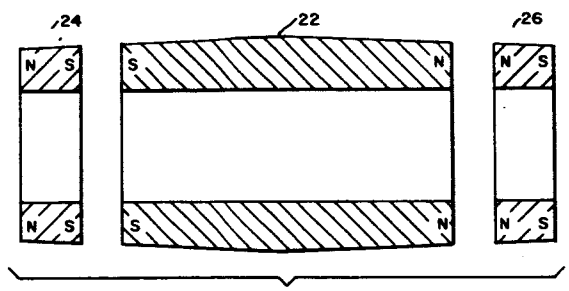

Fig. 2

WITNESSES
Leon J. Laza
James F. Young

INVENTOR
Gerhard W. Goetze
BY
Charles F. Renz
ATTORNEY

Figure 3.3.1. Permanent Magnet Focusing

APPENDIX A

Johnson-Nyquist and Amplifier Noise

It is more meaningful to compute the signal-to-noise ratio of the imaging or storage tube by including the noise contributions of the preamplifier following it. First of all, the imaging tube is a current source and most low-noise amplifiers are voltage amplifiers. A load resistance must therefore be provided, thereby introducing Johnson-Nyquist noise. The level of the voltage signal across the load resistance is quite small, so that it must be amplified in order that it can be used at another location. The amplifier used must introduce little noise of its own and must have sufficient gain so that the noise contribution of succeeding stages of amplification is negligible.

The need for a load resistance and the presence of stray capacity in the imaging tube, wiring and input circuit of the preamplifier implies a frequency dependence of the input network, which dictates an equilization network in later stages if the overall frequency response is to be constant over the required bandwidth.

The connective circuit between the imaging tube and the preamplifier network is shown below.

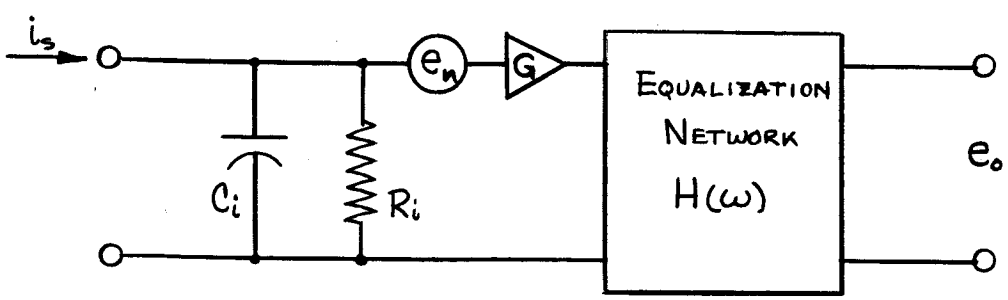

From this circuit it is possible to compute the noise power spectrum,

$$d(e_{o_n})^2 = G^2 |H(\omega)|^2 \left[\frac{4kTR_i\,df}{4\pi^2 f^2 R_i^2 C_i^2 + 1} + d(e_n^2) \right] \qquad (1)$$

Following convention,

$$d(e_n^2) = 4kTR_t\,df \qquad (2)$$

where e_n^2 is considered to originate in a fictitious resistor, R_t.

The quantity $H(\omega)$ represents the response of the equalization network, chosen so that

$$\left.\begin{aligned} |H(\omega)|^2 &= 4\pi^2 f^2 R_i^2 C_i^2 + 1 \;; \quad \text{for } f \le f_c \\ |H(\omega)|^2 &= 0 \;; \quad \text{for } f > f_c \end{aligned}\right\} \qquad (3)$$

Therefore:

$$d(e_{o_n})^2 = 4kTG^2 \left[R_i\,df + R_t(1 + 4\pi^2 f^2 R_i^2 C_i^2)df \right]; \quad \text{for } f \le f_c \qquad (4)$$

Integrating from 0 to f_c.

$$\overline{(e_{o_n})^2} = 4kTG^2 \left[R_i f_c + R_t f_c + \frac{4\pi^2 f_c^3 R_i^2 C_i^2 R_t}{3} \right]. \qquad (5)$$

If equation (5) is converted into an equivalent noise current referred to the input of the amplifier, it becomes

$$\overline{(\Delta i_n)^2} = \frac{\overline{(e_{o_n})^2}}{G^2 R_i^2} = \frac{4kTf_c}{R_i} \left[1 + \frac{R_t}{R_i} + \frac{4\pi^2 f_c^2 R_i R_t C_i^2}{3} \right]. \qquad (6)$$

If the equalization ratio is defined as

$$M = \frac{f_c}{\frac{1}{2\pi R_i C_i}} = 2\pi f_c R_i C_i \,, \qquad (7)$$

the noise current equation can be further simplified to

$$\overline{(\Delta i_n)^2} = 4kTf_c\left[\frac{1}{R_i} + \frac{R_t}{R_i^2}\left(1 + \frac{M^2}{3}\right)\right]. \qquad (8)$$

So far, nothing new has been introduced in the analysis, and equation (8) can be found in several references.[24,25,26,43] If it is "normalized" by dividing it by the bandwidth squared

$$\frac{\overline{(\Delta i_n)^2}}{f_c^2} = \overline{q_n^2} = 4kT\left[\frac{2\pi C_i}{M} + R_t(2\pi C_i)^2 f_c\left(\frac{1}{3} + \frac{1}{M^2}\right)\right], \qquad (9)$$

from which can be computed the noise fluctuation per cycle of bandwidth either in amperes per cycle, or in electrons per cycle of bandwidth. This becomes

$$q_n = \left\{4kT\left[\frac{2\pi C_i}{M} + (2\pi C_i)^2 R_t f_c\left(\frac{1}{3} + \frac{1}{M^2}\right)\right]\right\}^{\frac{1}{2}}. \qquad (10)$$

Equation (10) depends mostly upon the shunt capacity of the input to the amplifier and the equalization ratio, for a given bandwidth. Figure A-1 shows the noise fluctuation as a function of the equalization ratio for two values of input shunt capacity. In this graph the bandwidth has been taken to be 62.5 Kc/sec and the equivalent noise resistance of the tube R_t as 1000 ohms.

It can be seen that decreasing the shunt capacity C_i has the greatest effect upon decreasing the noise fluctuation for a given bandwidth. Lacking the ability of doing this, increasing the equalization ratio (by increasing the load resistance R_i) can also help to decrease the noise fluctuation. Since the curves in Figure C-1 have asymptotes, arising from

$$\lim_{M\to\infty}(q_n) = 4\pi C_i\left(\frac{kT R_t f_c}{3}\right)^{\frac{1}{2}}, \qquad (11)$$

the noise fluctuation can never be less than that given in (11). As Theile[24] shows, this leads to a maximum signal-to-noise ratio for an optimum value of load resistance.

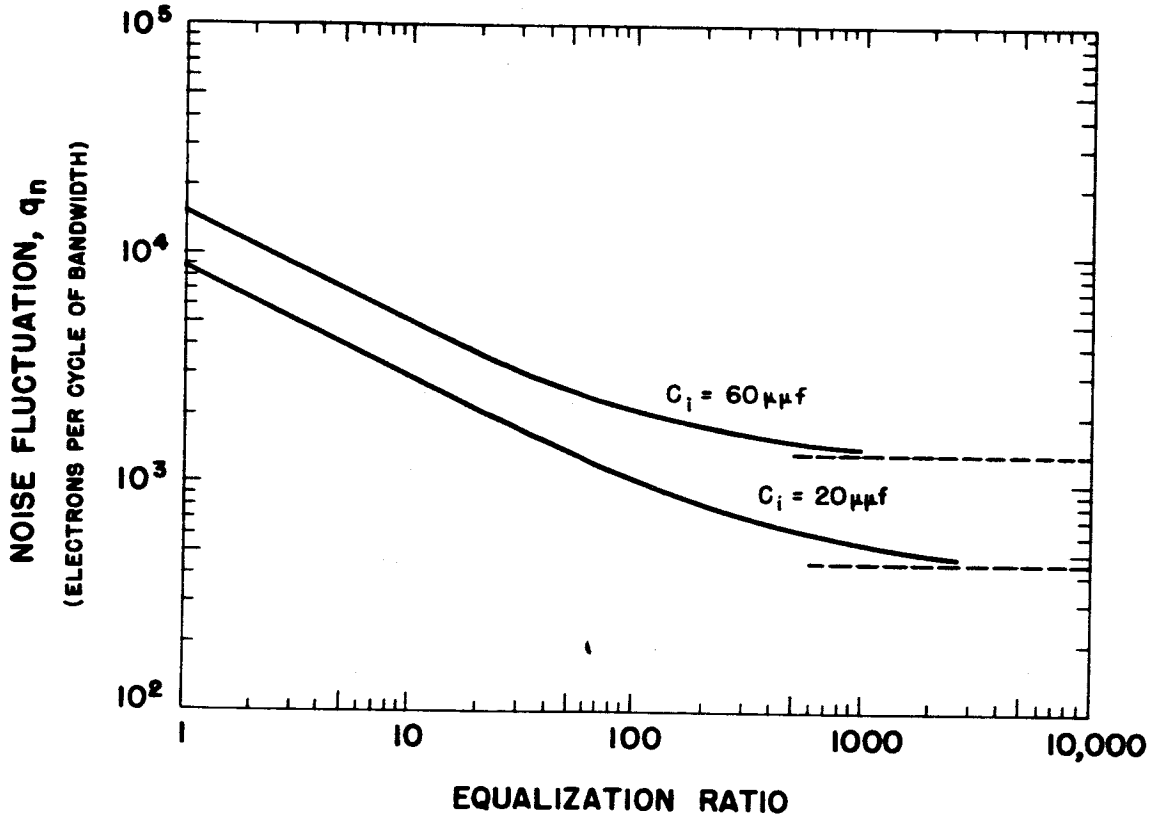

Figure A-1. Noise Fluctuation vs. Equalization Ratio

Certain factors normally preclude the use of high values of input resistance.* Grid leakage due to emission, soft X-rays, gas, etc., place a practical limit of one to two megohms on the grid resistance of most high G_m triodes. It should be possible to overcome this by returning the resistor to a low-frequency feedback network to stabilize the operating point so that a value up to 10 megohms can be used.

A second factor is concerned with a practical limit for equalization. When the gain of the first stage drops to unity, the noise of the second stage will dominate. A practical first stage at 100 Kc can have a maximum voltage gain of, say, 25 times at 100 Kc. Equalization by attenuation of the lower frequencies is permitted where the noise contribution of the later stages can be ignored. There will be a frequency, f_1, where the gain of the first stage drops to unity due to the low frequency attenuation and the relative noise due to the second and later stages becomes significant. However, the bandwidth increment from zero to that point is much less than f_1 to f_{max} and (since the lower frequencies are attenuated) the <u>total</u> noise contributed by these stages remains insignificant.

Instead of choosing the optimum resistance for maximum signal-to-noise, if we can be satisfied with a signal-to-noise ratio arbitrarily taken as 90% of the maximum it is possible to show by suitable manipulation of equation (6) that

$$\frac{R_i + R_t}{R_i^2} = 0.235 \left(\frac{4\pi^2 C_i^2 R_t f_c^2}{3} \right), \qquad (12)$$

thereby enabling the calculation of R_i for this compromise.

For normal TV rates corresponding to an f_c of 5 Mc/sec, the equalization ratio (for C_i = 30 pf) can be seen to be of the order of 20 to 50, and is often cited as the "practical limit". For lower bandwidths, such as used in the OA0, equalization ratios of 150 to 300 are possible.

---

*I am indebted to M. P. Siedband for the remainder of the remarks in this Appendix.

APPENDIX B

Effect of Low-Pass Filtering on Signal-to-Noise Ratio

In reference 43, Goldman treats the case of a rectangular pulse passing through a low-pass filter with a sharp cutoff at f_c, and a linear phase characteristic. Curves giving the derived pulse shapes at the filter output are reproduced in Figure B-1. The amplitude of the output signal G(t) shown in Figure B-1 is the value of the factor A_f in the body of the report, since it is the result of an input pulse of unity amplitude.

If a comparative signal-to-noise ratio is computed, Figure B-2 shows the result plotted against the reciprocal of k, (k = number of resolution elements per cycle of bandwidth). Figure B-2 implies that the maximum signal to noise ratio occurs at a value for k of approximately 1.5.

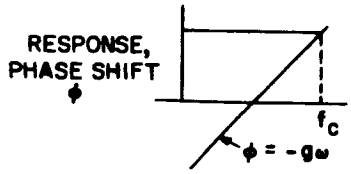

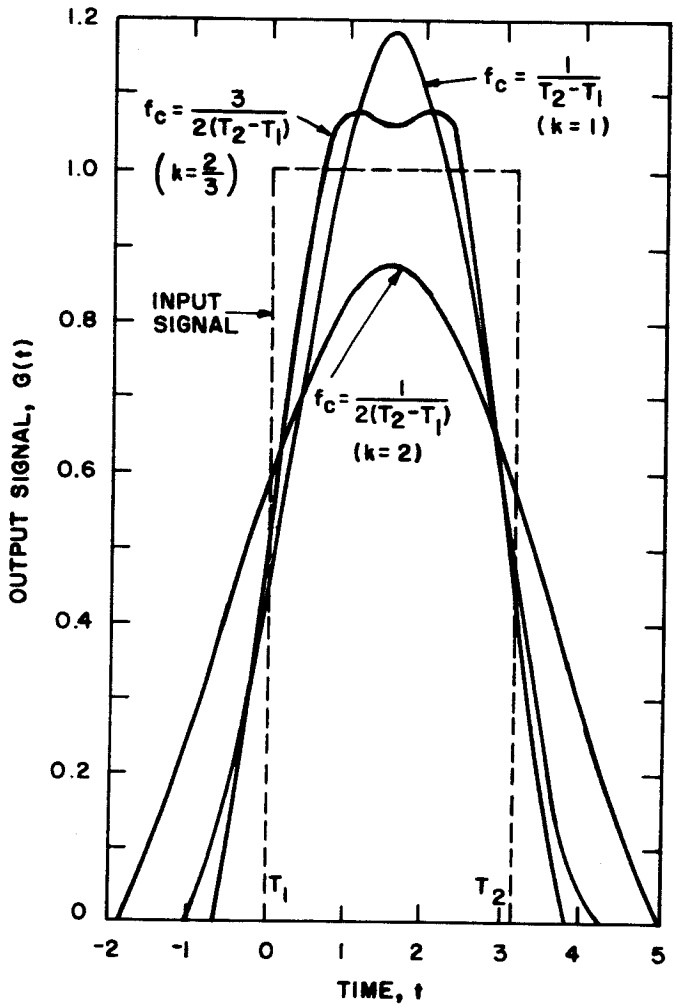

Figure B-1. Effect of Bandwidth on Pulse Shape
(After Goldman, p.83)
Low-pass Filter with Cutoff at f_c

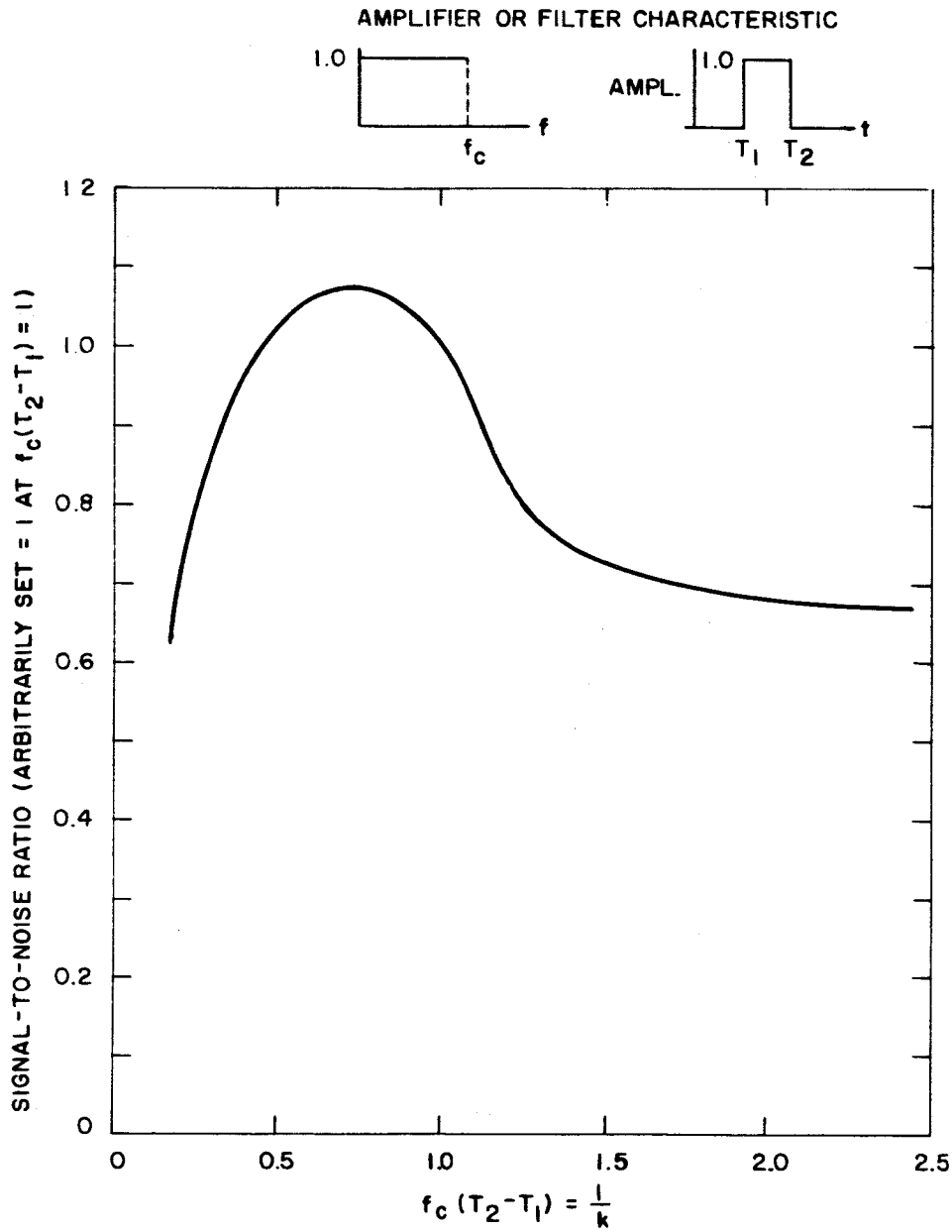

AFTER GOLDMAN, "FREQUENCY ANALYSIS, MODULATION AND NOISE", p99.

Figure B-2. Signal-to-Noise Ratio Vs. Number of Cycles per Resolution Element

APPENDIX C

Signal-to-Noise Analysis

1.0 INTRODUCTION

In order to assess the signal-to-noise qualities of the Grating Storage Camera Tube, the method proposed by deHaan[25] was adopted so that the contributions of the various gain processes within the tube would be apparent, and a parametric study would be possible.

DeHaan's thesis begins by stating that if n particles fall on a unit area of some substance in unit time, each will encounter a large number p of electrons. If there is a fixed chance q that an electron is excited, and a fixed chance r that an excited electron is emitted or raised to the conduction band, the average number of electrons emitted or participating in the conduction is $\bar{z} = \bar{n}pqr$. The mean square value of the total fluctuation in z is a summation in quadrature of the fluctuations in z due to the probability of emission r, of the fluctuations in z due to the probability of excitation q, and of the fluctuations in z due to the gaussian distribution of n in time, so that

$$\overline{(\Delta z)^2}_{TOTAL} = \bar{n}pqr + \bar{n}pqr^2 + \bar{n}p^2q^2r^2. \qquad (1)$$

If a value σ is defined as the number of electrons or particles produced on the average by an incoming particle, then $\sigma = pqr$ and (1) becomes, for $r \ll 1$;

$$\overline{(\Delta z)^2}_{TOTAL} = \bar{n}\sigma + \bar{n}\sigma^2 + \bar{n}\sigma r \approx \bar{n}\sigma(\sigma+1), \qquad (2)$$

for this physical mechanism, having a characterizing value σ, which can be

either a gain or a loss. Also, if j mechanisms occur in sequence, where

$$\bar{z} = \bar{n} \prod_{\ell=1}^{j} \sigma_\ell , \quad \text{So that } \sigma_\ell = p_\ell q_\ell r_\ell ; \qquad (3)$$
$$p_\ell \gg 1 , \; q_\ell \ll 1 , \; r_\ell \ll 1.$$

then

$$\overline{(\Delta z)^2}_{TOTAL} = \bar{n} \prod_{\ell=1}^{j} \sigma_\ell \left[\prod_{\ell=1}^{j} \sigma_\ell + \prod_{\ell=2}^{j} \sigma_\ell + \prod_{\ell=3}^{j} \sigma_\ell + \cdots + 1 \right]. \qquad (4)^*$$

Equation (4) is pivotal in the following analysis, since it expresses the noise fluctuation in terms of the system gains. It does not provide for excess noise in semiconductors or photoconductors, which must be added in quadrature in the same fashion as amplifier noise.

2.0 PROCEDURE

The Grating Storage Camera Tube has several gain mechanisms that can be employed to improve the signal-to-noise ratio obtainable. Figure 1 shows the sequence of gain mechanisms for the normal reading mode of the Grating Storage Camera Tube, and includes in b) and c) an assessment of the gains affecting the signal and reading beam branches, respectively. In like fashion, Figure 2 depicts the Vidicon reading mode for this tube. In both cases, the two branches shown each contribute noise: one branch noise contribution stems from the incoming photoelectrons and the physical processes they undergo; the second stems from the reading beam and the physical processes the reading beam electrons undergo. These two sources of noise are added in quadrature to the Johnson-Nyquist and amplifier noises.

---

*Equation (1) follows from (4) if $\sigma_1 = (pq)$ and $\sigma_2 = r$, so that

$$\overline{(\Delta z)^2}_{TOTAL} = \bar{n}(pq)r\{(pq)r + r + 1\} = \bar{n}p^2q^2r^2 + \bar{n}pqr^2 + \bar{n}pqr.$$

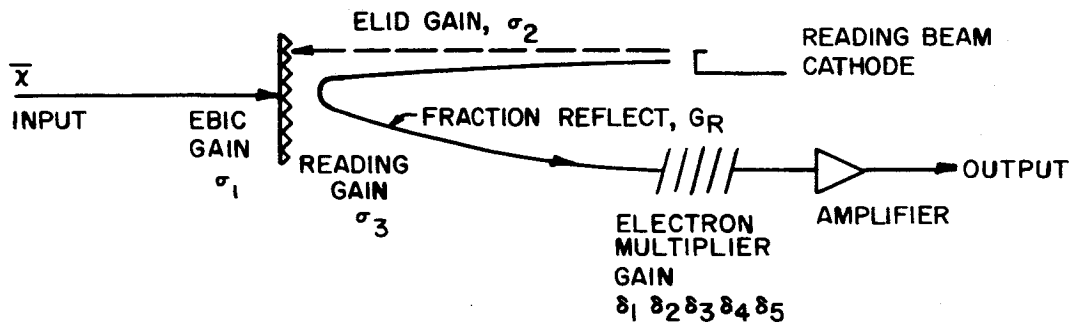

(a) SCHEMATIC DIAGRAM OF STORAGE AND READING MECHANISM

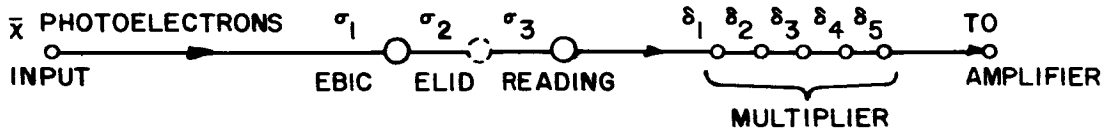

(b) SIGNAL FLOW GRAPH OF GAINS IN SIGNAL BRANCH

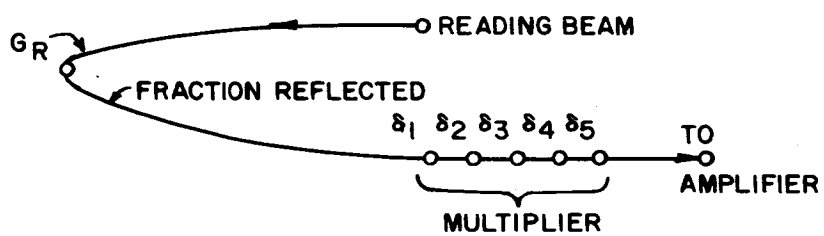

(c) SIGNAL FLOW GRAPH OF GAINS IN READING BEAM BRANCH

Figure C-1. Orthicon Reading Mode

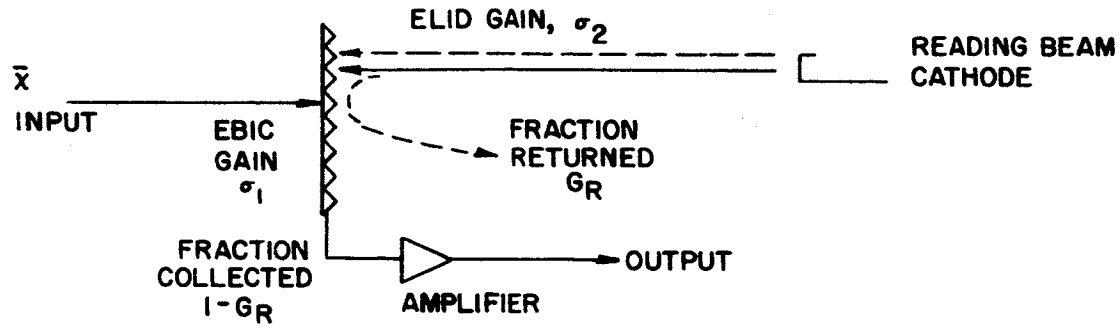

(a) SCHEMATIC DIAGRAM OF STORAGE AND READING MECHANISM

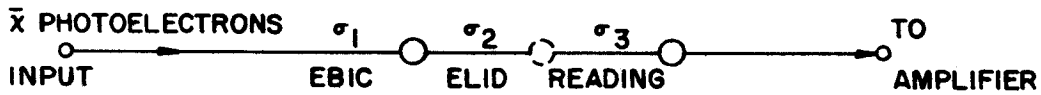

(b) SIGNAL FLOW GRAPH OF GAINS IN SIGNAL BRANCH

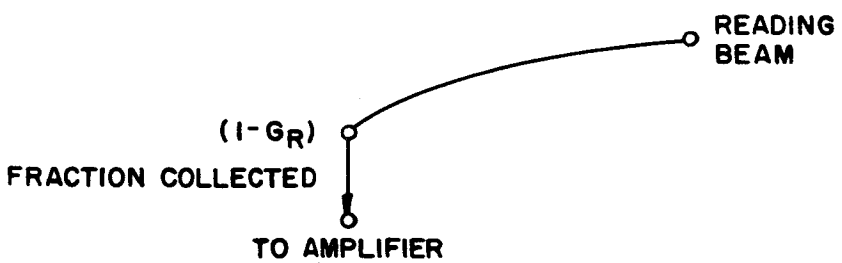

(c) SIGNAL FLOW GRAPH OF GAINS IN READING BEAM BRANCH

Figure C-2. Vidicon Reading Mode

As implied in the two figures, we shall consider two general cases: The signal-to-noise ratio when the Image Orthicon return beam and electron multiplier is used, called the orthicon mode of reading; and the signal-to-noise ratio when the signal is taken from the target, called the vidicon mode of reading.

3.0 TUBE GAINS

3.1 EBIC (Electron Bombardment Induced Conductivity)

This gain mechanism has a measured value of 7: i.e., for each incident photoelectron, seven electrons are discharged through the dielectric to the target base metal. $\sigma_1 = 7$, therefore.

3.2 ELID (Electron Latent Image Development)

It is possible to invoke another gain mechanism, that of Electrostatic Latent Image Development.* In this method, the charge pattern deposited upon the grating storage target is exposed to a flood beam of electrons having an energy corresponding to the first crossover. The parts of the target positive in voltage to this point become more positive, and those points negative become more negative, thereby effecting a gain. This gain depends upon the time of development (or exposure to flood beam electrons) and has a typical value of 10 for long time constant dielectrics. Therefore $\sigma_2 = 10$.

3.3 Reading Gain

A unique feature of the grating storage target is its triode modulating characteristic. That is, the reading gain is determined not only by the electrical storage capacity of the target, but also by the

*Appendix D

reading beam current. As in any storage tube, a voltage difference of $e/C_{e\ell}$ is developed for each resolution element per electron stored or removed from the dielectric surface. The triode characteristics of the target (Figure 3) imply that a certain fraction of the incident beam is returned or collected per volt of target potential difference. This fraction can be called the mutual transconductance factor of the target, g_m and has the dimensions of reciprocal volts.

The number of electrons affected by this potential difference of adjacent resolution elements in turn depends upon the reading beam current I_b, and the scanning time for a resolution limit, τ; and is given by

$$\bar{N} = \frac{I_b \text{ coul/sec } \tau \text{ sec/res.el}}{e \text{ coul/elect.}} = \frac{I_b \tau}{e} \frac{\text{electrons}}{\text{res. elem.}} \qquad (5)$$

In normal TV practice, the scanning time of a resolution element τ, is related to the bandwidth by

$$\tau \text{ sec/res.el.} = \frac{1}{k \frac{\text{elements}}{\text{cycle}} f_c \frac{\text{Cycles}}{\text{sec}}}, \text{ where } k = \frac{2 \text{ res. elem.}}{\text{Cycle}} \qquad (6)$$

The factor k can vary, however, depending upon the demands of the system.* In the general case, equation (5) becomes:

$$\bar{N} = \frac{I_b}{e k f_c} \frac{\text{electrons}}{\text{res. el.}}, \qquad (7)$$

Where $\bar{N}$ expresses the number of incident reading beam electrons, of which g_m are reflected (or do not get to the target), due to a small potential difference of $e\bar{\gamma}_s/C_a$; where $\bar{\gamma}_s$ is the number of stored photo-electrons per resolution element. The number of beam current electrons reflected or absorbed as the result of the signal is therefore

*Reference 43 and Appendix B

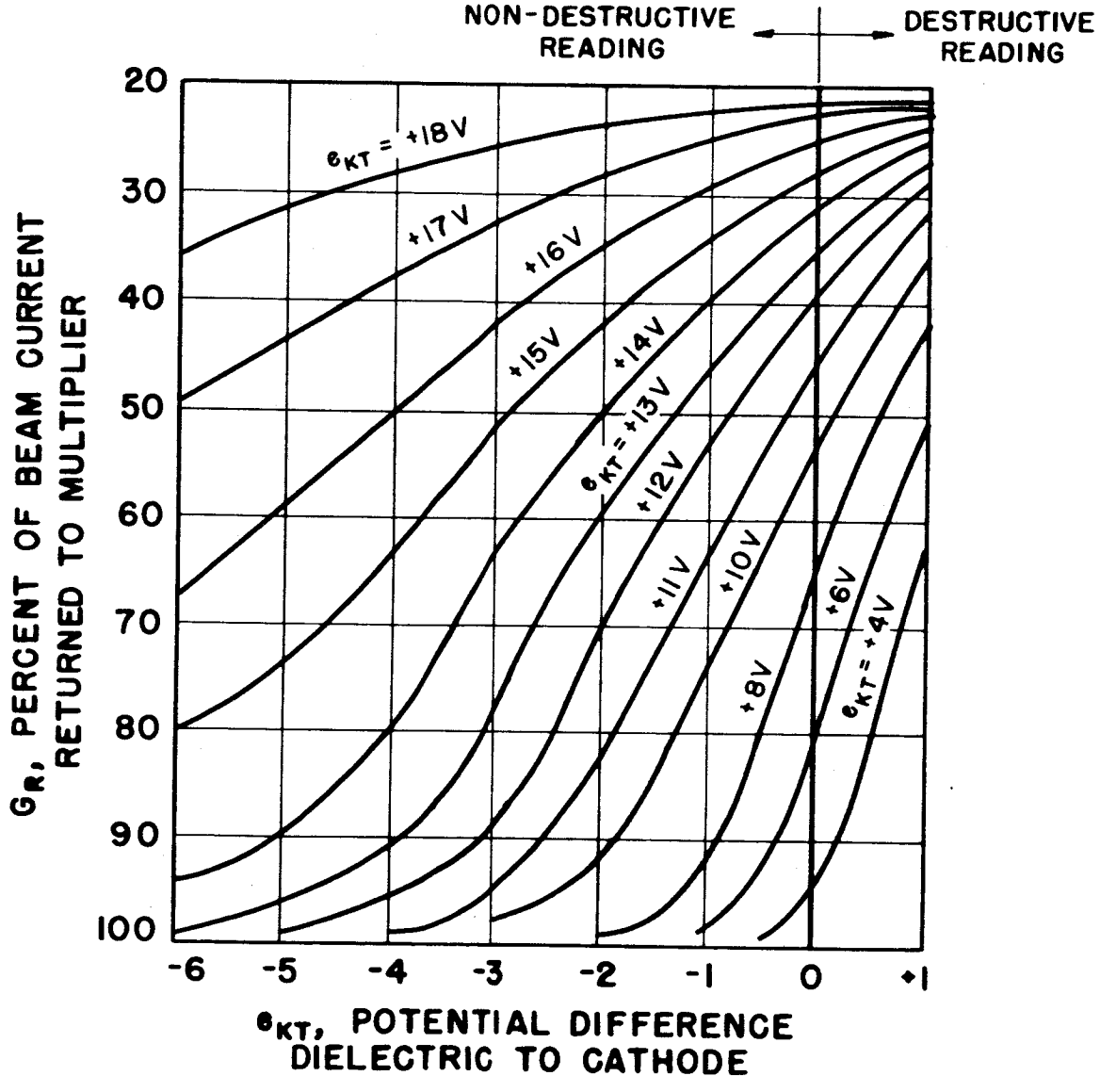

Figure C-3. Reading Transfer Characteristics

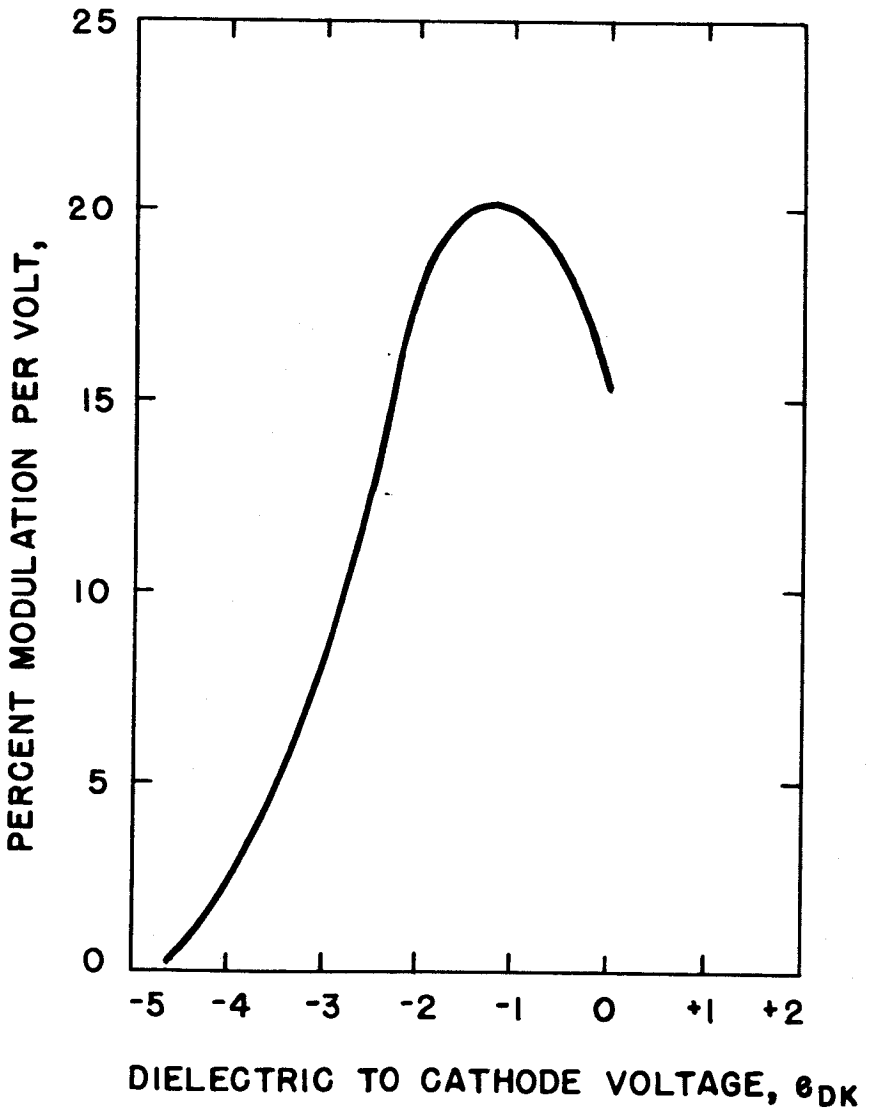

Figure C-4. Percent Small-Signal Modulation Vs. Dielectric to Cathode Voltage

$$\bar{i}_{rb} = \bar{I}_s \frac{g_m I_b}{C_{el} k f_c} ;$$

which implies that the reading gain σ_3, is

$$\sigma_3 = \frac{g_m I_b}{C_{el} k f_c} . \qquad (8)$$

If we assume a target base to cathode voltage of +11 volts and a dielectric to cathode voltage in the range of 0 to -2, the value of g_m is approximately 0.2 (volt)$^{-1}$. (Figure 4) For C_{el} = 35 x 10^{-15} farad, and f_c = 6.25 x 10^4 cycles/sec.

$$\sigma_3 = 0.914 \times 10^8 \frac{I_b}{k} . \qquad (9)$$

3.4 Multiplier Gain

In spite of the additional work involved, the writer prefers to consider the multiplier in terms of a sequential gain process and include it in the overall noise calculation. In general, the gain of the first dynode is low, and it will be taken as $\delta_1 = 0.8$. The succeeding dynodes will be considered as having their full gain, $\delta_2 = \delta_3 = \delta_4 = \delta_5 = 4$.

3.5 Beam Current

In addition to the small signal modulation factor g_m, the target also returns or absorbs, without destroying the stored signal, an amount of the incident beam current depending upon the operating point of the target. For the operating point given in 3.3, the fraction of beam current returned to the multiplier is $G_R = 0.64$ (obtained from Figure 3), and the fraction of beam current collected by the target is $(1 - G_R) = 0.36$.

3.6 Johnson-Nyquist and Amplifier Noise

The combined expression for the noise current of the input load resistance and amplifier is rederived in Appendix A and expressed in terms of the input load resistance R_1 and the Equalization Ratio M .

(10)

4.0 COMPUTATION OF SIGNAL

4.1 Vidicon Mode Reading

As a result of the various signal gains in the tube, for every incoming photoelectron per resolution element $\bar{\chi}$, $\bar{Z}_{VM}$ beam electrons arrive at the input to the amplifier according to the relation

$$\bar{Z}_{VM} = \sigma_1 \sigma_2 \sigma_3 A_v A_f \bar{\chi} \qquad (11)$$

where: $\sigma_1, \sigma_2, \sigma_3$ are the gains of the physical processes occurring in the tube,

A_v is the aperture or spatial response of the tube taken as 0.5 for the 25 micron resolution element (Figure 5),

A_f is the effect of the electrical low-pass filter on the pulse amplitude. If = 2 element/cycle,

A_f = 0.86 (See Appendix B)

The signal current at the output of the tube is therefore

$$(i_s)_{VM} = \frac{e}{T} \bar{Z}_{VM} \; ; \; \text{where: } T = \frac{1}{k f_c} \qquad (12)$$

so that

$$(i_s)_{VM} = k e f_c \sigma_1 \sigma_2 \sigma_3 A_v A_f \bar{\chi} \qquad (13)$$

4.2 Orthicon Mode Reading

The additional gain provided by the electron multiplier leads to

$$\bar{Z}_{OM} = (\sigma_1 \sigma_2 \sigma_3 A_v A_f) \delta_1 \delta_2 \delta_3 \delta_4 \delta_5 \bar{\chi} \qquad (14)$$

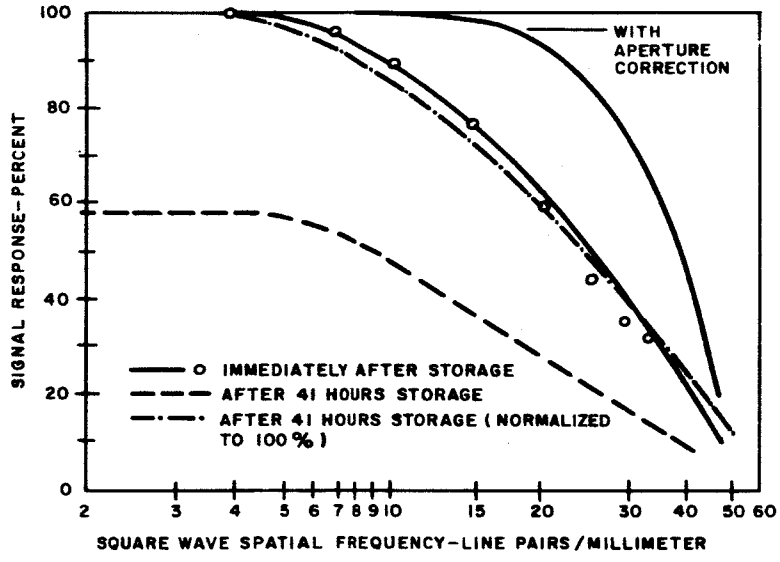

Figure C-5. Aperture Response of Optechon

5.0 COMPUTATION OF NOISE

5.1 Signal Noise

5.1.1 Signal Noise - Vidicon Mode of Reading

Since $$\overline{(\Delta z)^2} = \bar{\jmath}\,\sigma_1\sigma_2\sigma_3\,(\sigma_1\sigma_2\sigma_3 + \sigma_2\sigma_3 + \sigma_3 + 1) \quad (16)$$

the noise current is

$$\overline{(\Delta i_s)^2} = \frac{e^2}{T^2}\,\overline{(\Delta z)^2};$$

or

$$\overline{(\Delta i_s)^2}_{VM\text{-}ELID} = e^2k^2f_c^2\bar{\jmath}\,\sigma_1\sigma_2\sigma_3\,(\sigma_1\sigma_2\sigma_3 + \sigma_2\sigma_3 + \sigma_3 + 1), \quad (17)$$

for a three-gain system, with ELID,

and

$$\overline{(\Delta i_s)^2}_{VM} = e^2k^2f_c^2\bar{\jmath}\,\sigma_1\sigma_3\,(\sigma_1\sigma_3 + \sigma_3 + 1) \quad (18)$$

for a two-gain system.

5.1.2 Signal Noise - Orthicon Mode of Reading

Here we must take into account the dynode gains as in Section 4.2. The complete expression is (including ELID)

$$\overline{(\Delta i_s)^2}_{OM} = e^2k^2f_c^2\bar{\jmath}\,\sigma_1\sigma_2\sigma_3\delta_1\delta_2\delta_3\delta_4\delta_5\,(\sigma_1\sigma_2\sigma_3\delta_1\delta_2\delta_3\delta_4\delta_5 + \sigma_2\sigma_3\delta_1\delta_2\delta_3\delta_4\delta_5$$
$$\sigma_3\delta_1\delta_2\delta_3\delta_4\delta_5 + \delta_1\delta_2\delta_3\delta_4\delta_5 + \delta_2\delta_3\delta_4\delta_5 + \delta_3\delta_4\delta_5 + \delta_4\delta_5 + \delta_5 + 1)$$

since $\delta_1 \neq \delta_2 = \delta_3 = \delta_4 = \delta_5$ the above can be simplified to

$$\overline{(\Delta i_s)^2}_{OM-ELID} = e^2 k^2 f_c^2 \sum \sigma_1\sigma_2\sigma_3 \delta_1\delta_2^4 (\sigma_1\sigma_2\sigma_3\delta_1\delta_2^4 + \sigma_2\sigma_3\delta_1\delta_2^4 + \sigma_3\delta_1\delta_2^4 + \delta_1\delta_2^4 + \delta_2^4 + \delta_2^3 + \delta_2^2 + \delta_2 + 1) \quad (19)$$

with ELID ;

and

$$\overline{(\Delta i_s)^2}_{OM} = e^2 k^2 f_c^2 \sum \sigma_1\sigma_3\delta_1\delta_2^4 (\sigma_1\sigma_3\delta_1\delta_2^4 + \sigma_3\delta_1\delta_2^4 + \delta_1\delta_2^4 + \delta_2^4 + \delta_2^3 + \delta_2^2 + \delta_2 + 1) \quad (20)$$

without ELID.

5.2 Reading Beam Noise

The number of beam electrons incident upon a resolution element is the beam current I_b times the scanning time τ and the scanning time is given by (5). Therefore

$$N_b = \frac{I_b \frac{\text{Coul}}{\text{sec}} \tau \frac{\text{sec}}{\text{element}}}{e \text{ Coul/electron}} = \frac{I_b}{ekf_c} \frac{\text{electr.}}{\text{element}} \quad (5)$$

5.2.1 Vidicon Mode of Reading

$$\overline{(\Delta i_B)^2}_{VH} = e^2 k^2 f_c^2 N_b (1-G_R)[(1-G_R)+1] \quad (21)$$

Simplifying

$$\overline{(\Delta i_B)^2}_{VH} = ek f_c I_b (1-G_R)(2-G_R) \quad (22)$$

5.2.2 Orthicon Mode of Reading

$$\overline{(\Delta i_B)^2}_{OM} = [ekf_c] I_b [G_R \delta_1 \delta_2^4] [G_R \delta_1 \delta_2^4 + \delta_1 \delta_2^4 + \delta_2^4 + \delta_2^3 + \delta_2^2 + \delta_2 + 1] \quad (23)$$

5.3 Johnson-Nyquist and Amplifier Noise

Substituting in equation (10)

$$\left.\begin{aligned} &(kT) \text{ (for } 300^\circ K) = 0.026 \text{ eV} \\ &R_t = 3 \quad 10^2 \text{ ohms} \\ &R_i = 10^6 \text{ ohms} \\ &M = 11.8 \\ &f_c = 6.25 \times 10^4 \text{ cycles/sec} \end{aligned}\right\} \quad (24)$$

gives

$$\overline{(\Delta i_n)^2} = 1.05 \times 10^{-21} (\text{Amp})^2 \quad (25)$$

5.4 Priming Noise

Priming consists of charging the target to some negative potential V_p by means of deposition of electrons by a scanned or flood beam. If this process is based upon the minimum time required to deposit $\frac{C_{el} V_p}{e}$ electrons upon a resolution element by a current I_p, an indeterminacy is inevitable, and noise will be contributed. If this process is allowed to come to an equilibrium so that the dielectric is charged to cathode potential with respect to the positive metal grating, it can be expected that the fluctuation of charge upon the target will be very small. One way to look at it, is to consider a floating grid triode[26] where the noise is given by

$$\overline{(\Delta i_g)^2} = \frac{4kT\, df}{R_g}; \quad \text{where: } R_g = \frac{(kT_c)}{e\bar{I}_1} = \frac{0.026}{\bar{I}_1}$$

and I_1 is the grid current produced by electrons arriving at the grid. Assuming a good dielectric and a good vacuum (and therefore no ion bombardment) I_1 can be very small ($\ll$ 0.1 microamp) and consequently this noise contribution under the above conditions* can be neglected. We shall assume that this is generally the case.

5.5 Computation of Total Noise

5.5.1 Vidicon Mode of Reading

$$\overline{(\Delta i_{TOT})^2_{VM}} = \overline{(\Delta i_S)^2_{VM}} + \overline{(\Delta i_B)^2_{VM}} + \overline{(\Delta i_n)^2} \qquad (26)$$

For $\overline{(i_S)^2_{VM}}$ we have two cases: with and without ELID.

5.5.2 Orthicon Mode of Reading

$$\overline{(\Delta i_{TOT})^2_{OM}} = \overline{(\Delta i_S)^2_{OM}} + \overline{(\Delta i_B)^2_{OM}} + \overline{(\Delta i_n)^2}$$

Again, for $\overline{(i_S)^2_{OM}}$ we have two cases: with and without ELID.

*Hybrid conditions might be postulated; a fast scan, depositing enough electrons to charge to an intermediate voltage and a slow scan to bring the priming voltage to equilibrium conditions.

6.0 PARAMETRIC EQUATIONS

The signal-to-noise ratio is defined as

$$(S/N) = \frac{i_s}{\left[\overline{(\Delta i_{Tot})^2}\right]^{1/2}} \qquad (27)$$

where (i_s) is defined by the appropriate expressions given in Section 4.0 and $\overline{(\Delta i_{Tot})^2}$ by those given in Section 5.5. Since it is always possible to divide out the gain terms in expression (27), it can be simplified to

$$(S/N) = \frac{\bar{\chi}}{(\alpha \bar{\chi} + \beta)^{1/2}} \qquad (28)$$

In equation (28), the term α would include the effects of all the gain processes in the tube, including those of aperture response and electrical filter response, and would have a minimum value of 1. The term β would consist of the beam shot noise and amplifier-Johnson-Nyquist noise, modified by the tube gains. The asymptote to equation (28) can be determined quite easily for representative values of α and β, giving Figure 6. Figure 6 could give a quick estimate of the signal-to-noise variation as a function of photoelectrons incident upon a storage resolution element $\bar{\chi}$, knowing the tube gains, and from these calculating the values of α and β. From the results of the previous sections, the values of α and β can be expressed in terms of the parameters of the tube. Table I is a compilation of the α and β factors expressed parametrically, and Table II is a definition of symbols used in Table I.

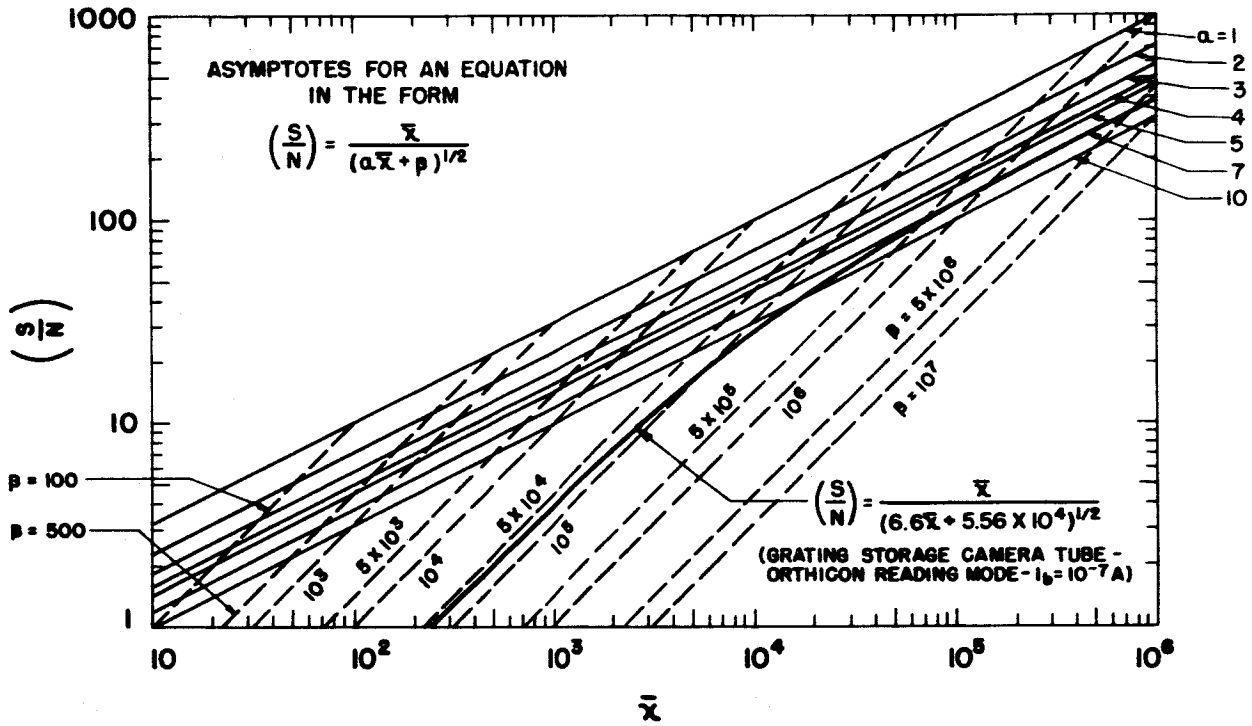

Figure C-6. Asymptotes for an Equation in the Form

TABLE I

Parametric Equations of Signal-to-Noise Ratio
In the Form

$$(S/N) = \frac{\bar{\chi}}{(\alpha\bar{\chi} + \beta)^{1/2}}$$

Vidicon Mode of Reading

$$\alpha = \frac{1}{(A_v A_f)^2}\left(1 + \frac{1}{\sigma_1} + \frac{k}{\sigma_1 a I_b}\right)$$

$$\beta = \frac{1}{e f_c I_b (\sigma_1 a A_v A_f)^2}\left[k(1-G_R)(2-G_R) + \frac{\overline{(\Delta i_n)^2}}{e f_c I_b}\right]$$

Orthicon Mode of Reading

$$\alpha = \frac{1}{(A_v A_f)^2}\left(1 + \frac{1}{\sigma_1} + \frac{k\Gamma_M}{\sigma_1 a I_b}\right)$$

$$\beta = \frac{1}{e f_c I_b (\sigma_1 a A_v A_f)^2}\left[k G_R(G_R + \Gamma_M) + \frac{\overline{(\Delta i_n)^2}}{e f_c I_b (\delta_1 \delta_2^{(4)})^2}\right]$$

Vidicon Mode of Reading with Electrostatic Latent Image Development (ELID)

$$\alpha = \frac{1}{(A_v A_f)^2}\left(1 + \frac{1}{\sigma_1} + \frac{1}{\sigma_1\sigma_2} + \frac{k}{\sigma_1\sigma_2 a I_b}\right)$$

$$\beta = \frac{1}{e f_c I_b (\sigma_1\sigma_2 a A_v A_f)^2}\left[k(1-G_R)(2-G_R) + \frac{\overline{(\Delta i_n)^2}}{e f_c I_b}\right]$$

Orthicon Mode of Reading with Electrostatic Image Development (ELID)

$$\alpha = \frac{1}{(A_v A_f)^2}\left(1 + \frac{1}{\sigma_1} + \frac{1}{\sigma_1\sigma_2} + \frac{k\Gamma_M}{\sigma_1\sigma_2 a I_b}\right)$$

$$\beta = \frac{1}{e f_c I_b (\sigma_1\sigma_2 a A_v A_f)^2}\left[k G_R(G_R + \Gamma_M) + \frac{\overline{(\Delta i_n)^2}}{e f_c I_b (\delta_1 \delta_2^{(4)})^2}\right]$$

TABLE II

DEFINITION OF SYMBOLS

(S/N)	Signal-to-noise ratio
$\bar{\gamma}$	Average number of photoelectrons per resolution element incident upon the storage target during an integration time.
$\bar{\gamma}_s$	Average number of electrons per resolution element stored on the target.
σ_1	Electron Bombardment Induced Conductivity (EBIC) gain.
σ_2	Electrostatic Latent Image Development (ELID) gain.
σ_3	Reading gain, expressed by $\sigma_3 = \frac{g_m I_b}{C_{ee} k f_c}$
g_m	Mutual transconductance factor of the target. Obtained from reading transfer characteristics (Figure 3.4). Dimensions are reciprocal volts.
I_b	Reading beam current, amperes.
C_{ee}	Electrical capacity of a resolution element, farads.
k	Number of resolution elements per cycle of bandwidth.
f_c	Bandwidth in cycles per second.
τ	Scanning time of a resolution element, in seconds per element.
a	Factor related to the reading gain σ_3 expressed by $a = \frac{g_m}{C_{ee} f_c} \frac{\text{sec-elem.}}{\text{coul-cycles}}$
δ_1	Gain of first dynode
$\delta_2, \delta_3 \cdots \delta_5$	Gain of subsequent dynodes
e	Electronic charge, 1.6×10^{-19} coul/electron.
A_f	Effect of electrical low-pass filter on the pulse amplitude Appendix B).
A_ν	Aperture response or spatial frequency response of the tube (Figure 5)
Γ_M	Noise factor associated with the multiplier, defined by $\Gamma_M = 1 + \frac{1}{\delta_1} + \frac{1}{\delta_1\delta_2} + \frac{1}{\delta_1\delta_2^2} + \frac{1}{\delta_1\delta_2^3} + \frac{1}{\delta_1\delta_2^4}$

TABLE II (Continued)

$\overline{(\Delta i_n)^2}$	Johnson-Nyquist and amplifier noise (compensated) defined by equation (10).
M	Equalization ratio, defined by $M = 2\pi f_c R_i C_i$
R_i	Load resistance at output of tube, ohms.
C_i	Shunt capacity of tube output and amplifier input, farads.
R_t	Equivalent series noise resistance of amplifier.
$(k T)$	Equipartition energy.
G_R	Fraction of beam current returned to multiplier by the grating storage target. Obtained from Figure 3.

APPENDIX D

Electrostatic Latent Image Development

In the Westinghouse Special Electron Devices Laboratory, we have invented an electronic process called Electrostatic Latent Image Development for which a patent has been applied, but there is as yet no formal paper dealing with this.

Most storage tubes require more electrons to be stored per resolvable element, in order to produce a sufficiently strong potential pattern to modulate the reading beam fully, than are required to carry the signal information. For example, a signal-to-noise ratio of stored signal charge of 100 may be obtained with as few as 10^5 electrons/element in the maximum signal. But 10^5 electrons on a typical elemental capacitor provides a voltage change of less than 0.1 volt, only 1% of that required to modulate the reading beam by the maximum possible amount. Hence, the writing speed can usually be increased by as much as 100 if a prestorage charge gain of 100 is made available. Direct secondary emission generally cannot provide as much gain as 10. Electron bombardment induced conductivity can provide gains up to 100 on short time constant semiconductors, but not more than 10 on good, long time constant dielectrics.

Electrostatic Latent Image Development has been demonstrated to provide a charge gain as high as 100. The process consists of bombarding the target, upon which a charge pattern has previously been stored, with a uniform flood or a uniform scan of electrons. The landing energy of these flood electrons is chosen to be on the negative slope of the secondary emission current curve, so that they have an energy per electron about equal to the voltage of the first crossover point of secondary emission. The incident flood or development electrons will have more or less energy upon landing in accordance with the stored potential pattern. At a region on the target which is only slightly below first crossover, the secondary emission ratio is only slightly below unity and electrons are deposited at only a slow rate. At another region on the target which is considerably below first crossover, the secondary emission is considerably below unity and electrons are deposited rapidly. Similarly,

at a region on the target which is only slightly above first crossover, the secondary emission ratio is only slightly greater than unity and electrons are removed slowly. At a region on the target which is considerably above first crossover, the secondary emission ratio is considerably greater than unity and electrons are removed rapidly. Thus during the time of development electrons are deposited or removed in greater or lesser amount according to the potential pattern already stored and in such a proportional manner that the potential pattern is enhanced.

The gain process is exactly that used in a dynatron oscillator, and stems from the negative resistance of this portion of the secondary emission characteristic.

The process must be carefully limited in the time of its application, else it will go to equilibrium.

Since electrons are deposited or removed in proportion to the number already stored, this is a pure gain process. Thus the process is a gain term for both the stored signal and the stored noise. No new information is added in the development process; but since the fluctuation in the number of electrons added is equal to the square root of this number, being a partition noise, the total noise is no greater than it would have been had all the electrons been deposited by the writing means. Therefore, the signal-to-noise ratio is no worse, and no information is lost by this development means. The process is very much analogous to the photographic development process.

Any dc shift in target voltage must be compensated by a corresponding shift in a reading bias voltage, for example, that of the reading gun cathode.

APPENDIX E

Crossed-Filament Light Source

Figure E-1 is an outline drawing of the crossed-filament light source used in the experimental investigation of the SEC-Vidicon beam bending. Basically, it consists of two separate crossed wires and two fiducial wires bracketing the crossed wires. Each 1 mil tungsten wire can be heated to a different brightness, although the outer fiducial wires are normally kept at some non-critical brightness and determine the linear extent of the display on the A-scope. Blackened light absorbing shields are provided to eliminate errors due to stray light reflectance.

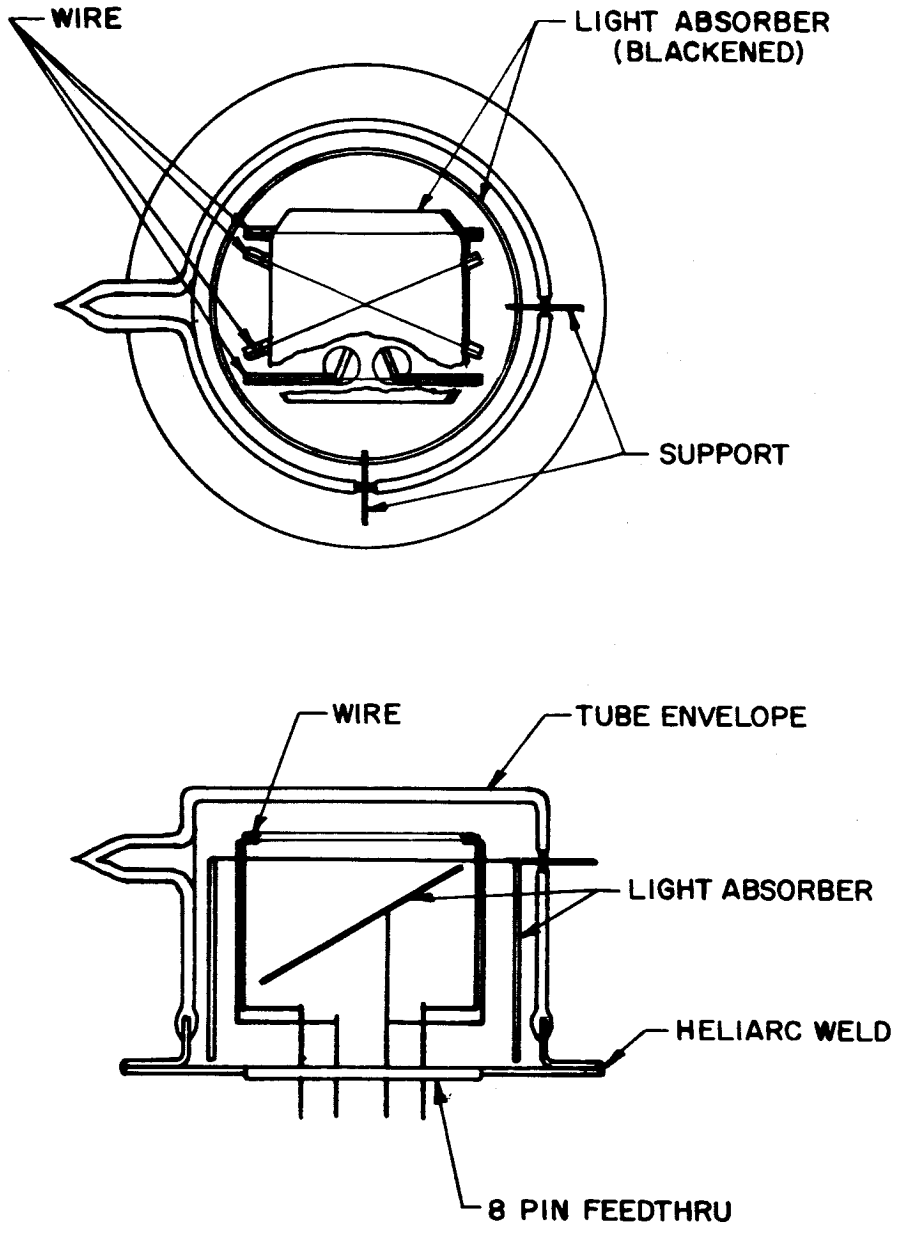

CROSSED FILAMENT LIGHT SOURCE

Figure E-1. Crossed Filament Light Source

References

1. W. C. Livingston, "Resolution Capability of the Image Orthicon Camera Tube Under Nonstandard Scan Conditions," JSMPTE, Vol 72, No. 10 (October 1963) pp 771-785.
2. R. K. H. Gebel, "Effects of Bright Point Light Sources on Low Level Image Orthicon Detectors," WADC Techn. Note 58-116; ASTIA Document No. AD-155503 (April 1958).
3. W. T. Powers, "Nondestructive Readout with a Field-Mesh Image Orthicon," Applied Optics, Vol. 3, No. 6 (June 1964) pp 673-675.
4. E. Luedicke, A. D. Cope, L. E. Flory, "Astronomical Image-Integration System Using a Television Camera Tube," Applied Optics, Vol. 3, No. 6 (June 1964) pp 677-689.
5. W. A. Baum, "The Detection and Measurement of Faint Astronomical Sources," "Astronomical Techniques," The University of Chicago Press (1960).
6. J. D. McGee, "Image Detection by Television Signal Generation," "Astronomical Techniques," The University of Chicago Press (1964).
7. W. C. Livingston, "Application of the Image Orthicon to Spectroscopy," "Astronomical Techniques," The University of Chicago Press (1960).
8. W. A. Baum, "The Potentialities of Photo-Electronic Imaging Devices for Astronomical Observatories," "Advances in Electronics and Electron Physics," Vol. XII, Academic Press (1960).
9. G. A. Morton, J. E. Ruedy, "The Low Light Level Performance of the Intensifier Orthicon," "Advances in Electronics and Electron Physics" Vol. XII, Academic Press (1960).
10. R. K. H. Gebel and L. Devol, "Some Early Trials of Astronomical Photography by Television Methods," "Advances in Electronics and Electron Physics," Vol. XII, Academic Press (1960).
11. D. J. Gibbons, "The Tri-Alkali Stabilized C. P. S. Emitron: A New Television Camera Tube of High Sensitivity," "Advances in Electronics and Electron Physics," Vol. XII Academic Press (1960).
12. R. P. Randall, "Charge Integration Experiments with a C. P. S. Emitron," "Advances in Electronics and Electron Physics," Vol. XII, Academic Press (1960).
13. R. L. Beurle and N. A. Slark, "An Experimental Image Storage Tube for the Detection of Weak Optical Images of Low Contrast," "Advances in Electronics and Electron Physics," Vol. XII, Academic Press (1960).
14. E. W. Dennison, "An Isophote Converter for Use With Signal-Generating Image Tubes," "Advances in Electronics and Electron Physics," Vol. XII, Academic Press (1960).

15. S. Miyashiro, Y. Nakayama, "Some Methods of Minimizing the Black Border Effect in the Image Orthicon Television Pickup Tube," "Advances in Electronics and Electron Physics," Vol. XVI, Academic Press (1962).

16. R. J. Schneeberger, G. Skorinko, D. D. Doughty, W. A. Feibelman, "Electron Bombardment Induced Conductivity Including its Application to Ultra-Violet Imaging in the Schuman Region," "Advances in Electronics and Electron Physics," Vol. XVI, Academic Press (1962).

17. W. A. Baum, "Laboratory Evaluation of Image Tubes for Astronomical Purposes," "Advances in Electronics and Electron Physics," Vol. XVI, Academic Press (1962).

18. J. A. Hynek, G. Barton, R. Ackens, and W. Powers, "Potentialities and Limitations of Image Scanning Techniques in Astronomy," "Advances in Electronics and Electron Physics," Vol. XVI, Academic Press (1962).

19. J. H. DeWitt, Jr., "A Report on the Image Orthicon Using Slow Readout," "Advances in Electronics and Electron Physics," Vol. XVI, Academic Press (1962).

20. W. C. Livingston, "Stellar Photometry with an Image Orthicon," "Advances in Electronics and Electron Physics," Vol. XVI, Academic Press (1962).

21. E. W. Dennison, "The Image Orthicon Applied to Solar Photometry," "Advances in Electronics and Electron Physics," Vol. XVI, Academic Press (1962).

22. R. K. H. Gebel, "The Potentialities of Electronically Scanned Photoconductive Image Detectors for Astronomical Uses," "Advances in Electronics and Electron Physics," Vol. XVI, Academic Press (1962).

23. C. B. Murray, Jr., A. Van der Ziel, "Measurements of Noise in Image Orthicons," IEEE Trans. on Electron Devices, Vol. ED-11, No. 8 (August 1964), pp 365-368.

24. R. Theile, "On the Signal-to-Noise Ratio in Television Storage Tubes," "Advances in Electronics and Electron Physics," Vol. XII, Academic Press (1960).

25. E. F. deHaan, "Signal-to-Noise Ratio of Image Devices," "Advances in Electronics and Electron Physics," Vol. XII, Academic Press (1960).

26. Van der Ziel, "Noise," Prentice Hall, Inc. (1956).

27. I. M. Krittman, John A. Inslee, "Discussion and Applications of Electrostatic Signal Recording," RCA Review Vol. 24 , No. 3 , (September 1963) pp 406-420.

28. F. B. Marshall, "Princeton AOAO Noise Considerations," Westinghouse Aerospace Division System Development Tech. Memo No. 404, (dated August 1964).

29. W. G. Reininger, A. S. Jensen, W. G. Beran, "Research in Advanced Photoelectric Information Storage," Technical Documentary Report No. RTD-TDR-63-4134, dated November 1963. Prepared under Contract No. AF33(657)8715, Project No. 6263, Task No. 626302, for Air Force Avionics Laboratory, Research and Technology Division, Air Force Systems Command, Wright-Patterson AFB, Ohio.

30. I. Limansky, "The Absence of Image Spreading in the Grating Storage Camera Tube," Westinghouse Electronic Tube Division Report ET-95-BEL-64-35 (dtd November 1964).

31. I. Limansky, "Beam Bending in the Grating Storage Target Tube - Report of Experimental Results," Westinghouse Electronic Tube Division Report ET-95-BEL-64-36, (dated December 1964).

32. R. S. Cortesi, "Compatibility of Electrostatically Focused Image Sections and Correlation Tubes Using TVIST Type Storage Targets," Westinghouse Aerospace Division, Systems Development Tech. Memo No. 403 (dated 29 July 1964).

33. A. S. Jensen, M. P. Siedband, K. J. Handel, "Secondary Emission Measurements of Semiconductors and Dielectrics," Westinghouse Electronic Tube Division Report ET-95-BEM-63-57 (dated 30 September 1963).

34. T. H. Moore, I. M. Krittman, "Sensing Characteristics of an Electrostatic Recording Camera," IEEE Trans. on Electron Devices, Vol. ED-11, No. 4, (April 1964) pp 183-190.

35. G. W. Geotze and A. H. Boerio, IEEE Proceedings 52, 1007 (1964). The Westinghouse Type No. for the first model described in this paper is WX-5419.

36. G. W. Goetze, "Advances in Electronics," Academic Press Inc., New York (1962) Vol. 16, p. 145.

37. G. W. Goetze, A. H. Boerio and M. Green, Journal of Applied Physics 35, 482 (1964).

38. R. S. Cortesi, "The Use of Image Tubes with Spectrometry," Westinghouse Aerospace Division Systems Development Tech. Memo No. 263, dated September 1963.

39. G. W. Goetze, "Continuously Variable Permanent Magnet for Imaging Purposes," U.S. Patent No. 3,155,860, dated 3 November 1964.

40. E. J. Sternglass, Rev. Sc. Instr. 26, 1202 (1955).

41. E. J. Sternglass and M. M. Wachtel, IRE Wachtel, IRE Trans. PGNS, Vol. NS-3, 29 (1956).

42. M. M. Wachtel, D. D. Doughty, G. W. Geotze, and E. J. Sternglass, Rev. Sc. Instr. 31, 576 (1960).

43. S. Goldman, "Frequency Analysis, Modulation, and Noise," McGraw Hill Book Co. Inc. (1948).

44. E. J. Sternglass, "Theory of Secondary Electron Emission and Electron Bombardment," Westinghouse Scientific Paper 6-94410-2-P9, July 23, 1957; Phys. Rev. 95, 609 (1954).

45. E. J. Sternglass, "Theory of Secondary Electron Emission by High-Speed Ions," Phys. Rev. 108, 1 (1957).

46. E. J. Sternglass and M. M. Wachtel, "Measurement of Low-Energy Electron Absorption in Metals and Insulators," Phys. Rev. 99, 646 (1955).

47. E. J. Sternglass and G. W. Goetze, "Field-Enhanced Transmission Secondary Emission for High-Speed Counting," IRE Trans Nucl. Sci., vol. NS-9, No. 3, June 1964.

48. R. J. Davis (private communication).

49. R. R. Beyer, G. W. Goetze, and D. D. Doughty, "A Method of Safe UVICON Operation," Westinghouse Research Report 64-9527-248-R1.

50. R. Theile, J. Telev. Soc. 9, 45 (1958).

51. See Appendix for description of the crossed-filament test-source used.

52. Martin Green, Second Interim Engrg. Report, "Exploratory Development of High Resolution Television Camera Tubes," Air Force Avionics Lab, Wright-Patterson AF33(615)1271.

53. Contract No. SD-22-12 (Smithsonian Astrophysical Laboratory - E.M.R.).